

Aus dem
Institut für Prophylaxe und Epidemiologie der Kreislaufkrankheiten
(IPEK)
Klinikum der Ludwig-Maximilians-Universität München



Role of non-classical monocytes in angiotensin II-induced cardiac remodelling

Dissertation
zum Erwerb des Doctor of Philosophy (Ph.D.)
an der Medizinischen Fakultät
der Ludwig-Maximilians-Universität München

vorgelegt von

Yi Xuan Shia

aus

Jahr

2025

Mit Genehmigung der Medizinischen Fakultät der
Ludwig-Maximilians-Universität München

Erstes Gutachten	: Prof. Dr. rer. nat. Sabine Steffens
Zweites Gutachten	: Prof. Dr. med. Christian Schulz
Drittes Gutachten	: Priv. Doz. Dr. Thomas Stocker
Viertes Gutachten	: Prof. Dr. Arthur Liesz
Dekan	: Prof. Dr. med. Thomas Gudermann

Tag der mündlichen Prüfung: 02.02.2025

Eidesstattliche Versicherung

Shia, Yi Xuan

Name, Vorname

Ich erkläre hiermit an Eides statt,
dass ich die vorliegende Dissertation mit dem Thema

Role of non-classical monocytes in angiotensin II-induced cardiac remodelling

selbständig verfasst, mich außer der angegebenen keiner weiteren Hilfsmittel bedient und alle Erkenntnisse, die aus dem Schrifttum ganz oder annähernd übernommen sind, als solche kenntlich gemacht und nach ihrer Herkunft unter Bezeichnung der Fundstelle einzeln nachgewiesen habe.

Ich erkläre des Weiteren, dass die hier vorgelegte Dissertation nicht in gleicher oder in ähnlicher Form bei einer anderen Stelle zur Erlangung eines akademischen Grades eingereicht wurde.

München, 05.12.2024

Ort, Datum

Yi Xuan Shia

Unterschrift Doktorand

The results of this work were presented at the following conferences:

Oral presentations:

- 10/2024 **IRTG1123 Annual Retreat**, Tutzing, Germany
Title: Role of non-classical monocytes in angiotensin II-induced cardiac remodelling
- 10/2022 **IRTG1123 Annual Retreat**, Tutzing, Germany
Title: Role of non-classical monocytes in heart failure

Poster presentations:

- 09/2024 **DGK Herztage 2024**, Hamburg, Germany
Title: Depletion of non-classical monocytes abolishes sex differences in angiotensin II-induced cardiac fibrosis.
- 06/2024 **II. Cardioimmunology Congress**, Bad Staffelstein, Germany
Title: Depletion of non-classical monocytes abolishes sex differences in angiotensin II-induced cardiac fibrosis.
- 06/2023 **IRTG1123 Annual Retreat**, Venice, Italy
Title: Sex differences in cardiac remodelling and circulating monocyte phenotype in a model of chronic angiotensin II infusion
- 04/2023 **89. DGK-Jahrestagung 2023**, Mannheim, Germany
Title: Sex differences in cardiac remodelling and circulating monocyte phenotype in a model of chronic angiotensin II infusion
- 09/2022 **DGK Herztage 2022**, Bonn, Germany
Title: Role of non-classical monocytes in angiotensin II-induced cardiac remodelling.

CONTENTS

LIST OF FIGURES	IV
LIST OF TABLES.....	VI
LIST OF ABBREVIATIONS	VII
1. SUMMARY	1
1. ZUSAMMENFASSUNG.....	1
2. INTRODUCTION	3
2.1 Heart failure	3
2.1.1 Heart failure with preserved or reduced ejection fraction	3
2.2 Sex-specific differences in heart failure development	4
2.3 Hypertensive heart disease	5
2.4 Adaptive and maladaptive cardiac remodelling	5
2.4.1 Decompensated cardiac hypertrophy	6
2.4.2 Cardiac fibrosis and extracellular matrix remodelling	7
2.4.2.1 Sex differences in cardiac fibrosis	8
2.4.2.2 Interstitial and perivascular fibrosis	9
2.4.2.3 Cardiac fibroblast activation and differentiation to myofibroblast.....	10
2.4.2.4 Role of endothelial cells during cardiac fibrosis	11
2.4.2.5 Endothelial-to-mesenchymal transition during cardiac fibrosis	12
2.4.3 Adverse cardiac inflammation	12
2.4.3.1 Sex differences in immune responses	13
2.4.3.2 Resident and recruited cardiac macrophages	13
2.4.3.3 Circulating classical and non-classical monocytes	14
2.4.3.4 Experimental models for studying the role of non-classical monocytes...	16
2.5 Angiotensin II infusion model of cardiac remodelling and heart failure	17
2.6 Study objectives and hypothesis	18
3. MATERIALS AND METHODS	19
3.1 MATERIALS	19
3.1.1 Chemicals and reagents	19
3.1.2 Buffers and solutions	20
3.1.3 Kits.....	20
3.1.4 Primers	20
3.1.5 Antibodies	21

3.1.6 Equipment.....	23
3.1.7 Software.....	23
3.2 METHODS	24
3.2.1 Mouse model	24
3.2.1.1 Subcutaneous osmotic minipump implantation	24
3.2.2 Tissue sampling.....	24
3.2.3 Histology	25
3.2.3.1 Paraffin sections preparation.....	25
3.2.3.2 Wheat germ agglutinin staining of paraffin sections	25
3.2.3.3 Sirius red staining of paraffin sections.....	26
3.2.4 RNA expression.....	27
3.2.4.1 RNA isolation.....	27
3.2.4.2 cDNA synthesis	28
3.2.4.3 Reverse transcription-quantitative real-time polymerase chain reactions ...	28
3.2.5 Flow cytometry.....	30
3.2.5.1 Sample preparation for heart and blood samples.....	30
3.2.5.2 Sample staining, data acquisition and analysis.....	30
3.2.6 Cell sorting.....	31
3.2.6.1 Sample preparation for cell sorting.....	31
3.2.6.2 Cell sorting for circulating Ly6C ^{hi} and Ly6C ^{lo} monocytes, cardiac fibroblasts, macrophages and endothelial cells sorting, and spleen B and T cells	31
3.2.7 Bulk RNA-seq	32
3.2.8 Non-invasive blood pressure measurement	33
3.2.9 Evans blue assay.....	33
3.2.10 Echocardiography.....	33
3.2.11 Statistical analysis	34
4. RESULTS	35
4.1 AngII treatment promotes cardiac hypertrophy independent of sex	35
4.2 Female mice are protected from AngII-induced cardiac fibrosis.....	36
4.3 AngII expands cardiac fibroblasts and induces pro-fibrotic genes only in males	38
4.4 AngII treatment downregulates genes associated with detoxifying reactive oxidative species in male cardiac fibroblasts	39
4.5 AngII promotes circulating and cardiac Ly6C ^{lo} monocyte expansion in females	43
4.6 AngII-treatment downregulates protective genes in male cardiac macrophages	47
4.7 Transcriptomic profiling of circulating Ly6C ^{hi} and Ly6C ^{lo} monocytes.....	51

4.8 Ang II treatment upregulates genes linked to antigen presentation and type I interferon response in female Ly6C ^{hi} monocytes.....	52
4.9 Ang II treatment upregulates genes linked to antigen presentation and cell killing in female circulating Ly6C ^{lo} monocytes	55
4.10 Gene expression of AT1R, ER α , and ER β in various cell types.....	56
4.11 <i>Nr4a1se_2</i> ^{-/-} mice as a Ly6C ^{lo} monocyte ablation model	58
4.12 <i>Nr4a1se_2</i> deficiency reverses anti-fibrotic effects in females with AngII infusion.....	60
4.13 <i>Nr4a1se_2</i> deficiency promotes the AngII-induced expansion of recruited macrophages in females.....	62
4.14 <i>Nr4a1se_2</i> deficiency promotes vascular permeability after AngII infusion in females	63
5. DISCUSSION.....	66
5.1 Female mice are protected from adverse cardiac fibrosis during AngII infusion	66
5.2 AngII promotes antigen processing and presentation in Ly6C ^{hi} and Ly6C ^{lo} monocytes during cardiac remodelling in females	67
5.3 AngII induces TLR7 signalling in female Ly6C ^{hi} monocytes	67
5.4 Impact of global <i>Nr4a1se_2</i> deficiency on various cell types	68
5.5 <i>Nr4a1se_2</i> deficiency promotes perivascular fibrosis	68
5.6 <i>Nr4a1se_2</i> deficiency increases endothelial permeability and oxidative stress	69
5.7 Study limitations and future perspectives	70
6. CONCLUSION.....	72
7. REFERENCES	73
8. ACKNOWLEDGEMENTS	83
9. AFFIDAVIT	84
10. CONFIRMATION OF CONGRUENCY	85
12. PUBLICATIONS AND ABSTRACT PRESENTATIONS.....	87
12.1 List of publications	87
12.2 List of abstracts.....	87

List of figures

Figure 1 Structural and functional characteristics of HFpEF and HFrEF.	4
Figure 2 The progression from adaptive to maladaptive cardiac remodelling upon chronic pressure overload.	6
Figure 3 Maladaptive concentric and eccentric cardiomyocyte hypertrophy.	7
Figure 4 Pathogenesis of cardiac fibrosis and diastolic dysfunction.	8
Figure 5 Collagen staining in cardiac sections from patients with heart failure.	9
Figure 6 Activation of cardiac fibroblasts and conversion to myofibroblasts.	10
Figure 7 Endothelial cells contribute to adverse cardiac remodelling.	11
Figure 8 Origin and functions of resident and recruited cardiac macrophages.	14
Figure 9 The roles of classical and non-classical monocytes during cardiac remodelling.	15
Figure 10 Cascade of the renin-angiotensin-aldosterone system.	17
Figure 11 Collagen content quantification using ImageJ.	27
Figure 12 Experimental design and gravimetric measurements upon 28 days of AngII infusion.	35
Figure 13 Cardiomyocyte cross-sectional area analysis after 28 days of AngII infusion.	36
Figure 14 Cardiac fibrosis after 7 to 28 days of AngII infusion.	37
Figure 15 Quantification of cardiac fibroblasts after 7 days of AngII infusion.	38
Figure 16 Cardiac pro-fibrotic gene expression after 7 days of AngII infusion.	39
Figure 17 Bulk RNA-seq analysis of sorted cardiac fibroblasts upon 7 days of AngII infusion.	41
Figure 18 Gene ontology analysis of DEGs in cardiac fibroblasts.	42
Figure 19 Gating strategy for leukocyte subsets in the blood and in the heart.	44
Figure 20 Circulating immune cell subsets upon 7 days of AngII infusion.	45
Figure 21 Cardiac myeloid cell subsets upon 7 days of AngII infusion.	46
Figure 22 Cardiac lymphoid subsets upon 7 days of AngII infusion.	47
Figure 23 Bulk RNA-seq analysis of sorted cardiac macrophages upon 7 days of AngII infusion.	49
Figure 24 Bulk RNA-seq analysis of DEGs in cardiac macrophages.	50
Figure 25 Transcriptomic profiling of circulating monocyte subsets after 7 days of AngII infusion.	51
Figure 26 Bulk RNA-seq analysis of sorted circulating Ly6C ^{hi} monocytes after 7 days of AngII infusion.	53
Figure 27 Type I IFN gene expression in circulating Ly6C ^{hi} monocytes after 7 days of AngII infusion.	54

Figure 28 Bulk RNA-seq analysis of sorted circulating Ly6C ^{lo} monocytes after 7 days of AngII infusion.....	55
Figure 29 Gene Ontology biological process analysis in circulating Ly6C ^{lo} monocytes after 7 days of AngII infusion.....	56
Figure 30 Phenotypic analysis of <i>Nr4a1se_2</i> ^{-/-} mice.....	59
Figure 31 Echocardiography analysis for cardiac function measurements after 28 days of AngII infusion.	60
Figure 32 Impact of <i>Nr4a1se_2</i> deficiency on AngII-induced cardiac fibrosis.	61
Figure 33 Cardiac leukocyte quantification in females after 7 days of AngII infusion.	62
Figure 34 Bulk RNA-seq analysis of sorted cardiac endothelial cells after 7 days of AngII infusion.....	64
Figure 35 Gene set enrichment analysis of cardiac ECs and Evans blue assay after 7 days of AngII infusion.	65
Figure 38 Contribution of reactive oxidative species in endothelial dysfunction.	70
Figure 39 Role of NCMs in AngII-induced cardiac remodelling	72

List of tables

Table 1 Chemicals and reagents	19
Table 2 Composition of buffers and solutions.....	20
Table 3 Kits	20
Table 4 Life technologies primers for RT-qPCR analysis	20
Table 5 Antibodies cocktail for heart staining panel A	21
Table 6 Antibodies cocktail for heart staining panel B	21
Table 7 Antibodies cocktail for blood myeloid panel	21
Table 8 Antibodies cocktail for lymphoid staining panel	22
Table 9 Antibodies cocktail for blood sorting panel.....	22
Table 10 Antibodies cocktail for heart sorting panel	22
Table 11 Equipment.....	23
Table 12 Software	23
Table 13 Gene expression of <i>Agtr1a</i> in each cell type	57
Table 14 Gene expression of <i>Esrra</i> in each cell type	57
Table 15 Gene expression of <i>Essrb</i> in each cell type.....	57
Table 16 Circulating immune cell counts in WT and <i>Nr4a1se_2^{-/-}</i> mice after 7 days of AngII infusion.....	62
Table 17 Cardiac immune cell counts in WT and <i>Nr4a1se_2^{-/-}</i> mice after 7 days of AngII infusion.....	63

List of abbreviations

α -sma	α -smooth muscle actin
ACE	Angiotensin-converting enzyme
ACK	Ammonium chloride potassium
ANOVA	Analysis of variance
AngII	Angiotensin II
APC	Allophycocyanin
AT1R	Angiotensin II type 1 receptor
AT2R	Angiotensin II type 2 receptor
BH2	7,8-dihydrobiopterin
BH4	Tetrahydrobiopterin
BP	Blood pressure
BV	Brilliant violet
Ca ²⁺	Calcium
CCL2	C-C motif chemokine ligand 2
CCR2	C-C motif chemokine receptor 2
COL1a2	Collagen type I alpha 2 chain
COL3a1	Collagen type III alpha 1 chain
CSA	Cross-sectional area
Ct	Threshold cycle
CTGF	Connective tissue growth factor
CXCL10	CXC-chemokine ligand 10
Cy	Cyanine
d	Days
DAMP	Damage-associated molecular pattern
DEG	Differentially expressed gene
DNase	Deoxyribonuclease
dH ₂ O	Distilled water
E2	17 β -estradiol
EC	Endothelial cell
ECM	Extracellular matrix
EDTA	Ethylenediaminetetraacetic acid
EndMT	Endothelial-to-mesenchymal transition
eNOS	Endothelial nitric oxide synthase
ER	Oestrogen receptor
FACS	Fluorescence-activated cell sorting
FITC	Fluorescein isothiocyanate
FOLR2	Folate receptor beta
FPKM	Fragments per kilobase of transcript per million mapped reads
FSC	Forward scatter
GAPDH	Glyceraldehyde-3-phosphate dehydrogenase
GOBP	Gene Ontology biological process
GSEA	Gene Set Enrichment Analysis
H ₂ O ₂	Hydrogen peroxide
H2-Ab1	Histocompatibility 2, class II antigen A, beta 1
HF	Heart failure

HFmrEF	Heart failure with mildly reduced ejection fraction
HFpEF	Heart failure with preserved ejection fraction
HFrEF	Heart failure with reduced ejection fraction
HHD	Hypertensive heart disease
HW/BW	Heart weight-to-body weight ratio
HW/TL	Heart weight-to-tibia length ratio
ICAM1	Intercellular adhesion molecule 1
IFN	Interferon
IL-1 β	Interleukin 1 β
IL-6	Interleukin 6
IRF	IFN regulatory factor
JAK2	Janus kinase 2
KHCO ₃	Potassium bicarbonate
KO	Knockout
LV	Left ventricle / left ventricular
LVEDV	Left ventricular end-diastolic volume
LVESV	Left ventricular end-systolic volume
LVID;d	Left ventricular diastolic internal diameter
LVID;s	Left ventricular systolic internal diameter
LYVE1	Lymphatic vessel endothelial hyaluronan receptor 1
MEFSK4	Murine embryonic fibroblast clone SK4
MHC	Major histocompatibility complex
MMP	Matrix metalloproteinase
mRNA	Messenger ribonucleic acid
MYD88	Myeloid differentiation primary response protein 88
NADPH	Nicotinamide adenine dinucleotide phosphate
Na ₂ EDTA	Disodium ethylenediaminetetraacetate dihydrate
NCM	Non-classical monocytes
NH ₄ Cl	Ammonium chloride
NF- κ B	Nuclear factor- κ B
NO	Nitric oxide
NOX	NADPH oxidase
NR4A1	Nuclear receptor subfamily 4 group A member 1
NR4A1SE_2	NR4A1 super-enhancer 2 deletion
O-cuff	Occlusion cuff
O ₂ ^{•-}	Superoxide anion
OH [•]	Hydroxyl radical
ONOO ⁻	Peroxynitrite
padj	Adjusted p-value
PBS	Phosphate buffered saline
PBMC	Peripheral blood mononuclear cells
PC	Principal component
PCA	Principal component analysis
PD-L1	Programmed death-ligand 1
PE	Phycoerythrin
PFA	Paraformaldehyde
PerCP	Peridinin-Chlorophyll-Protein
pH	Potential of hydrogen

PV	Perivascular
RAAS	Renin-angiotensin-aldosterone system
RFU	Relative fluorescence units
RNA	Ribonucleic acid
RNA-seq	RNA-sequencing
ROS	Reactive oxidative species
RT-qPCR	Reverse transcription-quantitative polymerase chain reaction
SD	Standard deviation
SEM	Standard error of the mean
SGLT2	Sodium-glucose cotransporter 2 inhibitors
SSC	Side scatter
STAT3	Signal transducer and activator of transcription 3
TAC	Transverse aortic constriction
TGF- β	Transforming growth factor- β
TIMD4	T-cell immunoglobulin and mucin domain containing 4
TIMP	Tissue inhibitor of metalloproteinase
TLR	Toll-like receptor
TNF	Tumour necrosis factor
VPR	Volume pressure recording
w/o	Without
WT	Wildtype

1. Summary

Heart failure (HF) occurs when the heart is unable to pump adequate blood volume to meet the metabolic demand of the body. There is a difference in the clinical prevalence of HF types in men and women, with women more prone to HF with preserved ejection fraction (EF; HFpEF), and men more prone to HF with reduced EF (HFrEF). However, experimental animal models of HF often include only one sex, which may limit the potential for translational application of the gained insights. Chronic hypertension can trigger cardiac remodelling, including immune activation, to compensate for the increased workload, which will eventually lead to the development of HFpEF or HFrEF in the long term. Angiotensin II (AngII) infusion is a well-established animal model of hypertensive cardiac fibrosis. The aim of this thesis was to investigate the sex-specific differences in AngII-induced cardiac remodelling and the involvement of immune cells in this process.

Male and female 8 to 10-week-old C57BL/6J wildtype (WT) and *Nr4a1* super-enhancer 2 subdomain knockout (*Nr4a1se_2^{-/-}*) mice, a transgenic model for selective non-classical monocyte (NCMs; Ly6C^{lo}) depletion, were subjected to vehicle (saline) or AngII infusion for 7 and 28 days. Circulating and cardiac leukocyte subsets were examined via flow cytometry. Differentially expressed genes (DEGs) in sorted circulating Ly6C^{lo} and Ly6C^{hi} monocytes, cardiac macrophages, fibroblasts, and endothelial cells (ECs) were assessed via bulk RNA sequencing. Cardiac inflammation and fibrosis were determined via mRNA expression analysis of respective factors and by histology.

Increased cardiac interstitial and perivascular fibrosis was observed in the WT male AngII-treated group after 7 and 28 days, associated with elevated pro-fibrotic gene (*Col1*, *Col3*, *Ctgf*, *Ccl2*, *Il-6*) expression as well as cardiac macrophage and fibroblast expansion compared to the female AngII-treated group. Notably, the relative proportion of NCMs in the heart increased in females, but not in males in response to AngII. This could be due to a higher Ly6C^{hi} to Ly6C^{lo} monocyte conversion rate and responsiveness to damage signals from damaged ECs, as suggested by higher expression levels of *Nr4a1* and *Tlr7* in female blood monocytes. In addition, transcriptomic profiling of cardiac macrophages and cardiac fibroblasts revealed a downregulation of genes related to adverse cardiac inflammation and fibrosis in the WT female AngII-treated group, which could contribute to cardioprotective effects during cardiac remodelling.

The resistance to AngII-induced adverse cardiac remodelling was lost in female *Nr4a1se_2^{-/-}* mice, showing a similar extent of cardiac fibrosis and pro-fibrotic gene expression compared to males. Furthermore, the extent of perivascular fibrosis was aggravated in *Nr4a1se_2^{-/-}*

AngII-treated male and female mice compared to WT mice. Bulk RNA-seq of cardiac ECs indicated that NCM deficiency shifted the phenotype of cardiac ECs to a transcriptomic signature associated with vascular permeability, extracellular matrix assembly, cardiac epithelial-to-mesenchymal transition and increased response to oxidative stress. In addition, Evans blue leakage confirmed increased vascular permeability in *Nr4a1se_2^{-/-}* AngII-treated mice compared to WT AngII-treated controls, while flow cytometry analysis revealed a higher number of recruited cardiac macrophage and cardiac fibroblast expansion.

Taken together, these findings suggest that an enhanced conversion into NCMs in WT females during hypertensive stress may help preserve cardiac endothelial integrity, limit inflammatory cell infiltration, and counterbalance cardiac fibrosis. Thus, the increased abundance of NCMs may explain at least in part the discrepancies in disease development between males and females in this mouse model.¹

1. Zusammenfassung

Herzinsuffizienz (HF) tritt auf, wenn das Herz nicht mehr in der Lage ist, eine ausreichende Blutversorgung zu gewährleisten, um den metabolischen Bedarf des Körpers zu decken. Es gibt geschlechtsspezifische Unterschiede in der klinischen Prävalenz verschiedener Formen von HF. Frauen neigen eher zu HF mit erhaltener Ejektionsfraktion (EF; HFpEF) und Männer eher zu HF mit reduzierter EF (HFrEF). Tierexperimentelle Studien haben bislang häufig nur ein Geschlecht berücksichtigt, was die Übertragbarkeit der hieraus gewonnenen Ergebnisse auf den Menschen einschränkt. Chronische Hypertonie führt zu kardialen Remodelling, einschließlich einer Immunantwort, um die erhöhte Arbeitsbelastung zu kompensieren, aber langfristig zu HFpEF oder HFrEF führen kann. Die chronische Angiotensin-II (AngII)-Infusion ist ein etabliertes Tiermodell für hypertensive Herzfibrose. Das Ziel dieses Projekts war es, geschlechtsspezifische Unterschiede im AngII-induzierten kardialen Remodelling und die Beteiligung von Immunzellen in diesem Kontext zu untersuchen.

Männliche und weibliche 8 bis 10 Wochen alte C57BL/6J Wildtyp (WT) und *Nr4a1* Super-Enhancer 2 Subdomäne Knockout (*Nr4a1se²^{-/-}*) Mäuse, einem Transgenmodell mit selektiver Defizienz von nicht-klassischen Monozyten (NCMs; Ly6C^{lo}), wurden einer Vehikel- (Kochsalz) oder AngII-Infusion über 7 bzw. 28 Tage ausgesetzt. Zirkulierende und kardiale Leukozyten wurden mittels Durchflusszytometrie untersucht. Differenziell exprimierte Gene wurden in isolierten zirkulierenden Ly6C^{lo}- und Ly6C^{hi}-Monozyten, kardialen Makrophagen, Fibroblasten und Endothelzellen (ECs) mittels Bulk-RNA-Sequenzierung ermittelt. Kardiale Entzündung und Fibrose wurden durch mRNA-Expressionsbestimmung der jeweiligen Faktoren und durch Histologie beurteilt.

Bei WT-Mäusen zeigte sich eine erhöhte kardiale interstitielle und perivaskuläre Fibrose in der männlichen AngII-behandelten Gruppe nach 7 und 28 Tagen, verbunden mit einer erhöhten Expression pro-fibrotischer Gene (*Col1*, *Col3*, *Ctgf*, *Ccl2*, *Il-6*) sowie einer Expansion von kardialen Makrophagen und Fibroblasten im Vergleich zur weiblichen AngII-behandelten Gruppe. Bemerkenswerterweise erhöhte sich bei AngII-Behandlung der relative Anteil an NCMs im Herzen der weiblichen Mäuse, nicht jedoch in den männlichen Mäusen. Dies könnte auf eine vermehrte Konversion von Ly6C^{hi} zu Ly6C^{lo} Monozyten und eine stärkere Reaktion auf Schadenssignale von geschädigten ECs zurückzuführen sein, wie durch höhere Expressionsniveaus von *Nr4a1* und *Tlr7* in Monozyten von weiblichen Tieren nahegelegt wird. Darüber hinaus zeigte die Transkriptomanalyse von kardialen Makrophagen und kardialen Fibroblasten in der Gruppe der weiblichen AngII-behandelten WT Mäuse eine niedrigere Expression von Genen, die mit schädlicher kardialer Entzündung und Fibrose in Verbindung stehen. Dies könnte zu kardioprotektiven Effekten während des Remodellings beitragen.

Ein Schutz gegenüber AngII-induzierter kardialer Fibrose war bei den weiblichen *Nr4a1se_2*^{-/-} Mäusen nicht mehr zu beobachten, die ein ähnliches Ausmaß an kardialer Fibrose und profibrotischer Genexpression wie die männlichen Mäuse zeigten. Darüber hinaus war das Ausmaß der perivaskulären Fibrose bei *Nr4a1se_2*^{-/-} AngII-behandelten männlichen und weiblichen Mäusen im Vergleich zu WT-Mäusen verstärkt. Die Transkriptomanalyse der kardialen ECs zeigte, dass die NCM-Defizienz zur vermehrten Expression von Genen beitrug, die mit vaskulärer Permeabilität, der Assemblierung der extrazellulären Matrix, der kardialen Epithel-zu-Mesenchymal-Transition und einer verstärkten Reaktion auf oxidativen Stress assoziiert sind. Der Evans-Blau-Test bestätigte zudem eine erhöhte vaskuläre Permeabilität bei *Nr4a1se_2*^{-/-} AngII-behandelten weiblichen Mäusen, was mit einer Zunahme von rekrutierten kardialen Makrophagen und Fibroblasten assoziiert war.

Zusammengefasst deuten diese Ergebnisse darauf hin, dass der erhöhte relative Anteil an NCMs in weiblichen WT Mäusen bei AngII-Behandlung dazu beitragen könnte, die kardiale Endothelintegrität zu erhalten, die Infiltration von Entzündungszellen zu begrenzen und somit der AngII-induzierten kardialen Fibrose entgegenzuwirken. Daher könnte der relative Anteil an NCMs zumindest teilweise die Diskrepanzen in der Krankheitsentwicklung und der therapeutischen Reaktionsfähigkeit bei Männern und Frauen erklären.

2. Introduction

2.1 Heart failure

Heart failure (HF) is a heterogeneous clinical syndrome affecting more than 64 million people worldwide.² HF happens when the heart cannot provide adequate cardiac output, which is the amount of blood pumped by the heart per minute, to meet the metabolic demand.³ An ageing population and the advances in treatment that reduce the acute mortality for patients with ischaemic heart disease without mitigating the risk of developing HF drive the increasing prevalence of HF.⁴

2.1.1 Heart failure with preserved or reduced ejection fraction

HF can be categorised based on the ejection fraction (EF). EF is defined as the percentage of stroke volume, the amount of blood ejected from the left ventricle (LV) in each contraction, over left ventricular end-diastolic volume (LVEDV), the volume of blood in the LV at the end diastole. EF reflects the heart's efficiency in pumping the blood out of the LV during each contraction.⁵ Therefore, EF is a functional and clinical parameter used for HF classification, including HF with reduced EF (HFrEF; EF <40%), HF with mildly reduced EF (HFmrEF; EF 40-49%), and HF with preserved EF (HFpEF; EF ≥50%).⁶ Under physiological conditions, EF lies around 50-70%.⁷

HFpEF is characterized by diastolic dysfunction and the most common cause is chronic pressure overload.⁸ In response to increased pressure derived mainly from vascular resistance, which is also known as afterload, the LV walls thicken. The thickening of the LV walls restricts LV compliance, impairing the ability of the ventricle to relax adequately and to accommodate blood filling during diastole.⁹ This in turn leads to an increase in LV end-diastolic pressure.¹⁰ Diseases commonly leading to HFpEF include hypertrophic cardiomyopathy, diabetes, obesity, aortic stenosis, and hypertension.^{11,12}

In contrast, HFrEF is characterized by systolic dysfunction and its primary cause is chronic volume overload.¹³ To accommodate the increased incoming blood volume, the LV walls stretch and dilate. Over time, the overstretched cardiomyocytes lose their ability to contract effectively. In addition, myocardial infarction is also a key factor driving HFrEF development.¹⁴ The loss of contractile cardiomyocytes after myocardial infarction impairs LV contractility, leading to a reduction in ejected blood during systole. The subsequently increased LVEDV leads to myocardial stretch, which promotes LV dilation and eccentric hypertrophy (Figure 1). Diseases commonly leading to HFrEF include dilated cardiomyopathy, myocardial infarction, mitral regurgitation, infectious diseases, and hypertension.^{8,12}

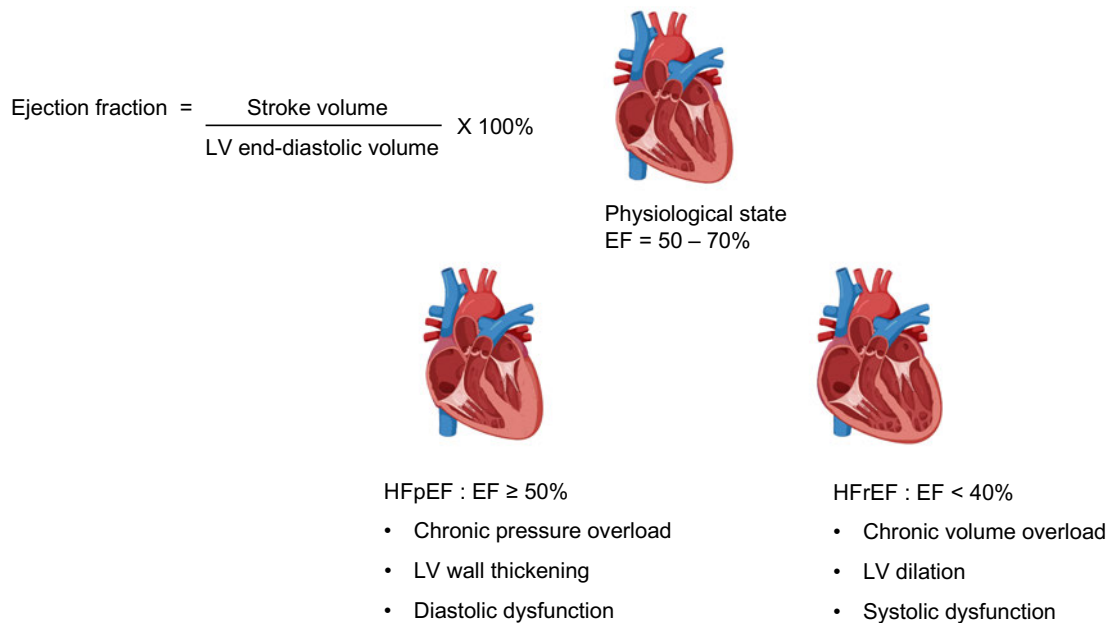


Figure 1 | Structural and functional characteristics of HFpEF and HFrEF.

Heart failure (HF) can be divided into two categories based on the ejection fraction (EF), which is defined as the percentage of stroke volume over left ventricular end-diastolic volume (LVEDV). Chronic pressure overload leads to HF with preserved EF (HFpEF), which is characterised by LV wall thickening and diastolic dysfunction. In contrast, chronic volume overload leads to HF with reduced EF (HFrEF), which is characterised by LV dilation and systolic dysfunction. (generated using BioRender.com)

Patients with HFpEF and HFrEF share similar symptoms, including dyspnoea, fatigue, limitations in exercise tolerance, and tissue congestion.^{8,15} While ageing and smoking increase the risk for both HFpEF and HFrEF, metabolic syndrome and a sedentary lifestyle enhance the likelihood of developing HFpEF.¹² The discovery of effective treatments for HFrEF has contributed to its declining prevalence over the last decades,¹⁵ whereas the prevalence of HFpEF is increasing by 10% per decade.¹² Based on several recent randomized clinical trials, the new clinical guidelines published by the European Society of Cardiology now recommend sodium-glucose cotransporter 2 inhibitors (SGLT2) such as Empagliflozin for the treatment of HFpEF patients, which are also effective in treating HFrEF patients and HF patients with type 2 diabetes.¹⁶ Positive clinical outcomes with reduced risk of cardiovascular death and hospitalisation are observed in HFpEF patients receiving Empagliflozin independent of the presence of diabetes.¹⁷ Nevertheless, further in-depth research into the efficacy of pharmacotherapy for HF subtypes with different underlying health conditions is urgently needed to improve the therapeutic management for each individual HF patient.

2.2 Sex-specific differences in heart failure development

Although the lifetime risk for HF is almost the same for men and women, there are significant differences in the manifestation of HF subtypes.¹⁸ Women are more likely to develop HFpEF with a longer life expectancy but worse health-related quality of life, while HFrEF is more

prevalent in men with a poor prognosis.^{19,20} The sex-based disparities encompass various aspects, including risk factors, clinical symptoms and the response to therapy.¹⁸

While ischaemic heart disease is the major cause of HF in men, hypertension and diabetes drive the risks for HF in women to a greater extent.¹⁸ Healthy men and women have distinctly different LV dimensions and functions, even after normalising to their body size. Furthermore, the LV chamber in women is smaller, resulting in a lower stroke volume. However, they have a higher resting heart rate to maintain a cardiac output similar to that in men.²¹ Studies also showed that women typically present with higher EF than men,²²⁻²⁵ indicating intrinsic sex differences in cardiac function under physiological conditions and in response to haemodynamic stress. In addition, women have higher systolic and diastolic LV stiffness than men at any given age, which is further aggravated by ageing.²⁶ Therefore, both sexes should be included in both clinical and animal research to address sex differences in disease development.

2.3 Hypertensive heart disease

Hypertension is the leading cause of cardiovascular disease worldwide with an increasing prevalence for HF.^{27,28} Long-term high blood pressure doubles the lifetime risk of HF compared to normal blood pressure.²⁹ Chronic hypertension can lead to hypertensive heart disease (HHD), which is associated with morphological and functional abnormalities of the LV, including concentric hypertrophy as its hallmark.³⁰ Unresolved pressure overload further aggravates LV wall thickening, resulting in diastolic dysfunction and the development of HFpEF. In the late stages of HHD, sustained pressure overload drives the manifestation of dilated cardiomyopathy and the development of HFrEF.³¹ In addition, non-haemodynamic mechanisms including immune alterations, oxidative stress, and endothelial dysfunction also contribute to the pathophysiology of HHD.^{32,33} HHD comes second (26.2%) among all causes of HF, closely behind ischaemic heart disease (26.5%).³⁴ Advancements in HHD treatment have failed to reduce the associated risk for HF, representing an unmet medical need with a huge clinical and socioeconomic burden.³⁵

2.4 Adaptive and maladaptive cardiac remodelling

The progress of HHD into HF involves a series of complex processes including adaptive and maladaptive cardiac remodelling. LV remodelling is the cellular, interstitial, structural and functional alteration of the heart in response to haemodynamic stress exerted on the LV.³⁶ Cardiac stress, such as pressure overload, initially triggers adaptive LV remodelling by cardiomyocyte hypertrophy that exerts compensatory effects to maintain cardiac output.

Although initial transient adaptive LV remodelling may be beneficial, long-term activation of the remodelling programme promotes the transition to maladaptive remodelling that exerts deleterious effects on the heart, predisposing to the development of HF and increasing cardiovascular morbidity and mortality.³⁷ Maladaptive LV remodelling during HF development encompasses decompensated cardiomyocyte hypertrophy, fibrosis, inflammation, apoptosis, and endothelial dysfunction (Figure 2).^{35,38}

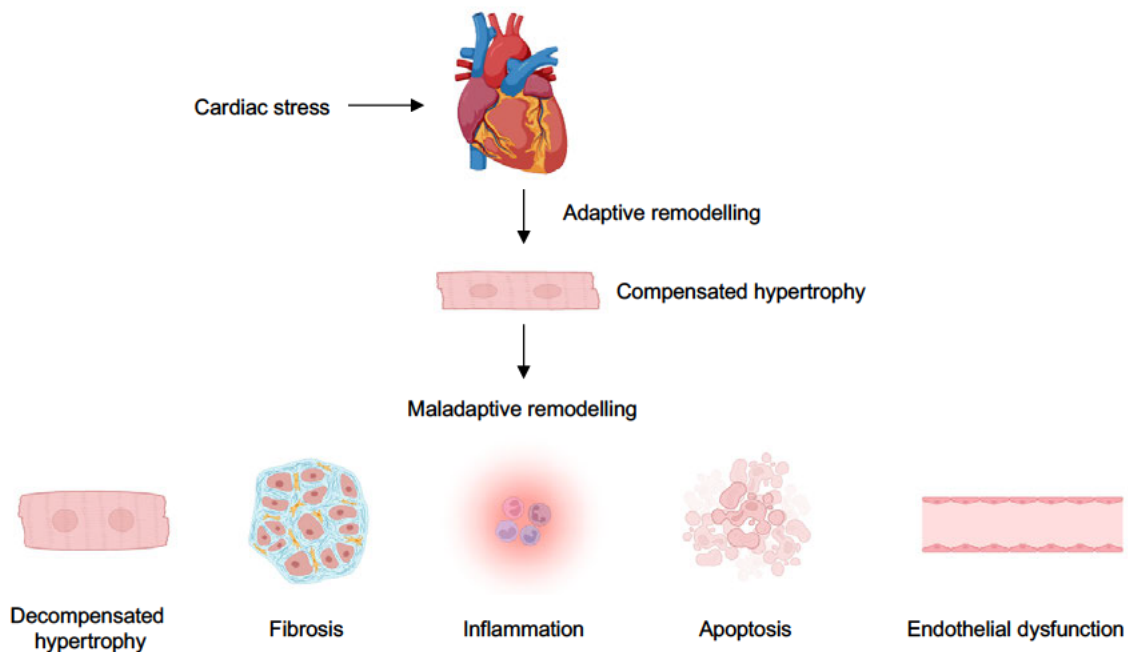


Figure 2 | The progression from adaptive to maladaptive cardiac remodelling upon chronic pressure overload.

When the cardiac wall stress increases, the left ventricle initiates adaptive cardiac remodelling such as compensated cardiomyocyte hypertrophy, to account for the extra cardiac burden. Persistent cardiac stress leads to the transition to maladaptive remodelling including decompensated cardiomyocyte hypertrophy, fibrosis, inflammation, apoptosis, and endothelial dysfunction, driving the progression towards heart failure. (generated using BioRender.com)

2.4.1 Decompensated cardiac hypertrophy

Cardiomyocyte hypertrophy is a key initial compensatory mechanism in response to pressure overload.³⁹ Cardiomyocytes constitute approximately 30% of the total cell number in the adult mammalian heart but account for 70 to 80% of the heart volume.⁴⁰ As cardiomyocytes are mostly terminally differentiated, they respond to cardiac stress by increasing in size instead of dividing. The sarcomere, the basic contractile unit of the cardiomyocyte, plays a crucial role during cardiomyocyte hypertrophy.⁴¹ Early pressure overload triggers initial adaptive hypertrophy by adding sarcomeres in parallel, which leads to an adaptive increase in cardiomyocyte size.³⁷ Chronic pressure overload drives the transition from adaptive hypertrophy to maladaptive hypertrophy, promoting HF pathogenesis. During maladaptive

concentric hypertrophy in HFpEF, sarcomeres are further added in parallel, contributing to the increase in cardiomyocyte diameter and LV wall thickening.⁴² Conversely, chronic volume overload leads to eccentric hypertrophy, where the sarcomeres are laid down in series, leading to cardiomyocyte lengthening and thinning of LV wall with the concurrent increase in LV lumen. In the long term, this can culminate in the transition to HFrEF (Figure 3).⁴² Cardiomyocyte hypertrophy further disrupts sarcomere composition and organisation, shifting from the predominant adult α -myosin heavy chain to the foetal β -myosin heavy chain, which consumes lower adenosine triphosphatase activity to conserve energy consumption, contributing to slower contractile velocity that impairs myocardial contractility.⁴³

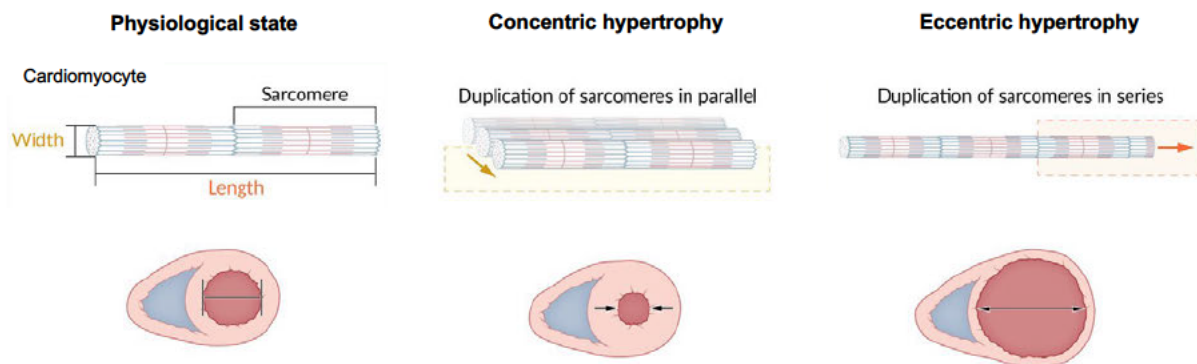


Figure 3 | Maladaptive concentric and eccentric cardiomyocyte hypertrophy.

Chronic pressure overload drives the transition from compensated cardiomyocyte hypertrophy to maladaptive concentric and eccentric cardiomyocyte hypertrophy. During concentric hypertrophy, sarcomeres are added in parallel, increasing the cardiomyocyte diameter, which leads to wall thickening while preserving contractility. In eccentric hypertrophy, sarcomeres are added in series, increasing cardiomyocyte cross-section that results in wall thinning, thereby impairing the contractile function of cardiomyocytes. Cross-sectional changes in LV diameter are indicated by arrows in the graphics above, with the LV cavity in red and the right ventricular cavity in blue. (adapted from AMBOSS.com)

2.4.2 Cardiac fibrosis and extracellular matrix remodelling

Cardiac fibrosis contributes to the development of HFpEF and HFrEF during maladaptive LV remodelling due to the disturbed balance between collagen deposition and degradation within the extracellular matrix (ECM).⁴⁴ ECM of the myocardium plays a crucial role in preserving structural integrity, electrical conduction, and mechanical function of the ventricles.⁴⁵ Excessive ECM accumulation disrupts electrical conduction, leading to rhythm disturbances and myocardial contractile dysfunction, thereby predisposing to arrhythmia and sudden cardiac death.⁴⁶ ECM deposition depends on the action of the cardiac fibroblast.³⁶ Cardiac fibroblasts located within the ECM actively secrete fibrotic mediators, including matrix metalloproteinase (MMP) 2, MMP9, tissue inhibitor of metalloproteinase (TIMP), transforming growth factor β (TGF- β) and connective tissue growth factor (CTGF).^{47,48} The expression of MMPs and TIMPs regulates the balance between collagen deposition and degradation, as TIMPs counteract MMPs to inhibit uncontrolled ECM degradation.⁴⁹ Unbalanced activation of

MMPs enhances matrix turnover, which leads to wall thinning and LV dilation,⁴⁹ thereby resulting in systolic dysfunction characteristic for HFrEF.

Chronic pressure overload triggers the differentiation of cardiac fibroblasts into myofibroblasts,⁵⁰ which synthesize type I and type III collagen.⁵¹ Type I collagen is the thicker fibre that provides tensile strength, while type III collagen is the thinner fibre that maintains the elasticity of the matrix network.¹² An increased type I/III collagen ratio and highly cross-linked collagen fibres enhance collagen insolubility and resistance to degradation, leading to excessive ECM accumulation and ventricular stiffness, thereby resulting in the characteristic diastolic dysfunction of HFpEF (Figure 4).

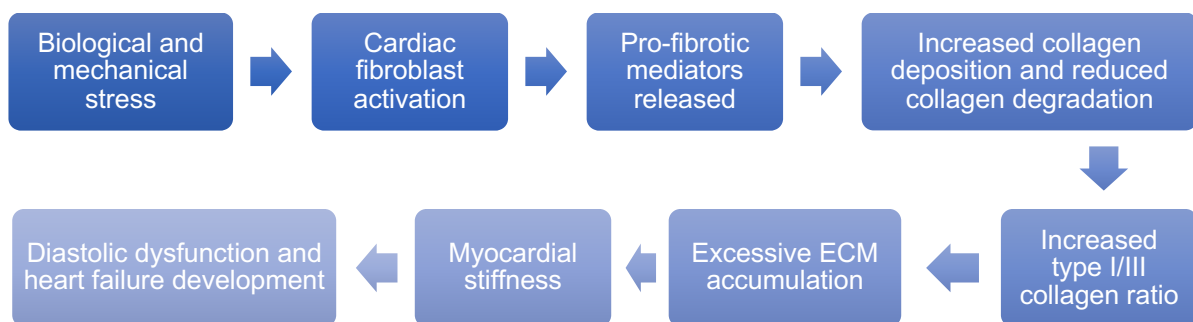


Figure 4 | Pathogenesis of cardiac fibrosis and diastolic dysfunction.

When the heart is subjected to biological and mechanical stress due to cardiac injury, cardiac fibroblasts get activated and release pro-fibrotic mediators. This leads to an increase in collagen deposition and a reduction in collagen degradation as well as increased type I/III collagen ratio, which eventually results in excessive extracellular matrix (ECM) accumulation. Disruption in ECM organisation contributes to myocardial stiffness that drives the progression to diastolic dysfunction and heart failure development.⁵²

2.4.2.1 Sex differences in cardiac fibrosis

The availability of sex hormones, especially 17 β -estradiol (E2) plays a crucial role in cardiac remodelling and fibrosis.⁵³ A higher concentration of circulating E2 contributes to cardioprotective effects, and a drop in the circulating levels in postmenopausal HF patients results in worsened myocardial fibrosis and diastolic dysfunction.^{54,55} Clinical studies of pressure overload with aortic stenosis patients showed an elevation in collagen gene expression in male patients, while female patients showed suppression in the expression of genes related to ECM assembly and inflammation.⁵⁶ Of note, the samples included in this study were obtained from age-matched male and female patients with a mean age of 55.6 or 55.8, respectively. In a rodent transverse aortic constriction (TAC) model, cardiac fibrosis in males was linked to androgen-dependent activation of TGF- β , and gonadectomy mitigated TAC-induced cardiac fibrosis.⁵⁷ Furthermore, ER β signalling is protective against cardiac

fibrosis and apoptosis in female mice via inhibition of inflammatory pathways and by maintenance of mitochondrial metabolism.^{58,59} These findings suggest a protective role of oestrogens against maladaptive cardiac fibrosis by modulating ECM deposition, while testosterone contributes to excessive collagen release.

2.4.2.2 Interstitial and perivascular fibrosis

Excessive interstitial diffuse deposition of collagen fibres within the myocardium promotes LV diastolic and systolic dysfunction, and the degree of severity determines the development of HF in HHD patients.⁵² The accumulation of collagen fibres may appear as microscars, representing reparative interstitial fibrosis. In contrast, reactive interstitial fibrosis often appears as thick fibrotic sheaths surrounding the perivascular area or as thick bands surrounding the cardiac muscle bundles (perimysial) and individual cardiomyocytes (endomysial).⁶⁰ Fibrosis in patients at an early stage of hypertrophic cardiomyopathy appears predominantly in the perivascular, perimysial, and endomysial areas, which is overtaken by microscars with disease progression (Figure 5).⁶¹

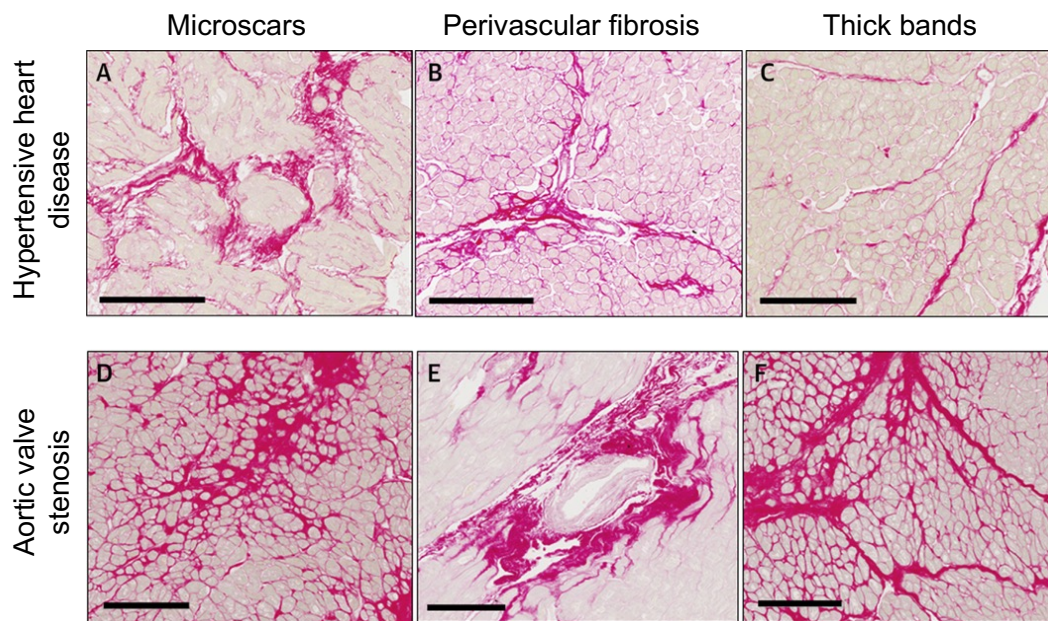


Figure 5 | Collagen staining in cardiac sections from patients with heart failure.

Sirius red staining of cardiac sections from patients with hypertensive heart disease (A-C) or aortic valve stenosis (D-F). Different types of interstitial fibrosis were identified: microscars (A, D), perivascular fibrosis (B, E) and thick bands (C, F). Scale bars = 200 μ m. (adapted from Díez et al., 2020)⁴⁴

In addition, collagen deposition usually increases from the outer epicardial to the inner endocardial third of the myocardium in patients with HHD, which is probably associated with wall stress, transmural pressure gradient, and coronary microcirculation alterations that cause relative endocardial ischaemia.⁴⁴ Myocardial interstitial and perivascular fibrosis lead to LV

diastolic dysfunction and HFpEF by exacerbating LV stiffness and impairing early diastolic LV filling. In LV systolic dysfunction and HFrEF, realignment of collagen fibres can impair force transmission from cardiomyocytes to the ventricular chamber, and the fibrotic sheaths that encircle the cardiomyocytes may restrict cardiomyocyte stretching during diastole, resulting in declined length-dependent force generation during systole.⁴⁴

2.4.2.3 Cardiac fibroblast activation and differentiation to myofibroblast

Cardiac fibroblasts are mainly derived from the proepicardium.⁶² However, they can also arise through epithelial/endothelial-to-mesenchymal transition.⁶³ Resident cardiac fibroblasts are dispersed throughout the heart, acting as a scaffold in the myocardium.⁶⁴ Under physiological conditions, the ECM in the adult heart is continuously subjected to compression and stretching forces generated by cardiac motion.⁶⁵ Cardiac fibroblasts play an important role in maintaining the homeostatic state of the ECM by regulating the expression of MMPs and TIMPs, thereby modulating the secretion and degradation of collagen fibres.⁶⁶ When subjected to cardiac stress, cardiac fibroblasts proliferate and convert to myofibroblasts with elevated α -smooth muscle actin (α -sma) expression and collagen deposition.⁶⁷ Single-cell RNA sequencing data revealed around 30 differentially expressed genes (DEGs) between activated myofibroblasts and resting fibroblasts, including type I collagen, type III collagen, and periostin.⁶⁸ The transition from cardiac fibroblast to myofibroblast is a complex process involving multiple factors such as TGF- β .⁶⁹ Activated myofibroblasts in turn can secrete TGF- β themselves without input from other cells creating a positive feedback loop that results in sustained fibrosis (Figure 6).^{70,71}

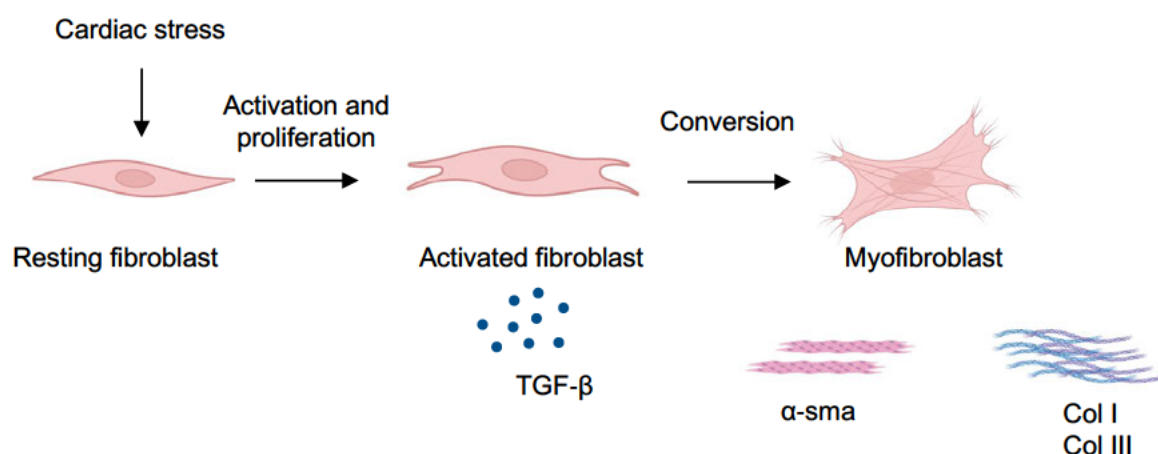


Figure 6 | Activation of cardiac fibroblasts and conversion to myofibroblasts.

In response to cardiac stress, resting fibroblasts are activated and proliferate. Activated cardiac fibroblasts release pro-fibrotic cytokines such as transforming growth factor- β (TGF- β) which drive the conversion to myofibroblasts. Myofibroblasts actively secrete α -smooth muscle actin (α -sma), type I (Col I) and III collagen fibres (Col III), leading to cardiac fibrosis. (generated using BioRender.com)

Cardiac fibroblasts and myofibroblasts respond to inflammation^{72,73} by releasing cytokines and chemokines to induce leukocyte infiltration into the heart.^{74,75} However, the composition of cytokines in the surrounding areas also affects the chemokine secretome of cardiac fibroblasts, leading to the infiltration of pro-inflammatory or anti-inflammatory monocytes.⁷⁶ The stretching of cardiac fibroblasts can induce mechanical stress that triggers the release of chemokines.⁶⁷ This contributes to elevated adhesion molecule expression on the endothelium and gelatinase expression to promote monocyte recruitment across the basolateral membrane.⁶⁷

2.4.2.4 Role of endothelial cells during cardiac fibrosis

Intercellular crosstalk is essential in both physiological cardiac development and maladaptive cardiac remodelling, particularly via factors released by cardiac endothelial cells (ECs).⁷⁷ There are two main types of ECs in the heart, the endocardial and the vascular ECs. Endocardial ECs are the innermost layer of the ventricular walls that separate the trabecular myocardium from the circulation, whereas vascular ECs primarily reside within the compact layers of the ventricular myocardium.⁷⁸

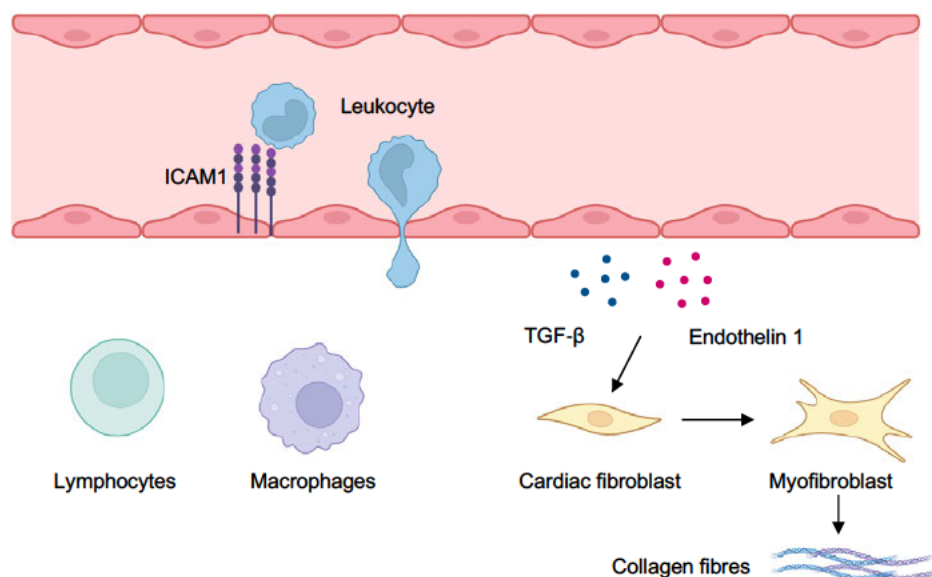


Figure 7 | Endothelial cells contribute to adverse cardiac remodelling.

During cardiac remodelling, endothelial cells increase the expression of adhesion molecules such as intercellular adhesion molecule 1 (ICAM1), promoting leukocyte infiltration including monocytes and lymphocytes. They also secrete pro-fibrotic factors such as transforming growth factor- β (TGF- β) and endothelin 1 that induce cardiac fibroblast conversion into myofibroblasts. Myofibroblasts secrete collagen fibres, thereby contributing to increased collagen deposition. (generated using BioRender.com)

In particular, vascular ECs are involved in cardiac fibrosis during cardiac remodelling via several indirect mechanisms (Figure 7). They facilitate leukocyte infiltration through elevated expression of adhesion molecules, secrete pro-fibrotic factors that activate cardiac fibroblasts, and stimulate tissue hypoxia through capillary rarefaction.⁷⁹ In mice with non-ischaemic heart

disease, increased intercellular adhesion molecule 1 (ICAM1) contributed to macrophage and lymphocyte recruitment⁸⁰ and the depletion of ICAM1 reduced neutrophil infiltration after ischaemic-reperfusion injury.⁸¹ Furthermore, cardiac ECs release pro-fibrotic cytokines such as TGF- β and endothelin 1 when subjected to angiotensin II (AngII) infusion in rats and mice,⁸² and the reduction in microvascular density was associated with aggravated myocardial interstitial fibrosis in HFpEF patients.⁸³

2.4.2.5 Endothelial-to-mesenchymal transition during cardiac fibrosis

ECs and mesenchymal cells derive from two different lineages with distinct phenotypes and functions.⁷⁸ Unlike ECs, which have an elongated shape, mesenchymal cells are stellate or spindle-shaped stromal cells without the expression of adherents and tight junctions. They move freely through the ECM and form the connective tissue that facilitates organ functions.⁸⁴ Mesenchymal cells play a critical role in contributing to the pool of fibroblasts and myofibroblasts in fibrotic diseases of multiple organs including the heart.⁸⁵

Lineage-tracing studies revealed that ECs and mesenchymal cells convert into each other both during cardiovascular development and pathogenesis. The transdifferentiation of ECs into mesenchymal cells, a process known as endothelial-to-mesenchymal transition (EndMT), occurs during heart development to form the cardiac valves. Studies have shown that EndMT is also involved in cardiovascular diseases such as myocardial infarction, atherosclerosis, and disease accompanying cardiac fibrosis.^{86,87} Conversely, the transdifferentiation of cardiac fibroblasts into ECs – also known as mesenchymal-to-endothelial transition – after cardiac injury promotes neovascularization.⁸⁸

2.4.3 Adverse cardiac inflammation

Activation of the immune system and cardiac inflammation that occurs during maladaptive LV remodelling contributes to cardiac injury,⁸⁹ driving the pathogenesis of HF. The inflammatory response induced by cardiac stress increases capillary wall permeability, enhancing inflammatory cell infiltration into the myocardium, and promoting pro-inflammatory cytokine and chemokine production including interleukin 6 (IL-6), IL-1 β , and CC-chemokine ligand 2 (CCL2).⁹⁰ Injured cardiomyocytes release damage-associated molecular patterns (DAMPs), inducing the production of inflammatory cytokines from the surrounding healthy cardiomyocytes and other cells in the heart, thereby creating a versatile signalling network for leukocyte recruitment and activation that leads to the worsening of inflammation.⁹¹ Macrophage expansion triggered by increased inflammatory cytokine levels in the

myocardium serves as a crucial aspect of cardiac inflammation, further enhancing inflammatory cytokines and nuclear factor- κ B (NF- κ B) expression within the myocardium.⁹²

2.4.3.1 Sex differences in immune responses

Biological sex also affects the immunological responses to self and foreign antigens involving genes and hormones. Women generally induce greater innate and adaptive immune responses than men.⁹³ The presence of androgen response elements as well as oestrogen response elements in the promoter regions of genes involved in innate immunity may thus result in dimorphic innate immune responses.⁹⁴ Transcriptomic research in mice showed that the gene expression along the toll-like receptor (TLR) pathways and the production of type I interferon (IFN) differs between sexes.^{94,95} For example, the TLR7 is encoded on the X chromosome, which may escape X inactivation and contribute to increased TLR7 expression in female mice.⁹⁶ When exposed to TLR7 ligands, peripheral blood mononuclear cells in female mice produce a higher amount of IFN α .⁹⁷ Furthermore, the transcriptional regulation of IFN regulatory factor 5 (IRF5) in female mice is regulated through oestrogen receptor α (ER α), which promotes higher production of IRF5 and IFN α following TLR7 ligand stimulation.⁹⁸ In addition, females also have a higher macrophage and neutrophil phagocytic activity and are more efficient at antigen presentation.^{99,100} In males, the immune cells have a higher expression level of TLR4, which leads to higher production of CXC-chemokine ligand 10 (CXCL10).¹⁰¹

Despite these clear indications of sex-specific mechanisms in the pathophysiology of HF, experimental studies in this context are lacking. Therefore, research into sex differences in the pathophysiology of HF, particularly the underlying immune response is urgently needed to uncover potential therapeutic targets to address the different clinical needs of men and women.

2.4.3.2 Resident and recruited cardiac macrophages

Cardiac macrophages are the most abundant immune cells in the healthy heart, interspersed throughout the myocardium, comprising 6 to 8% of non-cardiomyocyte cells in the adult mouse heart.¹⁰²⁻¹⁰⁴ Compared to monocytes, cardiac macrophages are characterised by increased expression of CD68, major histocompatibility class II (MHCII) and F4/80 in mice. Human macrophages can be distinguished from monocytes by their reduced CD14 expression.¹⁰⁵ Cardiac macrophages are involved in a variety of processes, including phagocytosis, cytokine production, immune surveillance, and electrical conductance.¹⁰⁶

Cardiac macrophages can be broadly categorised into resident and recruited macrophages based on their origin and the expression of C-C motif chemokine receptor 2 (CCR2).¹⁰² CCR2-

macrophages (resident macrophages), co-expressing T-cell immunoglobulin and mucin domain containing 4 (TIMD4), lymphatic vessel endothelial hyaluronan receptor 1 (LYVE1), and folate receptor beta (FOLR2),¹⁰⁷ are derived from embryonic origins and replenished by proliferative self-renewal, independent from monocyte input.^{108,109} In contrast, CCR2⁺ macrophages (recruited macrophages) derive from infiltrated circulating monocytes, which make up around 5 to 15% of all macrophages in a healthy heart.¹¹⁰ Resident and recruited macrophages have distinct functions in the heart. Whereas resident macrophages mainly participate in physiological cardiomyocyte hypertrophy, cardiac tissue regeneration, and functional recovery after cardiac injury,¹¹¹ recruited macrophages are involved in the initiation of inflammatory responses and further monocyte recruitment.¹¹² During cardiac remodelling and HF development, resident macrophages expand through local proliferation while recruited macrophages differentiate from infiltrated monocytes.¹⁰³ In the setting of hypertension in rodents, global ablation of macrophages aggravated cardiac function, but improved cardiac fibrosis, indicating that macrophages consist of heterogeneous subsets, each with distinct roles that can either protect against or contribute to disease progression (Figure 8).^{113,114}

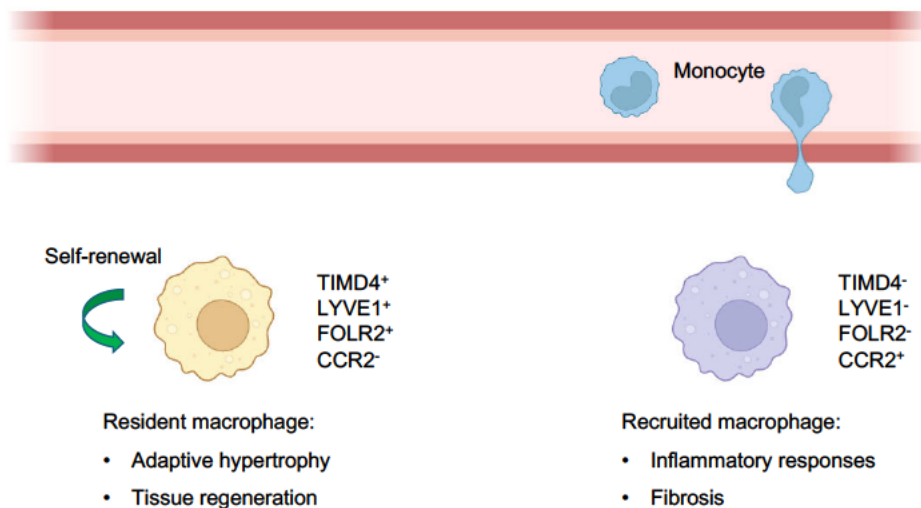


Figure 8 | Origin and functions of resident and recruited cardiac macrophages.

Resident macrophages (TIMD4⁺LYVE1⁺FOLR2⁺CCR2⁻) seed the heart during embryonic development and have the ability to self-renew through proliferation. They are involved in adaptive cardiomyocyte hypertrophy and tissue regeneration. In contrast, recruited macrophages (TIMD4⁻LYVE1⁻FOLR2⁻CCR2⁺) depend on the input from circulating monocytes and are involved in inflammatory responses and interstitial fibrosis during cardiac remodelling. (generated using BioRender.com)

2.4.3.3 Circulating classical and non-classical monocytes

Monocytes are part of the mononuclear phagocyte system that also encompasses macrophages and dendritic cells. Based on their surface expression markers, monocytes can be categorised into classical (CMs; Ly6C^{hi}) and non-classical monocytes (NCMs; Ly6C^{lo}).¹⁰⁵ Within the circulation, CMs have a relatively short half-life of 20 to 24 hours before gradually

converting into NCMs, which have a half-life of approximately 2 days.¹¹⁵ In the presence of inflammation, CMs are recruited to the inflammatory site and infiltrate the tissue, while NCMs are thought to remain in the vasculature, at least under most experimental conditions studied so far.¹¹⁶⁻¹¹⁸ NCMs can extend their half-life from around 2 days to 11 days to enhance immune surveillance and maintain vascular homeostasis during inflammation.¹¹⁹

CMs are defined as CD14⁺CD16⁻ in humans and Ly6C^{hi} in mice, both expressing high levels of CCR2.^{117,120} They are derived either from the bone marrow or extramedullary haematopoietic sites including the spleen. In the circulation, classical monocytes make up over 90% of all circulating monocytes.¹¹⁷ They travel to the site of injury in a CCR2-dependent manner and participate in the innate immune response by releasing tumour necrosis factor α (TNF- α), nitric oxide (NO) and other inflammatory mediators or differentiating into macrophages and dendritic cells. Furthermore, a recent study in mice also showed that CMs could activate adaptive immune responses through antigen presentation to T cells.¹²¹ In contrast, NCMs are defined as CD14⁻CD16⁺ in humans and Ly6C^{lo} in mice, both also express high levels of CX3C motif chemokine receptor 1 (CX3CR1).^{122,123} In the circulation, Ly6C^{lo} monocytes can arise through the conversion from Ly6C^{hi} monocytes. However, alternative routes for the development of Ly6C^{lo} monocytes independently of Ly6C^{hi} monocytes may also exist.¹¹⁶ NCMs are constantly patrolling on the luminal side of the vascular endothelium both under physiological state and during inflammation, playing a crucial role in immune surveillance (Figure 9).¹¹⁶

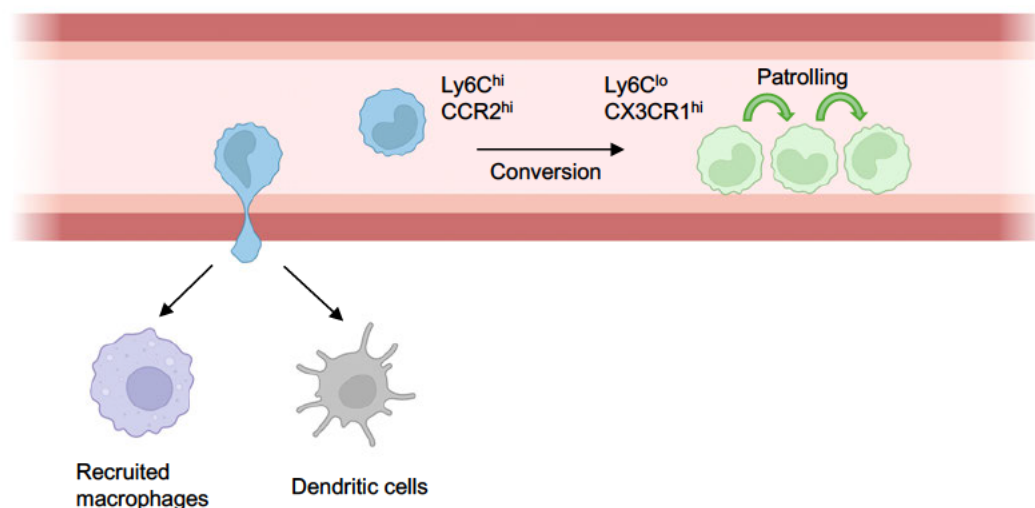


Figure 9 | The roles of classical and non-classical monocytes during cardiac remodelling.

Classical monocytes (Ly6C^{hi}CCR2^{hi}) usually convert into Ly6C^{lo} monocytes in the circulation within 24 hours or infiltrate into the interstitium, giving rise to recruited macrophages and dendritic cells. Non-classical monocytes (Ly6C^{lo}CX3CR1^{hi}) are constantly patrolling the endothelium for immune surveillance and maintaining vascular integrity. (generated using BioRender.com)

Recent studies have demonstrated that Ly6C^{lo} monocytes can extravasate into the lung interstitium and convert into macrophages with antigen-presenting properties.^{124,125} However, in the heart, the extravasation of NCMs and the transition to macrophages remains controversial.¹²⁶ A study in mice with myocardial infarction revealed that NCMs infiltrate into the heart at a later phase following myocardial infarction, promoting anti-inflammation and cardiac regeneration.¹²⁷ In addition, there is also a third subset of monocytes, the intermediate monocytes. They are defined as CD14⁺CD16⁺ in humans and Ly6C^{int} in mice. Despite their high CX3CR1 expression, these cells exhibit inflammatory characteristics and do not participate in vasculature patrolling.¹¹⁹

2.4.3.4 Experimental models for studying the role of non-classical monocytes

Nuclear receptor subfamily 4 group A member 1 (*Nr4a1*) is a transcription factor highly expressed in NCMs for Ly6C^{lo} monocyte development. Mice with *Nr4a1*^{-/-} have significantly lower numbers of Ly6C^{lo} monocytes in bone marrow, spleen, and blood. The remaining NCMs in *Nr4a1*^{-/-} mice have nearly lost the vascular patrolling function, and the few NCMs found in the bone marrow present abnormal morphology with higher apoptosis susceptibility.¹²⁸ Therefore, *Nr4a1*^{-/-} mice have been widely used as a mouse model to study the role of NCMs in different experimental settings. However, *Nr4a1*^{-/-} failed to ablate NCMs without affecting *Nr4a1* expression and function in other cell types, including macrophages.¹²⁸ Studies have shown that *Nr4a1* helps mitigate macrophage inflammatory responses, and *Nr4a1* deficiency facilitates cell migration and enhances phagocytic activity¹²⁹. Furthermore, *Nr4a1* deficiency enhances CCR2 expression on Ly6C^{hi} monocytes, facilitating myocardium infiltration and the differentiation into highly inflammatory macrophages that contribute to adverse cardiac outcomes¹³⁰. In addition, a study in mice also showed that overexpression of *Nr4a1* in T cells prevents their differentiation to effector T cells, leading to immunosuppression, while *Nr4a1* deficiency overcomes T cell tolerance and amplifies effector function.¹³¹ In B cells, *Nr4a1* plays a role in modulating the affinity of B cell receptors and *Nr4a1* deletion results in selective expansion of B cells with high antigen affinity.¹³²

Recently, a new transgenic mouse model for selective NCM depletion has been established by targeting the super-enhancer 2 (E2) subdomain of *Nr4a1* located 4 kb upstream of the transcription start site. Mice that lack the E2 subdomain (*Nr4a1se_2*^{-/-}) showed Ly6C^{lo} monocyte deficiency while preserving *Nr4a1* gene expression in other cell populations including macrophages under steady state as well as during inflammation.¹³³ Thus, *Nr4a1se_2*^{-/-} mice emerge as a more suitable loss-of-function tool for studying NCM.

2.5 Angiotensin II infusion model of cardiac remodelling and heart failure

Small animals, especially mice, are widely used as an experimental model to study the pathophysiology of HF due to their high degree of homology to the human genome, relatively short breeding cycles, and lower housing costs compared to other animal models.¹³⁴ The AngII infusion model is a well-established hypertension and cardiac remodelling model.¹³² It involves a technically simple surgery, where an osmotic minipump filled with AngII is implanted subcutaneously at the flank of the mouse.

AngII is part of the renin-angiotensin-aldosterone system (RAAS).¹³⁵ Angiotensinogen produced by the liver is converted into angiotensin I via renin, an enzyme secreted by the kidney. Angiotensin-converting enzyme (ACE) released by the lungs catalyses the conversion from angiotensin I to AngII. Chronic infusion with AngII causes persistent stimulation of the AngII type I receptor (AT1R), leading to vasoconstriction, elevated arterial blood pressure, and the initiation of cardiac remodelling.¹³⁶ Furthermore, AngII acts on the adrenal cortex, which promotes the production of aldosterone, increasing sodium and water reabsorption, thereby increasing blood volume and blood pressure (Figure 10). In contrast to the immediate pressure overload observed in the transaortic constriction model, AngII-induced cardiac remodelling and HF progress at a slower rate over time. This progression more closely resembles the clinical course of HHD in patients, making the AngII infusion model particularly advantageous.¹³⁴

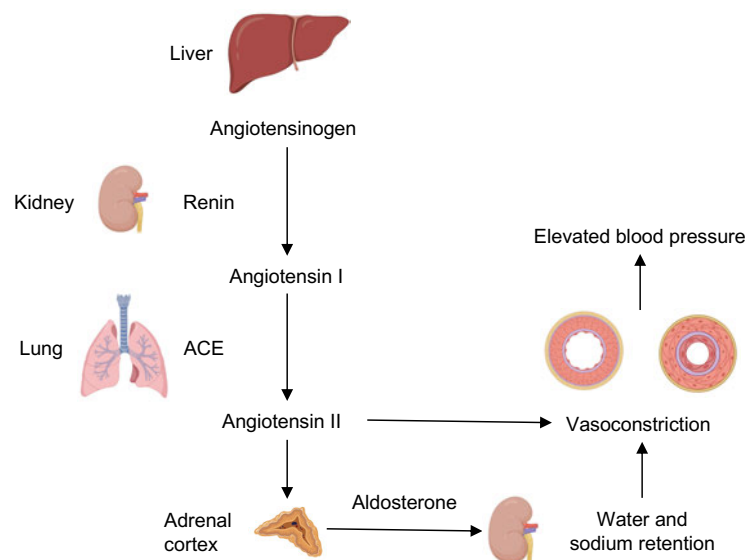


Figure 10 | Cascade of the renin-angiotensin-aldosterone system.

The renin-angiotensin-aldosterone system starts with the renin produced by the kidney acting on angiotensinogen released by the liver, forming angiotensin I. Angiotensin I is converted to AngII by angiotensin-converting enzyme (ACE) released from the lungs. AngII acts directly on the blood vessels, causing vasoconstriction. In addition, AngII acting on the adrenal cortex stimulates the secretion of aldosterone, leading to water and sodium retention, which also results in vasoconstriction and increased blood pressure. (generated using BioRender.com)

2.6 Study objectives and hypothesis

The paucity of sex-specific animal studies during cardiac remodelling and HF limits the potential for translating experimental findings into clinical practice. Moreover, research suggests that distinct subsets of monocytes may contribute differently to the downstream events of cardiac inflammation – including cardiac regeneration, healing, or progressive impairment of cardiac function – and thereby the clinical outcome of HF patients. In particular, research into the causal role of NCMs during HF development may contribute to a more profound understanding of HF development and the mechanisms of immune crosstalk and intercellular communication between cardiac macrophages, fibroblasts, and ECs during cardiac remodelling. Therefore, the principal objectives of this project can be delineated as follows:

1. Elucidate sex-specific differences during AngII-induced cardiac remodelling
2. Investigate the role of NCMs during AngII-induced cardiac remodelling
3. Characterise phenotypical and functional changes of cardiac ECs upon *Nr4a1se_2* depletion

3. Materials and methods

3.1 Materials

3.1.1 Chemicals and reagents

Table 1 | Chemicals and reagents

Chemicals / Reagents	Company
Albumin	Carl Roth GmbH & Co. KG, Karlsruhe, Germany
Angiotensin II	Sigma-Aldrich Chemie GmbH, Munich, Germany
β -mercaptoethanol	Sigma-Aldrich Chemie GmbH, Munich, Germany
Buffer RLT Plus	Qiagen, Hilden, Germany
Chloroform	Merck KGaA, Darmstadt, Germany
Collagenase type I	Sigma-Aldrich Chemie GmbH, Munich, Germany
Collagenase type XI	Sigma-Aldrich Chemie GmbH, Munich, Germany
Counting beads	Thermo Fisher Scientific, Waltham, USA
Direct red 80	Sigma-Aldrich Chemie GmbH, Munich, Germany
DNase I	Sigma-Aldrich Chemie GmbH, Munich, Germany
Ethanol	VWR Chemicals BDH, Radnor, USA
Entellan [®]	Merck KGaA, Darmstadt, Germany
Evans blue	Sigma-Aldrich Chemie GmbH, Munich, Germany
Formamide	Sigma-Aldrich Chemie GmbH, Munich, Germany
Hoechst 33342	Thermo Fisher Scientific, Waltham, USA
Hyaluronidase	Sigma-Aldrich Chemie GmbH, Munich, Germany
Ketamine	Serumwerk Bernburg AG, Bernburg, Germany
Immu-Mount [™]	Thermo Fisher Scientific, Waltham, USA
Isoflurane	CP-Pharma Handelsgesellschaft mbH, Burgdorf, Germany
Metacam [®] meloxicam	Boehringer Ingelheim Pharma GmbH, Ingelheim am Rhein, Germany
Octenisept [®] antiseptic	Schülke & Mayr GmbH, Norderstedt, Germany
Paraformaldehyde	Sigma-Aldrich Chemie GmbH, Munich, Germany
PBS Dulbecco w/o Ca ²⁺	Biochrom GmbH, Berlin, Germany
Picric acid 1.2%	Sigma-Aldrich Chemie GmbH, Munich, Germany
QIAzol [®] lysis reagent	Qiagen, Hilden, Germany
RNasin [®] Plus	Promega Corporation, Wisconsin, USA
Ribonuclease inhibitor	
Saline 0.9%	Fresenius Kabi GmbH, Bad Homburg vor der Höhe, Germany
Wheat germ agglutinin	Thermo Fisher Scientific, Waltham, USA
Xylazine	Wirtschaftsgenossenschaft deutscher Tierärzte eG, Niedersachsen, Germany
Xylene	Fisher Scientific, Loughborough, United Kingdom

3.1.2 Buffers and solutions

Table 2 | Composition of buffers and solutions

Solutions	Composition
0.1% Sirius Red solution	0.1% Sirius Red solution (v/v), 1.2% picric acid (pH 2.0) (v/v)
ACK lysis buffer	150 mM NH ₄ Cl, 10 mM KHCO ₃ , 0.1 mM Na ₂ EDTA, pH 7.4
Blocking solution	CD16/CD32, 1:1000 dilution in PBS
Cells lysis buffer	1% β -mercaptoethanol in Buffer RLT Plus
Counting beads solution	CountBright™ Absolute Counting Beads (C36950, Invitrogen), 1:30 dilution in FACS buffer
Digestion cocktail	450 U/mL Collagenase Type I, 125 U/mL Collagenase Type XI, 60 U/mL DNase I, 60 U/mL Hyaluronidase, 200 U/mL Ribonuclease Inhibitor in PBS
FACS buffer	0.5 % (w/v) albumin in PBS

3.1.3 Kits

Table 3 | Kits

Kit	Company
GoTaq® Probe qPCR master mix	Promega GmbH, Walldorf, Germany
PrimeScript™ RT reagent kit	Takara Bio, Shiga, Japan
RNeasy® Plus Micro Kit	Qiagen, Hilden, Germany

3.1.4 Primers

Primers and probes used for reverse transcription-quantitative polymerase chain reaction (RT-qPCR) were purchased from Life Technologies. Life Technologies provides a primer-probe mix which contains a TaqMan probe with fluorescein amidite (FAM) at the 5' end that serves as the reporter dye and a minor groove binder with a non-fluorescent quencher (MGB-NFQ) at the 3' end.

Table 4 | Life technologies primers for RT-qPCR analysis

Gene	Accession no.	Assay ID
<i>Col1a2</i>	NM_007743.2	Mm00483888_m1
<i>Col3a1</i>	NM_009930.2	Mm01254476_m1
<i>Ctgf</i>	NM_010217.2	Mm01192933_g1
<i>Ccl2</i>	NM_011333.3	Mm00441242_m1
<i>Gapdh</i>	NM_008084.3	Mm99999915_g1
<i>Ifnb1</i>	NM_010510.1	Mm00439552_s1

<i>Il6</i>	NM_031168.1	Mm00446190_m1
<i>Nr4a1</i>	NM_010444.2	Mm01300401_m1

3.1.5 Antibodies

Table 5 | Antibodies cocktail for heart staining panel A

Antigen	Clone	Host	Conjugation	Dilution	Provider	Ref no.
CD11b	M1/70	Rat	Pacific Blue	1:500	BioLegend	101224
CD11c	HL3	Hamster	BV786	1:200	BD Biosciences	563735
CD45	30-F11	Mouse	BV605	1:500	BioLegend	103139
CD64	X54-5/7.1	Mouse	APC	1:500	BioLegend	139306
LYVE1	ALY7	Rat	Alexa Fluor™ 488	1:200	Invitrogen	53-0443-82
Ly6C	HK1.4	Rat	BV510	1:500	BioLegend	128033
Ly6G	1A8	Rat	APC-Cy7	1:500	BioLegend	127623
MHCII	M5/114.15.2	Rat	Alexa Fluor™ 700	1:200	Invitrogen	56-5321-82
PD-L1	10F.9G2	Rat	PE	1:200	BioLegend	124308
TIMD4	RMT4-54	Rat	PE-Cy7	1:200	BioLegend	130009

Table 6 | Antibodies cocktail for heart staining panel B

Antigen	Clone	Host	Conjugation	Dilution	Provider	Ref no.
CD3	17A2	Rat	APC-Cy7	1:100	BD Biosciences	560590
CD4	GK1.5	Rat	FITC	1:100	Invitrogen	11-0041-85
CD8a	53-6.7	Rat	PE-Cy7	1:200	Invitrogen	25-0081-82
CD11b	M1/70	Rat	Pacific Blue	1:500	BioLegend	101224
CD19	eBio1D3	Rat	PerCP-Cy5.5	1:500	Invitrogen	45-0193-82
CD31	MEC13.3	Rat	PE	1:1000	BioLegend	102507
CD45	30-F11	Mouse	BV605	1:500	BioLegend	103139
MEFSK4	mEF-SK4	Rat	APC	1:200	Miltenyi Biotec	130-120-802
MHCII	M5/114.15.2	Rat	Alexa Fluor™ 700	1:200	Invitrogen	56-5321-82

Table 7 | Antibodies cocktail for blood myeloid panel

Antigen	Clone	Host	Conjugation	Dilution	Provider	Ref no.
CCR2	475301	Rat	BV786	1:200	BD Biosciences	747966
CD11b	M1/70	Rat	PerCP	1:200	BioLegend	101230

CD11c	HL3	Hamster	FITC	1:200	BD Biosciences	561045
CD45	30-F11	Mouse	BV605	1:500	BioLegend	103139
CD115	AFS98	Rat	APC	1:500	Invitrogen	17-1152-82
F4/80	BM8	Rat	PB	1:500	BioLegend	123124
Ly6C	HK1.4	Rat	BV510	1:500	BioLegend	128033
Ly6G	1A8	Rat	APC-Cy7	1:500	BioLegend	127623
MHCII	M5/114.15.2	Rat	Alexa Fluor™ 700	1:200	Invitrogen	56-5321-82
PD-L1	10F.9G2	Rat	PE	1:200	BioLegend	124308

Table 8 | Antibodies cocktail for lymphoid staining panel

Antigen	Clone	Host	Conjugation	Dilution	Provider	Ref no.
CD3	17A2	Rat	FITC	1:500	BD Biosciences	555274
CD4	GK1.5	Rat	APC-H7	1:500	BD Biosciences	560181
CD8a	53-6.7	Rat	PE-Cy7	1:200	Invitrogen	25-0081-82
CD19	eBio1D3	Rat	PE	1:500	Invitrogen	12-0193-82
CD45.2	104	Mouse	APC	1:1000	BD Biosciences	558702

Table 9 | Antibodies cocktail for blood sorting panel

Antigen	Clone	Host	Conjugation	Dilution	Provider	Ref no.
CD11b	M1/70	Rat	Pacific Blue	1:500	BioLegend	101224
CD45.2	104	Mouse	FITC	1:1000	BD Biosciences	553772
CD115	AFS98	Rat	APC	1:500	Invitrogen	17-1152-82
Ly6C	AL-21	Rat	PE-Cy7	1:1000	BD Biosciences	560593
Ly6G	1A8	Rat	APC-Cy7	1:500	BioLegend	127623

Table 10 | Antibodies cocktail for heart sorting panel

Antigen	Clone	Host	Conjugation	Dilution	Provider	Ref no.
CD11b	M1/70	Rat	Pacific Blue	1:500	BioLegend	101224
CD31	MEC13.3	Rat	PE	1:1000	BioLegend	102507
CD45.2	104	Mouse	FITC	1:1000	BD Biosciences	553772
CD64	X54-5/7.1	Mouse	PerCP-Cy5.5	1:500	BioLegend	139308
Ly6C	AL-21	Rat	PE-Cy7	1:1000	BD Biosciences	560593
Ly6G	1A8	Rat	APC-Cy7	1:500	BioLegend	127623
MEFSK4	mEF-SK4	Rat	APC	1:200	Miltenyi Biotec	130-120-802

3.1.6 Equipment

Table 11 | Equipment

Equipment	Company
CUT 6062 Fully automatic precision microtome	SLEE medical GmbH, Mainz, Germany
FACSAria III cell sorter	BD Biosciences, New Jersey, USA
FACSCanto II	BD Biosciences, New Jersey, USA
Hot Plate 062	Labotect GmbH, Rosdorf, Germany
Leica ASP200S Tissue Processor	Leica Biosystems, Wetzlar, Germany
Leica EG1150 Tissue Embedding System	Leica Biosystems, Wetzlar, Germany
Leica THUNDER Imager 3D Tissue	Leica Microsystems, Wetzlar, Germany
LSRFortessa™ X-20	BD Biosciences, New Jersey, USA
NanoPhotometer® NP80	Implen GmbH, Munich, Germany
QuantStudio™ 6 Pro Real-time PCR System	Thermo Fisher Scientific, Waltham, USA
Qubit 4 Fluorometer	Thermo Fisher Scientific, Waltham, USA
Rodent NIBP CODA® Monitor Sets	ADInstruments, Sydney, Australia
TissueLyser LT	Qiagen, Hilden, Germany
Vevo® 3100 imaging system	FUJIFILM VisualSonics, Toronto, Canada

3.1.7 Software

Table 12 | Software

Software	Company
Design and Analysis Software 2.6.0	Thermo Fisher Scientific, Waltham, USA
EndNote 20	Clarivate, Philadelphia, USA
FlowJo 10.8.1	BD Biosciences, New Jersey, USA
g:Profiler	ELIXIR, Tartu, Estonia
GraphPad Prism 10.0	GraphPad Software Inc., USA
GSEA 4.3.2	Broad Institute, Massachusetts, USA
ImageJ	National Institutes of Health, Maryland, USA
LabChart	ADInstruments, Sydney, Australia
Leica Application Suite X (LAS X)	Leica Microsystems, Wetzlar, Germany
RStudio	Posit Software, Boston, USA
Vevo Lab	FUJIFILM VisualSonics, Toronto, Canada

3.2 Methods

3.2.1 Mouse model

C57BL/6J mice were purchased from Janvier Labs and served as wildtype (WT) mice. Mice with *Nr4a1*^{se_2} depletion (RRID:IMSR_JAX:030204)¹³³ were originally generated by C. Hedrick's lab (La Jolla, CA, USA) and bred in-house to serve as NCM knockout (KO) mice. The *Nr4a1*^{se_2} regulatory region was mutated using CRISPR/Cas9 technology. Up to five mice were housed in each separately ventilated cage. The housing facility maintained a 12-hour light-dark cycle with a temperature of 23°C and 60% relative humidity. All animal procedures were performed in adherence to the ethical principles declared in the Directive 2010/63/EU, the government of Upper Bavaria (ROB-55.2.2532.Vet_02-18-114 and ROB-55.2.2532.Vet_02-23-157) and the ARRIVE guidelines.

3.2.1.1 Subcutaneous osmotic minipump implantation

Male and female mice aged between 8 to 10 weeks were randomly subjected to angiotensin II (AngII) or saline infusion for 7 or 28 days. Mice were weighed one day before the surgery for osmotic minipump preparation. The pumps (ALZET 1004, Durect) were filled with 1.5 µg/g/day AngII (4474-91-3, Sigma, dissolved in 0.9% saline) or an equivalent volume of 0.9% saline (6605514, Fresenius Kabi) which served as a control. To ensure a steady infusion rate immediately after implantation, the prefilled pumps were activated by incubation in 0.9% saline for at least 24 hours at 37°C before the implantation. Mice were anaesthetised via inhalatory isoflurane at a concentration of 1.5% mixed with 98.5% oxygen at a flow rate of 1 L/min and laid prone on a hot plate set at 37°C to maintain physiological body temperature. The neck area was disinfected with Octinesept® antiseptic (04830483, Schülke) and a small skin incision was made. After subcutaneous insertion of the pump, the incision was closed with 5-0 silk sutures (IO10171L, Serag Wiessner). 100 µL Meloxicam (2 mg/kg) was subcutaneously injected immediately, 6 and 24 hours after the intervention.

3.2.2 Tissue sampling

At each study endpoint (7 days and 28 days), mice were euthanised by intraperitoneal injection of overdosed xylazine (120 mg/kg) and ketamine (10 mg/kg). After weighing the mouse, the peritoneum and thorax were opened. Blood was taken from the right ventricle and kept in ethylenediaminetetraacetic acid (EDTA) tube on ice until further processing. The body circulation was perfused with 10 mL phosphate buffered saline (PBS) infused via LV. The weight of the heart was measured to determine cardiac hypertrophy and consequently cut into several sections. The section used for flow cytometry was placed in a tube with PBS and

placed on ice until further processing. The section used for ribonucleic acid (RNA) isolation was placed in a tube, snap-frozen with liquid nitrogen, and stored at -80°C until further processing. The midventricular section used for histology was placed in a tube with 4% paraformaldehyde (PFA) at 4°C for fixation and subsequent paraffin embedding. The left tibia was excised to measure the length for heart weight normalisation.

3.2.3 Histology

3.2.3.1 Paraffin sections preparation

Midventricular sections placed in 4% PFA for at least 24 hours at 4°C were processed using Leica ASP200S Tissue Processor with a routine overnight programme. Briefly, the tissue was dehydrated with increasing concentration of ethanol, cleared by xylene, and infiltrated with histological wax. Processed tissues were embedded in paraffin using Leica EG1150 Tissue Embedding System and cut into $5\text{ }\mu\text{m}$ sections using CUT 6062 Fully automatic precision microtome. The cut sections were transferred into a water bath, followed by transfer onto Superfrost[®] Plus microscope slides. The slides were dried on a heating plate overnight at 45°C .

3.2.3.2 Wheat germ agglutinin staining of paraffin sections

To assess cardiomyocyte hypertrophy, midventricular paraffin sections were stained with wheat germ agglutinin (Alexa Fluor[™] 647 conjugate, W32466, Invitrogen) to label the plasma membrane for fluorescence imaging. Hoechst (Invitrogen, H3570) was used for nuclei staining and the sections were mounted with Immu-Mount[™] (Thermo Scientific, 9990402). A detailed staining protocol is described below:

Procedure	Substance	Time
Deparaffinisation	Xylene	2 x 5 min
Rehydration	100% ethanol	2 min
	90% ethanol	2 min
	70% ethanol	2 min
Washing	dH ₂ O	5 min
	PBS	5 min
Staining	Wheat germ agglutinin (1:200) and Hoechst (1:500) in PBS	60 min
Washing	PBS	5 min
	PBS	5 min
Mounting	Immu-Mount [™]	

Images were taken at 20x magnification using Leica THUNDER Imager 3D Tissue. The cross-sectional area (CSA) of a minimum of 50 cardiomyocytes in the LV per mouse was measured using ImageJ.

3.2.3.3 Sirius red staining of paraffin sections

To determine the development of fibrosis in LV, midventricular paraffin sections were stained with Sirius red solution. The staining protocol is described below:

Procedure	Substance	Time
Deparaffinisation	Xylene	2 x 5min
Rehydration	100% ethanol	2 min
	90% ethanol	2 min
	70% ethanol	2 min
Washing	dH ₂ O	5 min
Staining	0.1% Sirius Red solution	30 min
Washing	dH ₂ O	Rinse
	dH ₂ O	Rinse
Dehydration	90% ethanol	2 min
	100% ethanol	2 min
	Xylene	2 x 5 min
Mounting	Entellan®	

For total fibrosis quantification, tile scans were taken in 10x magnification using Leica THUNDER Imager 3D Tissue to visualise the whole section. Area fraction of the collagen fibres and cardiomyocytes were quantified using ImageJ by applying threshold for collagen fibres and cardiomyocytes accordingly (Figure 11A). Collagen content was determined using the following formula:

$$\text{Collagen content (\%)} = \frac{\text{Area fraction of collagen fibres (\%)}}{\text{Area fraction of cardiomyocytes (\%)}}$$

For perivascular (PV) fibrosis quantification, images containing vessels were taken at 10x magnification. The extent of fibrosis surrounding the vessel was outlined using ImageJ, and the threshold for collagen fibres and vessel smooth muscle cells was applied (Figure 11B). Collagen content was determined using the above formula. Three vessels of each sample were measured for PV fibrosis.

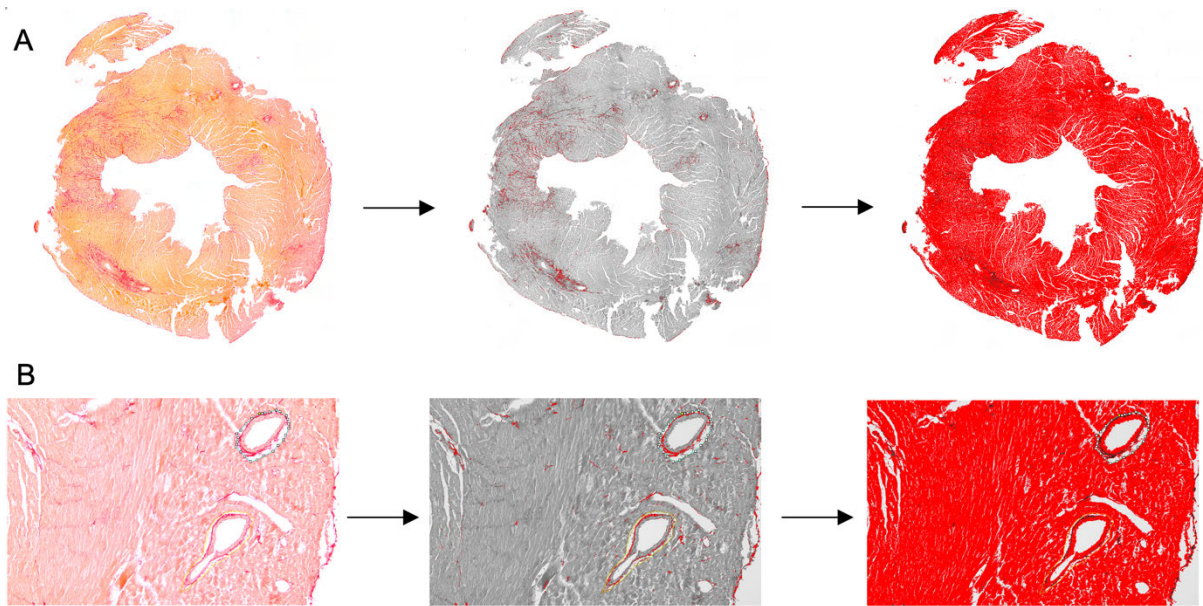


Figure 11 | Collagen content quantification using ImageJ.

A. Tile scans taken in 10x magnification were converted to RGB stack and the image in green channel was used for threshold application. The threshold for the collagen fibres was first applied (middle) and the area fraction was measured, followed by the threshold for cardiomyocyte (right). **B.** Image containing the vessels was taken in 10x magnification. The region of interest surrounding the vessels was traced using the 'polygon selection' (blue tracing) in ImageJ. The threshold for the collagen fibres (middle) and vessel smooth muscle cells (right) was applied and measured.

3.2.4 RNA expression

3.2.4.1 RNA isolation

For gene expression analysis in whole heart lysate, heart sections that were frozen during tissue sampling were pulverised. The tissue was kept frozen by adding liquid nitrogen during pestling. 1 mL QIAzol[®] lysis reagent (79306, Qiagen), a monophasic solution of phenol and guanidium isothiocyanate, was added to the pulverised heart tissue samples for cell disruption and cell components solubilisation. Metal beads were added into each tube, and the tissues were homogenised using TissueLyser LT at 50 rpm/s for 2 min. The homogenised lysates were transferred to new tubes, and 200 μ L chloroform was added to facilitate the phase separation of RNA from DNA and protein. The tubes were mixed by inverting 30 times and were left at room temperature for 5 min. The tubes were then centrifuged at 12,000 g for 5 min. The supernatant was used for RNA isolation.

For *Nr4a1* expression analysis, the snap-frozen sorted B and T cells from the spleen were thawed on ice and 350 μ L cells lysis buffer was added.

RNA was isolated using the RNeasy[®] Plus Micro Kit (74034, Qiagen) according to the manufacturer's protocol. Briefly, the sample was transferred to gDNA Eliminator spin columns for genomic DNA removal. 70% ethanol was added to the flow-through and transferred to

RNeasy MinElute spin columns for RNA binding. Buffer RW1 was added to the RNeasy MinElute spin columns to facilitate the binding of RNA to the column membrane. Buffer RPE was then added to the RNeasy MinElute spin columns, followed by 80% ethanol for washing. Finally, the RNeasy MinElute spin columns were placed in new 1.5 mL collection tubes and RNase-free water was added directly to the centre of the spin column membranes to elute the RNA. The concentration of the eluted RNA was measured using NanoPhotometer® NP80. The RNase-free water used for RNA elution was used for blank measurement.

3.2.4.2 cDNA synthesis

Reverse transcription (RT) of RNA to complementary deoxyribonucleic acid (cDNA) was performed using PrimeScript™ RT reagent kit (RR037A, Takara Bio). The master mix composition for one reaction (required for reversely transcribing 1 µg RNA) is described below.

Reagent	Volume
5X PrimeScript Buffer	2 µL
PrimeScript RT Enzyme Mix I	0.5 µL
Oligo dT Primer (50 µM)	0.5 µL
Random 6 mers (100 µM)	2 µL
1 µg RNA	X µl
RNase-free water	up to 10 µL (final volume)

The RT reaction mixture tubes were incubated at 37°C for 15 min, followed by 15 s of heat treatment at 85°C to inactivate the reverse transcriptase. The tubes were then placed on ice for a few minutes and RNase-free water was added to dilute the cDNA to a final concentration of 10 ng/µL. For each batch of newly synthesised cDNA, a reaction tube without the addition of RNA, but with the respective volume of RNase-free water instead, was included as the RT negative control.

3.2.4.3 Reverse transcription-quantitative real-time polymerase chain reactions

To assess the expression of genes related to LV hypertrophy, interstitial fibrosis, and inflammation, RT-qPCR were performed using GoTaq® Probe qPCR Master Mix (A6102, Promega) with carboxy-X-rhodamine as the reference dye. 2.3 ng cDNA were used for the amplification of each gene, and all samples were run in duplicates in a 96-well FastGene® Fast PCR plate (FG-03890-50, Nippon Genetics). The RT-qPCR reaction mixture (final volume 20 µL) was composed as follows:

Life Technologies primer-probe mix	
Reagent	Volume
cDNA (10 ng/μL)	4.60 μL
Primer-probe mix	0.50 μL
RNase-free water	4.50 μL
Master mix	10.40 μL

A template-free control was included for each gene by replacing cDNA with RNase-free water in the RT-qPCR reaction mix. RT-qPCR was performed with QuantStudio™ 6 Pro Real-time PCR System using fast cycling mode:

Reaction	Temperature	Time
Activation of the enzyme	95°C	20s
Denaturation	95°C	1s
Annealing and extension	60°C	20s

} 40 cycles

The amplification results were analysed using QuantStudio™ Design and Analysis Software (version 2.6.0). The same threshold cycle (Ct) value was applied for each gene throughout the study to ensure consistency and reliable comparison of gene expression at different study time points. *Glyceraldehyde-3-phosphate dehydrogenase (Gapdh)* was used as the reference housekeeping gene. Ct values of the target genes for each sample were normalised against the Ct mean value of the housekeeping gene of the respective sample to obtain ΔCt . $\Delta\Delta\text{Ct}$ was calculated by subtracting the average ΔCt of each treatment group from the average ΔCt of the control group. Throughout all gene expression analyses of the project, “male saline 7d” (male mice treated with saline and analysed at 7 days post-intervention) served as the control group. The fold changes of gene expression relative to the control group were expressed by calculating the $2^{-\Delta\Delta\text{Ct}}$. The equations mentioned above are shown below:

$$\Delta\text{Ct} = \text{Ct (target gene)} - \text{Ct (reference housekeeping gene)}$$

$$\Delta\Delta\text{Ct} = \Delta\text{Ct (treatment group)} - \Delta\text{Ct (control group)}$$

$$\text{n-fold of gene expression} = 2^{-\Delta\Delta\text{Ct}}$$

3.2.5 Flow cytometry

3.2.5.1 Sample preparation for heart and blood samples

To quantify the leukocyte subsets during cardiac remodelling, flow cytometry was performed for heart and blood samples. Heart sections collected in PBS during tissue sampling at 7 days post-intervention were transferred to a 24-well plate. One mL digestion cocktail was added to each well and the sections were cut into small pieces with Vannas-Tübingen Spring Scissors (15003-08, Fine Science Tools). The plate was incubated at 37°C for 1 hour. Digested heart tissues were homogenised by pipetting up and down, followed by transfer to a 70 µm filter placed on a 50 mL Falcon® tube. 5 mL FACS buffer was added, and the tubes were centrifuged at 1400 rpm for 5 min. The supernatants were discarded and 700 µL FACS buffer was added for resuspension. 500 µL cell suspension was transferred to a FACS tube for heart staining panel A (Table 5) and 200 µL cell suspension for heart staining panel B (Table 6).

For blood samples, 350 µL blood collected in EDTA tube during tissue sampling at 7 days post-intervention was transferred to the FACS tube for blood myeloid staining panel (Table 7) and 50 µL for lymphoid staining panel (Table 8). To lyse erythrocytes, 2 mL and 1 mL ACK lysis buffer was added for each panel sample, respectively. The tubes were incubated on ice for 20 min, followed by centrifugation at 1400 rpm for 5 min. The supernatants were discarded, and 1 mL ACK lysis buffer was added for the second erythrolysis. The tubes were incubated on ice for 10 min, followed by centrifugation at 1400 rpm for 5 min. The supernatants were discarded, 1 mL FACS buffer was added for washing and the tubes were centrifuged at 1400 rpm for 5 min. The supernatants were discarded.

3.2.5.2 Sample staining, data acquisition and analysis

To prevent non-specific binding of the antibodies, 50 µL blocking solution was added to each tube and incubated for 5 min at room temperature. Subsequently, antibodies cocktail was added (100 µL for heart samples and 50 µL for blood samples), and the tubes were incubated in the dark at 4°C for 30 min. Samples were washed by adding 500 µL FACS buffer and centrifuged at 1400 rpm for 5 min. After discarding the supernatant, the cell suspensions were resuspended with 300 µL FACS buffer, followed by transfer to a FACS tube with a cell strainer cap (35 µm nylon mesh) and centrifugation at 1400 rpm for 5 min. The cell strainer cap was removed and counting beads solution was added (600 µL for heart samples and 300 µL for blood samples with myeloid staining panel). The tubes were kept in the dark at 4°C until data acquisition. Flow cytometry data were acquired using LSRFortessa™ X-20 for heart samples and blood samples with myeloid staining panel. The data were analysed using FlowJo 10.8.1.

3.2.6 Cell sorting

3.2.6.1 Sample preparation for cell sorting

To determine the *Nr4a1* gene expression level by RT-qPCR, T and B cells of WT and KO mice were sorted. The spleen from the baseline mouse without any intervention was collected in a tube with 1 mL PBS, was kept on ice and subsequently placed on a 70 μ L filter attached to a 50 mL Falcon[®] tube and minced with a 2 mL syringe plunger flange. 5 mL FACS buffer was added, and the tubes were centrifuged at 1400 rpm for 5 min. The supernatants were discarded, and 1 mL ACK lysis buffer was added for erythrolysis. The tubes were incubated on ice for 5 min, followed by centrifugation at 1400 rpm for 5 min. The supernatants were discarded, and 1 mL FACS buffer was added for washing, followed by centrifugation at 1400 rpm for 5 min. The supernatants were discarded, and the cells were resuspended in 500 μ L FACS buffer.

To investigate changes in the transcriptome, circulating Ly6C^{hi} and Ly6C^{lo} monocytes, cardiac fibroblasts, macrophages and ECs were sorted 7 days after AngII infusion. Blood samples and heart sections collected during tissue sampling were processed according to 3.2.5.1.

The samples were stained with 100 μ L antibodies cocktail for the lymphoid staining panel (Table 8), antibodies cocktail for blood sorting panel (Table 9), and antibodies cocktail for heart sorting panel (Table 10) for the spleen, blood and heart samples respectively according to 3.2.5.2.

3.2.6.2 Cell sorting for circulating Ly6C^{hi} and Ly6C^{lo} monocytes, cardiac fibroblasts, macrophages and endothelial cells sorting, and spleen B and T cells

The samples were sorted using FACS Aria III cell sorter and the number of cells sorted for each population is shown below:

Cells	Number
Ly6C ^{hi} monocytes	10,000
Ly6C ^{lo} monocytes	10,000
Cardiac fibroblasts	10,000
Cardiac macrophages	5,000
Cardiac endothelial cells	10,000
Spleen B cells	500,000
Spleen T cells	500,000

After sorting, the tubes were centrifuged at 1400 rpm for 5 min and the supernatants were discarded. The cells were resuspended in 100 μ L cells lysis buffer, snap-frozen with liquid nitrogen and stored at -80°C until further processing.

3.2.7 Bulk RNA-seq

To analyse the transcriptome of Ly6C^{hi} monocytes, Ly6C^{lo} monocytes, cardiac fibroblasts, macrophages, and ECs 7 days post-intervention, bulk RNA-seq was performed. Frozen sorted cells were thawed on ice and transferred to a semi-skirted 96-well PCR plate (652290, Greiner Sapphire Microplates). The plate was tightly sealed with an aluminium seal (391-1275, VWR) and kept on dry ice while transported to Eva Briem and Daniel Richter (AG Enard, Anthropology and Human Genomics, LMU Munich) for further processing (RNA extraction, sequencing and raw data pre-processing) according to the protocols published on protocols.io (<https://doi.org/10.17504/protocols.io.s9veh66>).¹³⁷ In brief, 50 μ L cell lysate was used for RNA sequencing. The samples were digested with Proteinase K and DNase I. Uniquely barcoded oligodT primers were used for cDNA synthesis and samples for the same library were pooled. Pre-amplification was performed for 11 to 14 cycles determined by the initial input per library. PicoGreen dsDNA Assay Kit (Thermo Scientific, P11496) was used for cDNA quantification and Bioanalyzer HS DNA chip (Agilent, 5067–4626) for cDNA quality assessment. Libraries were constructed NEB Next Ultra II FS Kit (E6177S, New England Biolabs) according to the prime-seq specifications. The libraries were quantified and qualified with the HS DNA chip on the Bioanalyzer and sequenced using Illumina HiSeq 1500 at an average depth of 10.6 million reads per sample. The reads were first demultiplexed using deML, followed by filtering and mapping to the mouse genome (mm10, GRCm38). The reads were then counted using zUMIs (version 2.5.5) with STAR.¹³⁸

Differential gene expression analysis was performed in RStudio using R version 4.3.1 with DESeq2 package. DEGs were determined as genes with an adjusted p-value (p_{adj}) < 0.05. Up- and downregulated DEGs for each group comparison were listed separately for functional enrichment analysis using g:Profiler.¹³⁹ Gene set enrichment analysis (GSEA) with the aggregate score approach was performed using GSEA 4.3.2^{140,141} (Gene sets database: m5.go.bp.v2023.1.Mm.symbols.gmt; Chip platform: MSigDB.v2023.1.Mm.chip).¹⁴² Venn diagrams were created using BioVenn.¹⁴³ Gene sets were considered significantly enriched with a normalised enrichment score (NES) of more than 1 or less than -1 and a false discovery rate (FDR) of less than 0.25.

3.2.8 Non-invasive blood pressure measurement

To assess the blood pressure of the mice, non-invasive blood pressure (NIBP) measurements were performed under basal condition and upon 28 days of AngII infusion using Rodent NIBP CODA[®] Monitor Sets. The mice were lightly anaesthetised with <1% isoflurane mixed with 99% oxygen at a flow rate of 1 L/min and laid prone on a hot plate to maintain the body temperature at 37°C. The occlusion cuff (O-cuff) was placed near the base of the tail followed by the sliding of the volume pressure recording (VPR) cuff up the tail until it reached the O-cuff. The O-Cuff and VPR Cuff sensors were connected to the CODA[®] monitor and the measurements were started. At least five continuous cycles were taken for each mouse and the systolic and diastolic blood pressure were analysed using LabChart.

3.2.9 Evans blue assay

To investigate the vascular permeability of the heart, Evans blue assay was performed after 7 days of AngII infusion. 0.5% Evans blue was prepared by dissolving the Evans blue powder (E2129, Sigma) in 0.9% saline. The mice were anaesthetised with 1.5% isoflurane mixed with 98.5% oxygen at a flow rate of 1 L/min and laid prone on a hot plate to maintain the body temperature at 37°C. The tail was disinfected with Octinesept[®] antiseptic and 200 µL Evans blue solution (40 mg/kg) was injected intravenously into the tail vein. The mice were sacrificed with overdosed xylazine (120 mg/kg) and ketamine (10 mg/kg) 70 min after the injection. The blood was withdrawn from the right ventricle and the heart was perfused with 10 mL PBS. After weighing the heart, the heart was transferred to a tube with 1 mL Formamide (17899, Thermo Fischer). The tubes were incubated in a shaking incubator for 24 hours at 55°C. The tubes were centrifuged at 1400 rpm for 5 min to pellet any remaining tissue fragments. 200 µL of supernatant was used for measuring the absorbance at 635 nm using Qubit 4 Fluorometer. 200 µL Formamide were used as blank. The relative fluorescence units obtained were normalised to the heart weight.

3.2.10 Echocardiography

To assess cardiac function and morphology after AngII infusion, echocardiography was performed using Vevo[®] 3100 imaging system at 28 days post-intervention. Mice were first anaesthetised with 3% isoflurane mixed with 97% oxygen in an induction chamber, which was then transferred to a nose cone supplying with 1.5% isoflurane mixed with 98.5% oxygen at a flow rate of 1 L/min. Mice were laid supine on a hot plate to maintain the body temperature at 37°C. A rectal probe was inserted in the rectum to monitor the body temperature, and the paws were attached to the electrodes embedded in the heated platform to monitor the heart rate and respiratory rate recording to suppress respiratory artefacts. Depilatory cream was used to

remove the fur on the chest area. Long and short axes of the LV were acquired in B- and M-mode. The data were analysed using Vevo Lab. Three cardiac cycles recorded in M-mode of the short axis were used for calculating the heart rate, LV end-diastolic volume, LV end-systolic volume, LV diastolic internal diameter (ID), LV systolic ID, ejection fraction, and fractional shortening.

3.2.11 Statistical analysis

Statistical analysis was performed using GraphPad Prism 10.0 software. Data from RT-qPCR analysis are shown as geometric mean \pm geometric standard deviation (SD). All other data are shown as mean \pm standard error of mean (SEM). Two-way analysis of variance (ANOVA) with Sidak's multiple comparisons test was performed to determine 1) significant differences between the sexes for each treatment group and 2) differences between the treatment groups within each sex group. Unpaired t-test was used when there were only two groups. All calculated p-values are two-sided. Differences with a $p < 0.05$ were considered statistically significant.

4. Results

4.1 AngII treatment promotes cardiac hypertrophy independent of sex

To study the effects of biological sex on AngII-induced cardiac remodelling, 8- to 10-week-old male and female WT mice were randomly subjected to either AngII or saline infusion via minipump implantation for 7 or 28 days (Figure 12A). As a more pronounced cardiac hypertrophy can usually be detected at a later time point, cardiac hypertrophy was assessed by heart gravimetry and cardiomyocyte size at day 28 of AngII infusion. As expected, females had in general lower body and heart weights than males, irrespective of AngII, while the AngII infusion reduced body weight only in males when compared to the vehicle group. A significant decrease in body weight was observed in the AngII-treated male group compared to the saline-treated group (Figure 23B). Heart weight, heart weight/body weight ratio (HW/BW), and heart weight/tibia length ratio (HW/TL) were significantly increased in both sexes upon AngII infusion, indicating a similar extent of hypertrophic growth (Figure 12C-E).

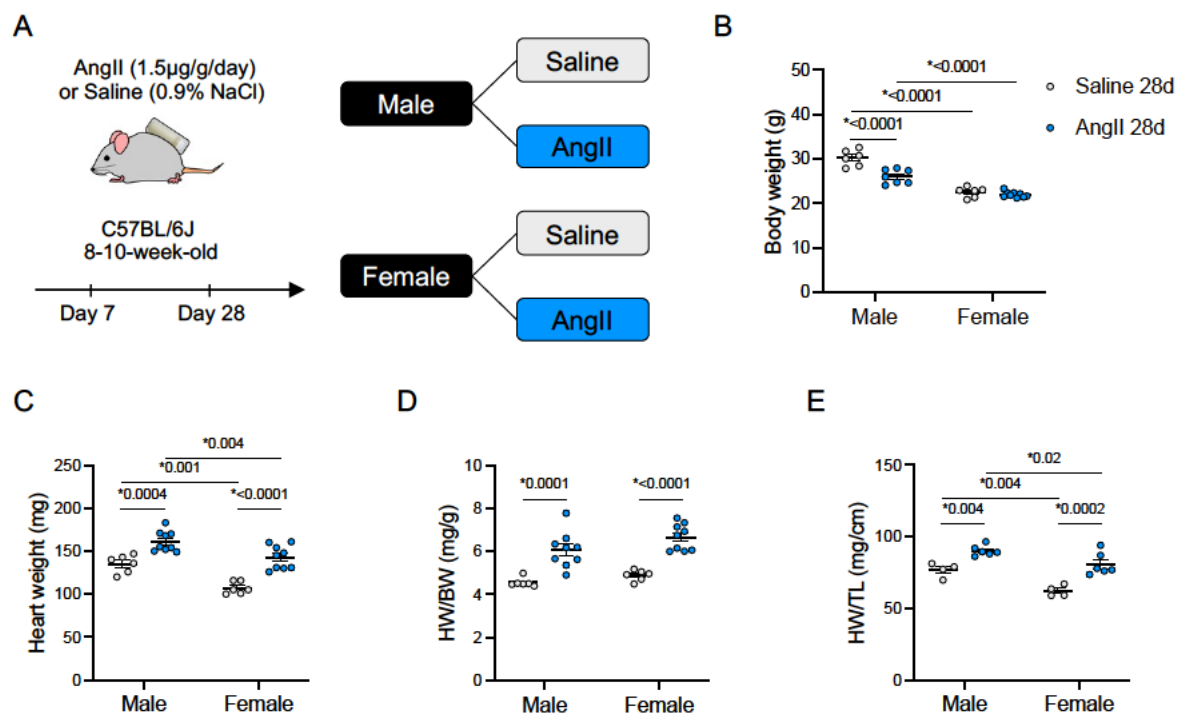


Figure 12 | Experimental design and gravimetric measurements upon 28 days of AngII infusion.

A. Wildtype male and female mice were randomly assigned to two groups for minipump implantation containing AngII or saline for 7 or 28 days. **B-E.** Body weight, heart weight, heart weight/body weight ratio (HW/BW), and heart weight/tibia length ratio (HW/TL) were measured after 28 days of AngII infusion. Each dot represents a mouse. (n=4-9). Data are shown as mean \pm SEM. Two-way ANOVA with Sidak's multiple comparisons; p<0.05 was considered significant.

This also held true for cardiomyocyte thickening as investigated by cross-sectional area (CSA) measurements of wheat germ agglutinin-stained cardiomyocytes (Figure 13). These data suggest that AngII-induced cardiac hypertrophy is not affected by biological sex differences.

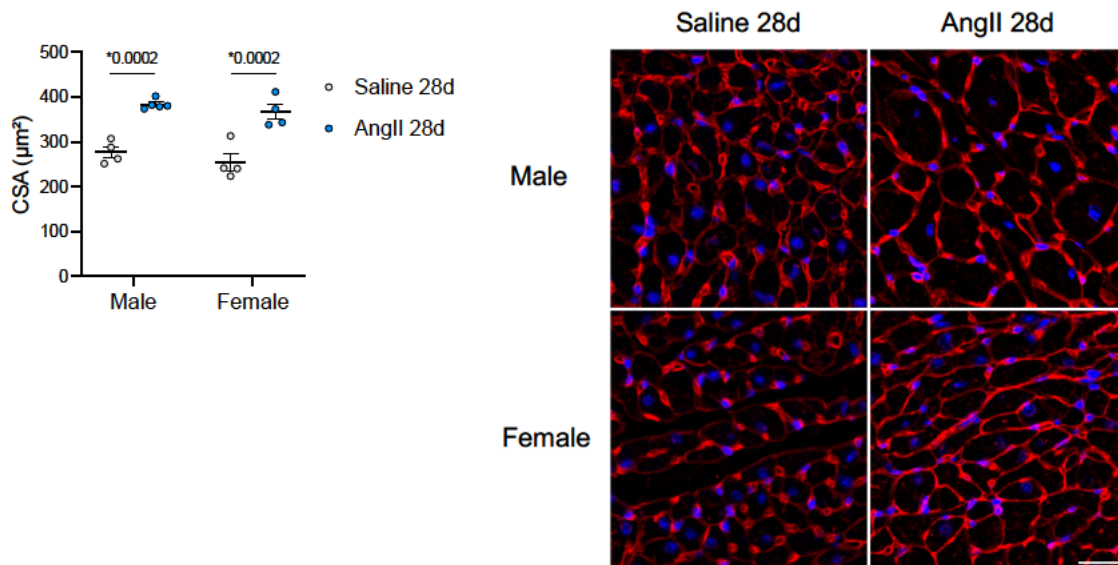


Figure 13 | Cardiomyocyte cross-sectional area analysis after 28 days of AngII infusion

Cardiomyocyte cross-sectional area (CSA) was measured after 28 days of AngII treatment. Representative images of wheat germ agglutinin staining of midventricular transverse sections were taken in 20x magnification (scale bar=25 μm). At least 50 cells per heart were quantified on 5-10 images taken in the left ventricular region. Each dot represents a mouse. (n=4-5). Data are shown as mean \pm SEM. Two-way ANOVA with Sidak's multiple comparisons; $p < 0.05$ was considered significant.

4.2 Female mice are protected from AngII-induced cardiac fibrosis

To investigate the effects of biological sex on the initiation of cardiac fibrosis during AngII-induced cardiac remodelling, cardiac transverse sections were stained with Sirius red solution for collagen content quantification. After 7 days of AngII treatment, males presented a prominent increase in collagen disposition in the heart. However, no significant increase in cardiac fibrosis was observed in females. Likewise, perivascular (PV) fibrosis was significantly increased by AngII in males, but not females (Figure 14A). A similar pattern of cardiac fibrosis was observed upon 28 days of AngII infusion (Figure 14B). The relative amount of cardiac fibrosis was generally higher after 28 days of AngII treatment compared to 7 days of treatment. Again, a significant difference in comparison to the vehicle group was only observed in AngII-treated males, but not in females.

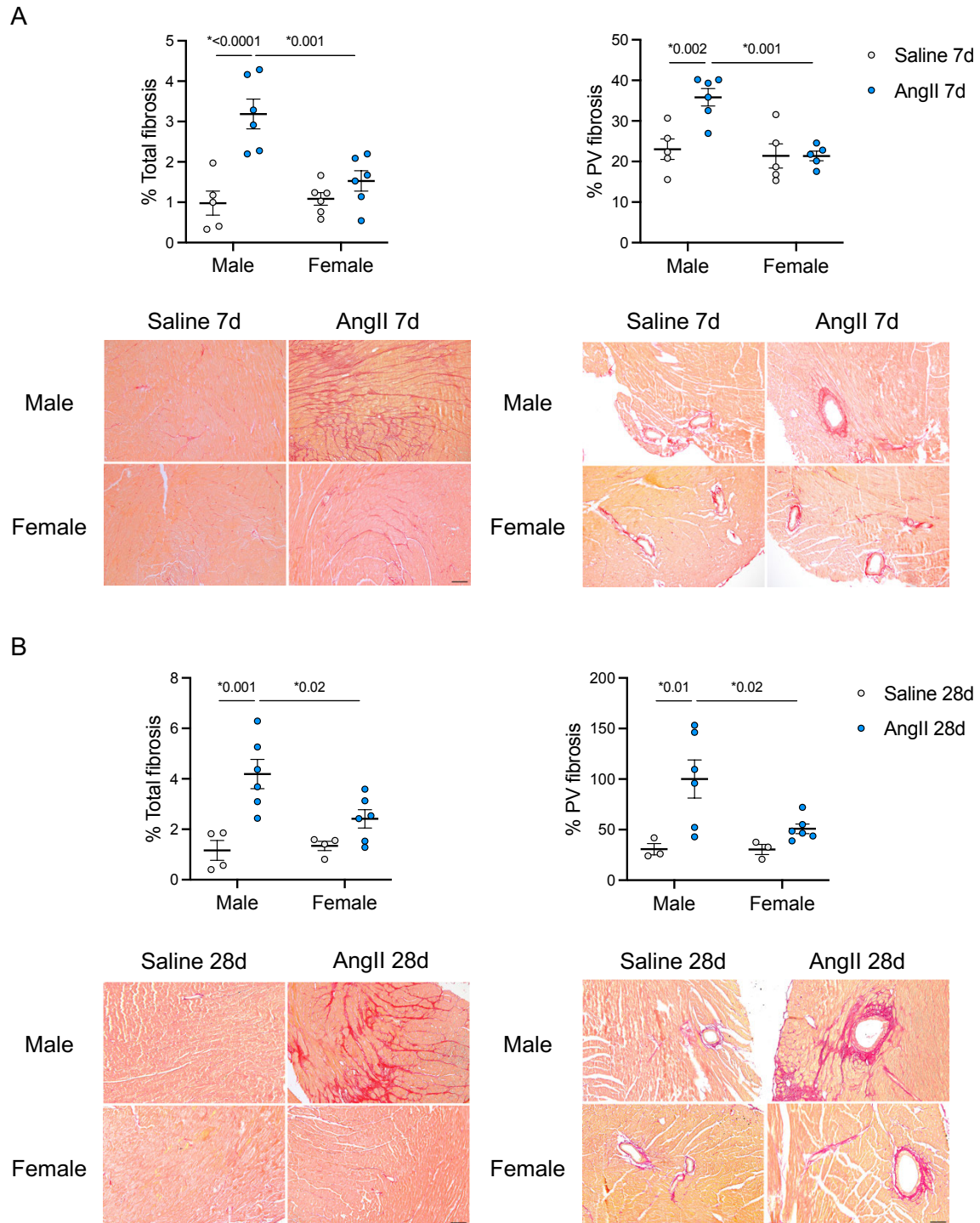


Figure 14 | Cardiac fibrosis after 7 to 28 days of AngII infusion.

A-B. Interstitial and perivascular (PV) fibrosis were measured after 7 days (**A**) and 28 days (**B**) of AngII infusion. Representative images of Sirius red staining of midventricular transverse sections were taken in 10x magnification (scale bar=100μm). Tile scans taken in 10x magnification for each sample were used for total fibrosis quantification. Three coronary vessels per mouse heart were analyzed for PV fibrosis. Each dot represents a mouse (n=3-6). Data are shown as mean ± SEM. Two-way ANOVA with Sidak's multiple comparisons; $p < 0.05$ was considered significant.

4.3 AngII expands cardiac fibroblasts and induces pro-fibrotic genes only in males

To further investigate the biological sex effects on cardiac fibrosis, the expansion of cardiac fibroblasts and pro-fibrotic gene expression in the heart was measured via flow cytometry and RT-qPCR, respectively. Cardiac fibroblasts were identified by flow cytometry in digested hearts based on the fibroblast marker MEFSK4 and further gated as CD45⁺CD31⁻ (Figure 15A). In line with the fibrosis staining results, females did not show an expansion of cardiac fibroblasts, while males had significantly more cardiac fibroblasts after 7 days of AngII infusion (Figure 15B-C). Furthermore, pro-fibrotic genes including collagen 1a2 (*Col1a2*), collagen 3a1 (*Col3a1*), connective tissue growth factor (*Ctgf*), C-C motif chemokine ligand 2 (*Ccl2*), and interleukin 6 (*Il-6*) were significantly induced after AngII infusion in males but not in females (Figure 16). Taken together, these results indicate that females are protected against AngII-induced cardiac fibrosis despite comparable hypertrophic responses.

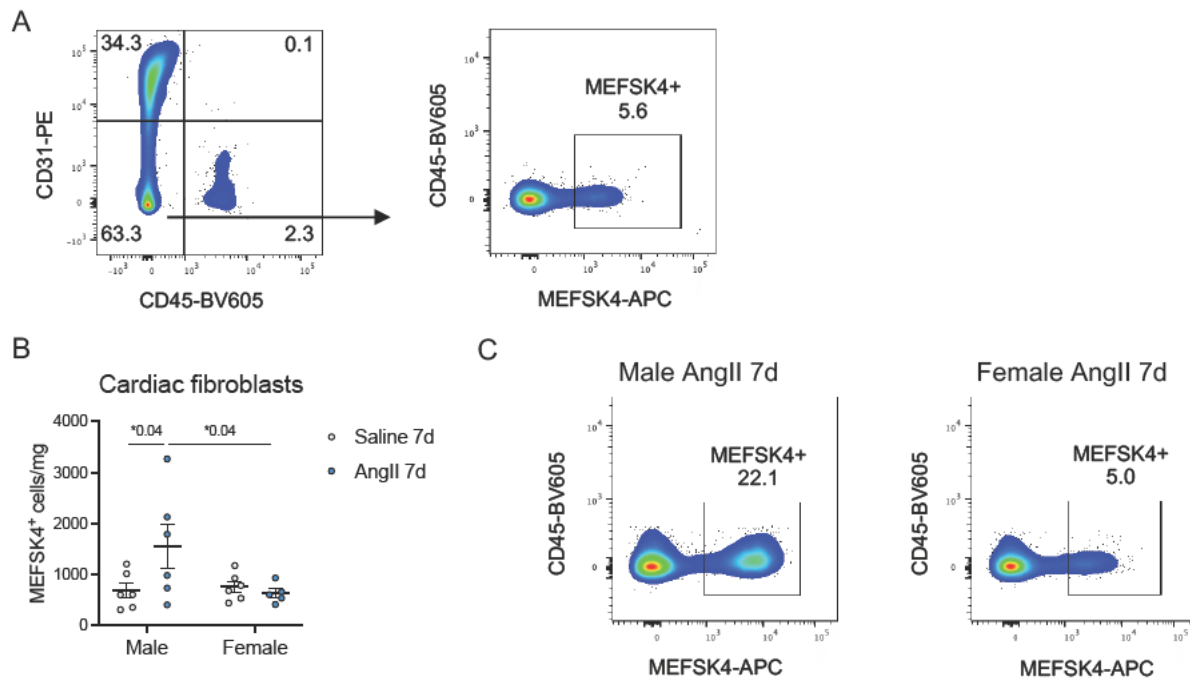


Figure 15 | Quantification of cardiac fibroblasts after 7 days of AngII infusion.

A. Flow cytometry gating for cardiac fibroblast (CD45⁺CD31⁻MEFSK4⁺). **B.** Flow cytometric analysis of the number of cardiac fibroblasts per mg heart after 7 days of AngII treatment. (n=5-6). **C.** Representative FACS plot and MEFSK4⁺ of cardiac fibroblasts in AngII-treated mice, with the percentage of gated MEFSK4⁺ indicated. In panel **B**, each dot represents a mouse and data are shown as mean ± SEM. Two-way ANOVA with Sidak's multiple comparisons; p<0.05 was considered significant.

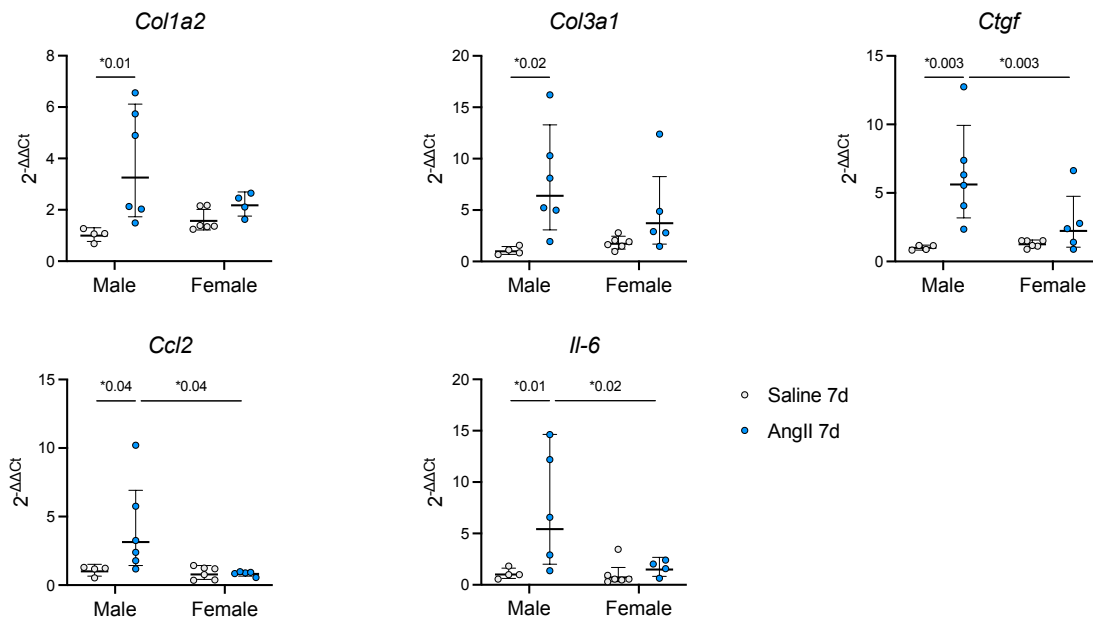


Figure 16 | Cardiac pro-fibrotic gene expression after 7 days of AngII infusion.

Gene expression analysis (RT-qPCR) to detect pro-fibrotic genes encoding for collagen 1a2 (*Col1a2*), collagen 3a1 (*Col3a1*), connective tissue growth factor (*Ctgf*), C-C motif chemokine ligand 2 (*Ccl2*), and interleukin 6 (*Il-6*) in heart lysates after 7 days of AngII treatment. *Gapdh* was used as the reference gene. Data are normalised over male saline 7d. (n=4-6). Each dot represents a mouse. Data are shown as geometric mean \pm geometric SD. Two-way ANOVA with Sidak's multiple comparisons; $p < 0.05$ was considered significant.

4.4 AngII treatment downregulates genes associated with detoxifying reactive oxidative species in male cardiac fibroblasts

Cardiac fibroblasts, the main drivers of cardiac fibrosis,¹⁴⁴ were sorted for bulk RNA-seq in order to assess global transcriptomic changes during AngII-induced cardiac fibrosis. Since changes in fibrosis and pro-fibrotic gene expression were already evident after 7 days of AngII treatment, this time point was chosen for the transcriptomic analysis. The principal component analysis (PCA) plot showed a clear clustering of the saline and AngII groups (principal component (PC1), 39% of variance), and of the male AngII versus female AngII groups (Figure 17A). The comparison between male AngII-treated and male saline-treated groups provided the highest number of differentially expressed genes (DEGs=854), followed by the comparison between female AngII-treated and female saline-treated groups (DEGs=506). While 134 DEGs were detected for the comparison between male saline-treated and female saline-treated groups, the comparison between male AngII-treated and female AngII-treated groups gave the lowest number of DEGs (DEGs=34) (Figure 17B).

The volcano plots showed that, in both male and female, several upregulated genes in the AngII-treated groups compared to saline groups are related to ECM remodelling and assembly. These include *Col1a1*, *Col3a1*, *Fn1*, *Lox*, and *Timpt1*.^{145,146} Furthermore, AngII infusion in

males led to the downregulation of genes associated with detoxifying reactive oxidative species (ROS), such as *Hspa1a*, *Gpx3*, and *Atg7*,¹⁴⁷⁻¹⁴⁹ which could enhance oxidative stress. In contrast, the downregulated genes in the female AngII-treated group are involved in fibroblast activation and signalling, such as *Smad3*, *Klf9*, and *Ddr2*,¹⁵⁰⁻¹⁵² which could partly explain the observed prevention of extensive collagen deposition in response to cardiac stress in females (Figure 17C-D).

Next, a Venn diagram was constructed to determine unique and common DEGs in males and females upon AngII treatment. Of the 506 DEGs observed in AngII-treated females, 192 (37.9%) did not overlap with the DEGs in AngII-treated males. In addition, 540 out of 854 genes (63.2%) were uniquely regulated in male AngII-treated mice. Furthermore, 314 DEGs were commonly up- or downregulated by AngII, independent of sex (Figure 17E).

Functional enrichment analysis for the gene ontology biological process (GOBP) revealed that the shared upregulated DEGs in AngII-treated groups were involved in ECM organisation, TGF- β receptor signalling, and EndMT, while the downregulated DEGs were associated with cell communication and differentiation (Figure 18A). The genes uniquely differentially upregulated in the male AngII-treated group were linked to cell migration, while downregulated genes were associated with cell communication, heart contraction, and epithelial cell proliferation. GO terms cell differentiation, programmed cell death, and cellular response to growth factor stimulus were associated with both up- and downregulated DEGs (Figure 18B). Lastly, among the genes that were uniquely differentially regulated in the AngII-treated female group, the upregulated genes were associated with response to stress, autophagy and apoptosis, while the downregulated were related to cell differentiation and communication (Figure 18C). Taken together, these data suggest that female cardiac fibroblasts may be more resistant to AngII-induced stress responses through mechanisms involving autophagy and apoptosis, thereby resulting in a less activated state, while male cardiac fibroblasts have a reduced ability to detoxify ROS, resulting in pro-fibrotic remodelling.

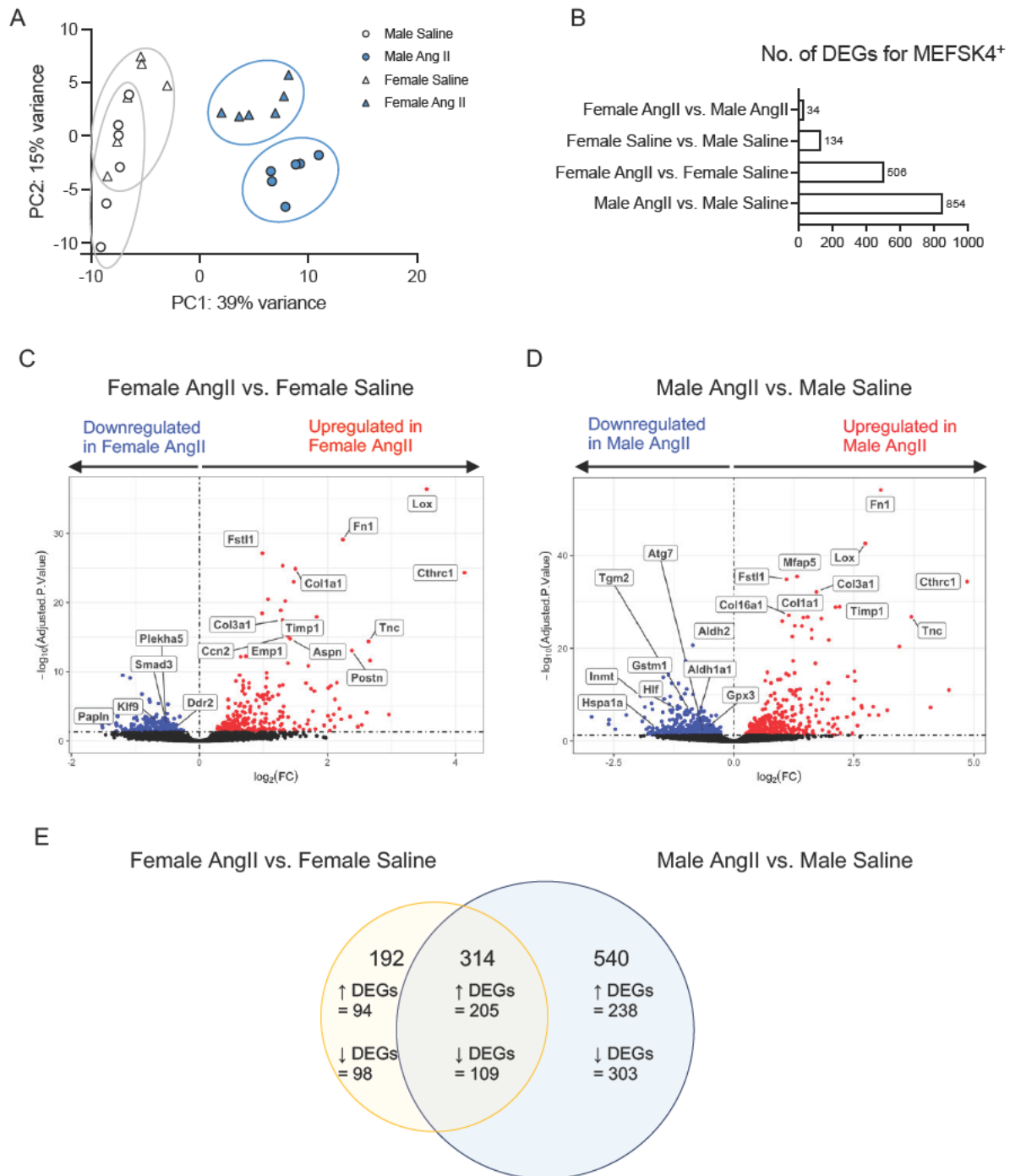


Figure 17 | Bulk RNA-seq analysis of sorted cardiac fibroblasts upon 7 days of AngII infusion.

Male and female cardiac fibroblasts were sorted (10,000 cells per sample) for bulk RNA sequencing after 7 days of AngII or vehicle treatment ($n=6$ per group). **A.** Principal component analysis (PCA) plot to visualize the heterogeneity of transcriptomic profiles between the experimental groups. Each symbol represents a mouse. **B.** Number of differentially expressed genes (DEGs) with $\text{padj} < 0.05$ and $\text{FC} > \pm 0.2$ for each comparison. **C-D.** Volcano plot with up- (red) and downregulated (blue) DEGs in female AngII (**C**) and male AngII (**D**) compared with their respective saline group. **E.** Venn diagram of DEGs ($\text{padj} < 0.05$) in female AngII (yellow) vs. male AngII (blue). Both the total number of DEGs and the number of up- and downregulated DEGs are indicated.

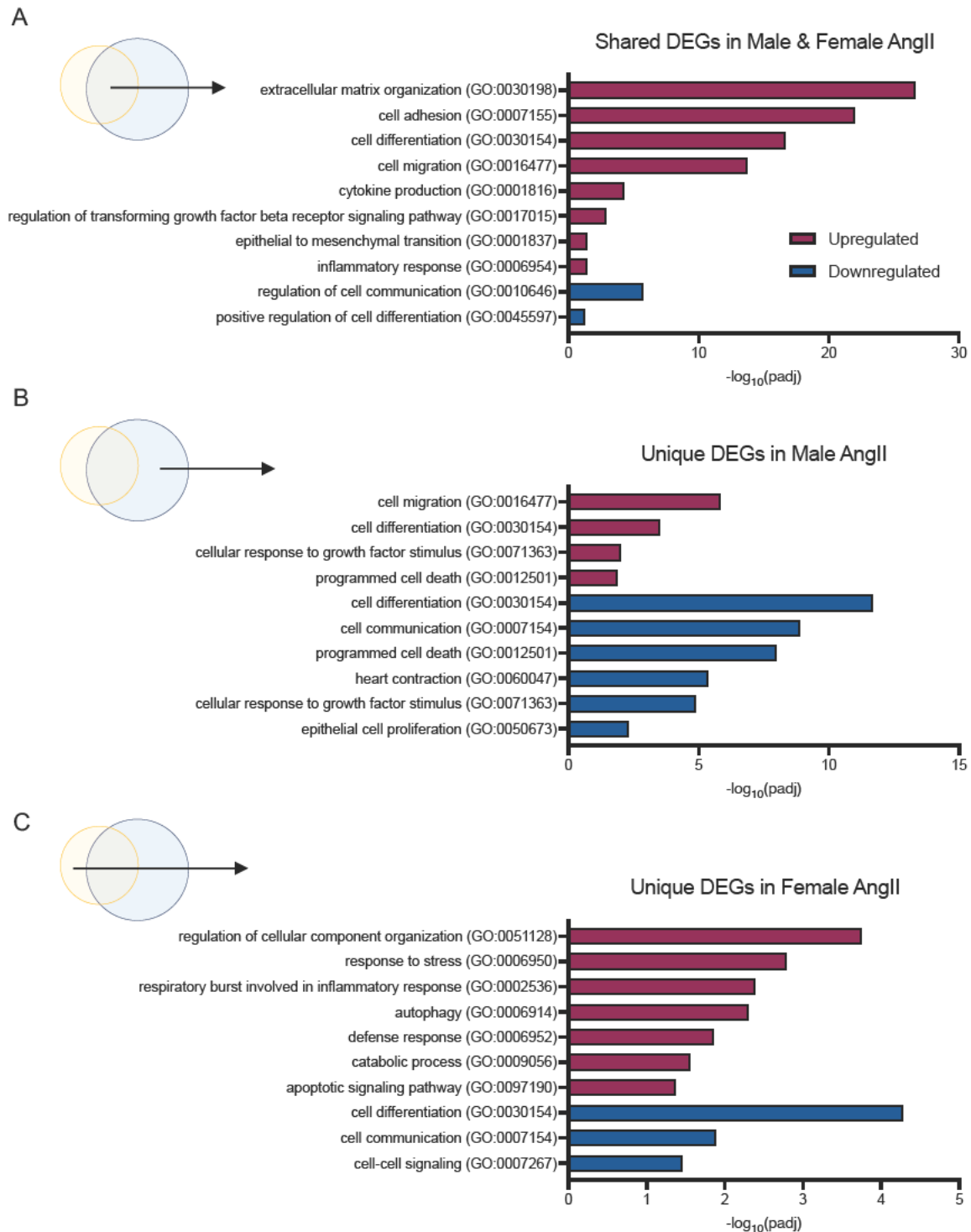


Figure 18 | Gene ontology analysis of DEGs in cardiac fibroblasts.

Gene ontology biological process (GOBP) terms associated with shared DEGs in both AngII-treated groups (**A**), unique DEGs in male AngII vs. male saline (**B**) or unique DEGs in female AngII vs. female saline (**C**), performed using g:Profiler based on the results shown in the previous Figure.

4.5 AngII promotes circulating and cardiac Ly6C^{lo} monocyte expansion in females

Inflammation is known to contribute to cardiac remodelling, and sex differences in immune cells have been reported. Therefore, the next aim was to investigate the effects of sex differences in the driving of cardiac inflammation during AngII-induced cardiac remodelling. Flow cytometry was used to determine the changes in the distribution of the circulating and cardiac leukocyte subpopulations (Figure 19).

AngII-treated males had significantly higher neutrophil counts compared to saline-treated males and AngII-treated females (Figure 20A). Although the total number of monocytes was comparable between the groups, AngII-treated females presented a shift in the relative proportion of monocyte subsets, with a reduction in the Ly6C^{hi} subset and an increase in both the Ly6C^{int} and Ly6C^{lo} subsets compared to AngII-treated males (Figure 20A-B). Furthermore, CD8⁺ T cells were higher in the female AngII-treated group compared to the male AngII-treated group (Figure 20C). No significant differences between the groups were observed in the other analysed leukocyte subsets, namely the total number of myeloid cells, B cells, T cells, and CD4⁺ T cells (Figure 20A, C).

Differently from the blood, the myeloid cell counts in the heart were significantly increased in male AngII-treated group. Among the myeloid cell subsets, AngII infusion induced an expansion of neutrophils in male AngII-treated group compared to female AngII-treated group (Figure 21A). Similar to the blood, a shift in the relative proportion of monocyte subsets was observed. It was found that females generally have a lower relative proportion of cardiac Ly6C^{hi} monocytes than males, irrespective of treatment. Upon AngII infusion, the relative proportion of cardiac Ly6C^{int} monocytes increased in females compared to their corresponding saline-treated group and the male AngII-treated group. The relative proportion of Ly6C^{lo} monocytes decreased in males upon AngII treatment compared to their corresponding saline-treated group and the female AngII-treated group (Figure 21B-C). In addition, macrophages in AngII-treated males, particularly of recruited macrophages (CD64⁺TIMD4⁻) counts, were significantly increased compared to saline-treated males and AngII-treated females (Figure 21D-E). Of note, no changes in cardiac lymphocyte subsets were found between the groups (Figure 22).

Taken together, an increase in recruited cardiac macrophages in the AngII-treated male group may promote adverse cardiac inflammation and fibrosis, whereas a higher relative proportion of Ly6C^{lo} monocytes in the females after AngII infusion may potentially contribute to protective effects against maladaptive cardiac fibrosis.

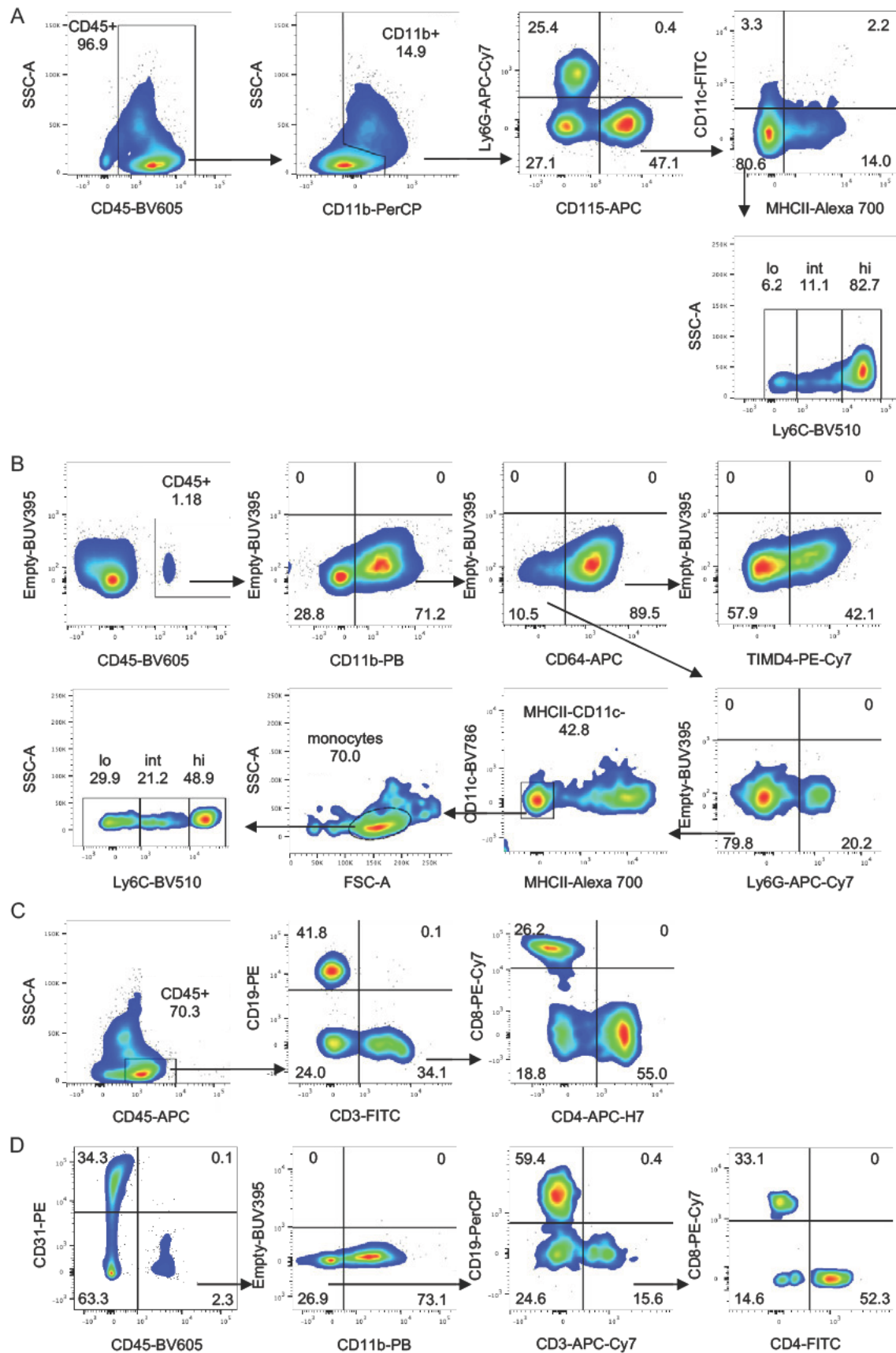


Figure 19 | Gating strategy for leukocyte subsets in the blood and in the heart.

Flow cytometry gating for blood myeloid cells (A), cardiac myeloid cells (B), blood lymphoid cells (C), and cardiac lymphoid cells (D).

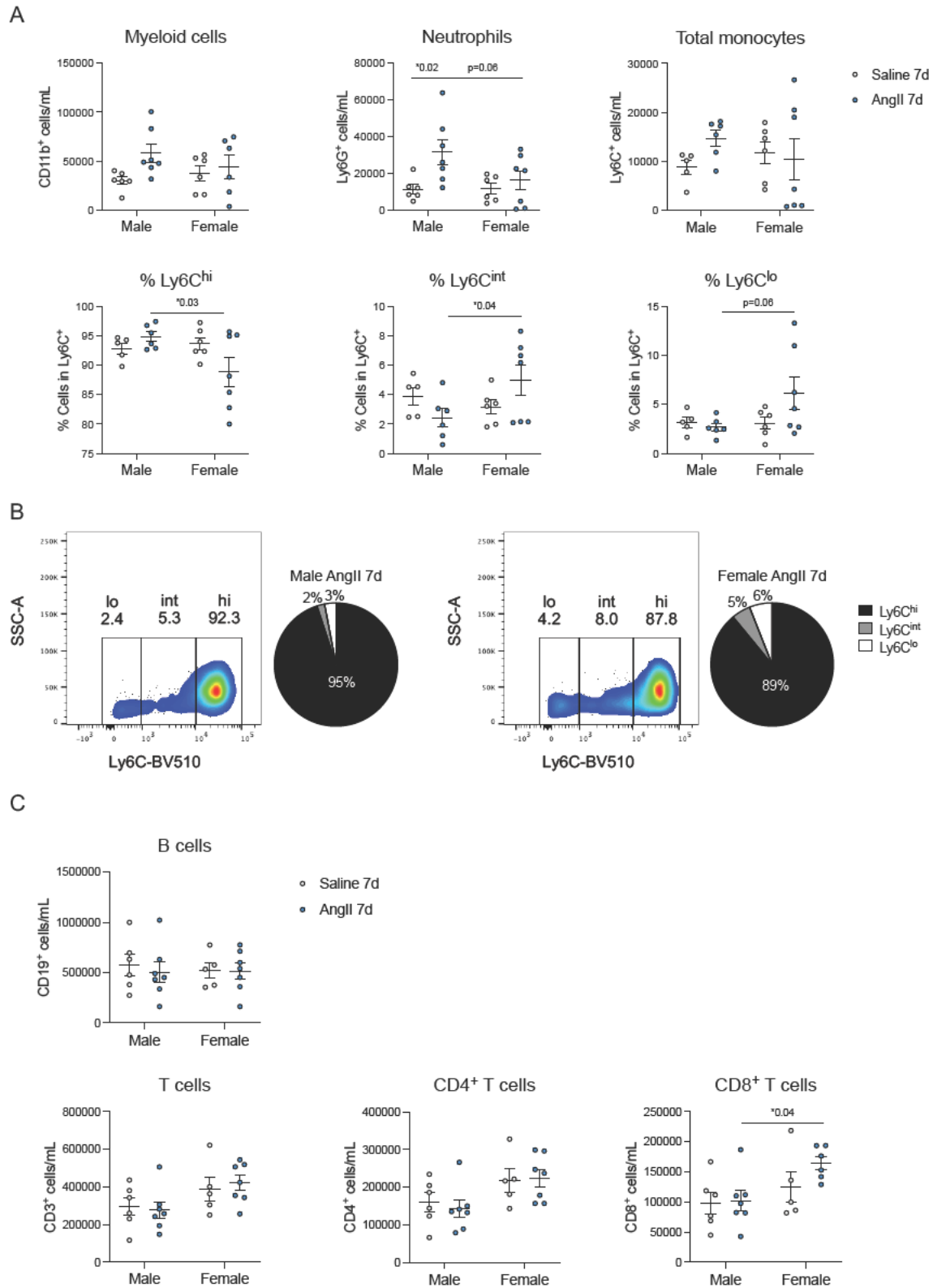


Figure 20 | Circulating immune cell subsets upon 7 days of AngII infusion.

Flow cytometric analysis of the number of circulating myeloid (**A**) and lymphoid cell subsets (**C**) after 7 days of AngII treatment. **B**. Representative FACS plots and pie chart of Ly6C⁺ monocyte subset average distribution for male AngII 7d (left) and female AngII 7d (right). Each dot represents a mouse (n=6-7). Data are shown as mean ± SEM. Two-way ANOVA with Sidak's multiple comparisons; p<0.05 was considered significant.

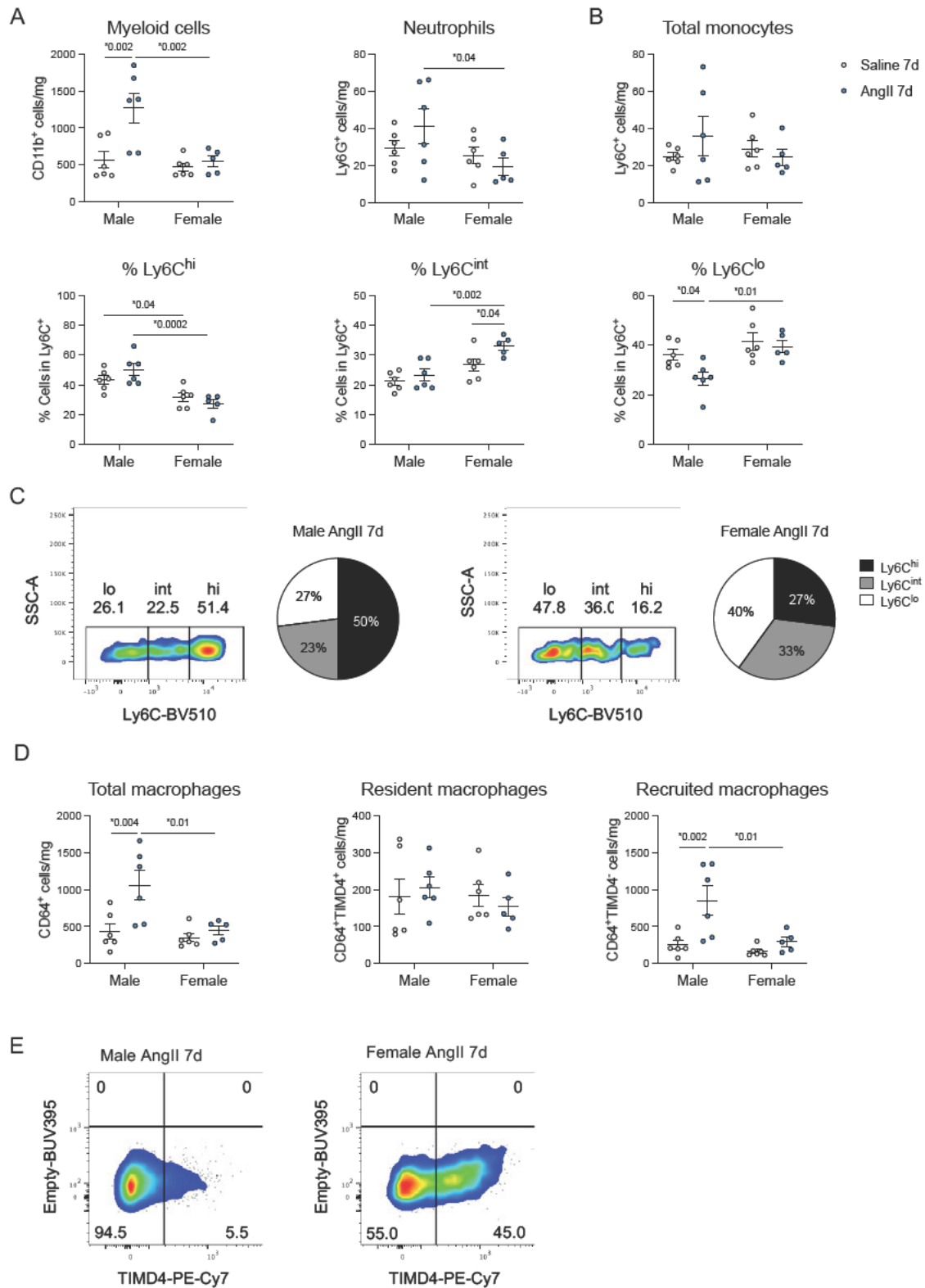


Figure 21 | Cardiac myeloid cell subsets upon 7 days of AngII infusion.

A,B,D. Flow cytometric analysis of the number of myeloid cell subsets normalised to heart weight after 7 days of AngII treatment. **C.** Representative FACS plots and pie charts of Ly6C⁺ monocyte subset gating and average distribution for male AngII 7d (left) and female AngII 7d (right). **E.** Representative FACS plots of recruited macrophages (CD64⁺TIMD4⁺) for male AngII 7d (left) and female AngII 7d (right). (n=5-6). Each dot represents a mouse. Data are shown as mean ± SEM. Two-way ANOVA with Sidak's multiple comparisons; p<0.05 was considered significant.

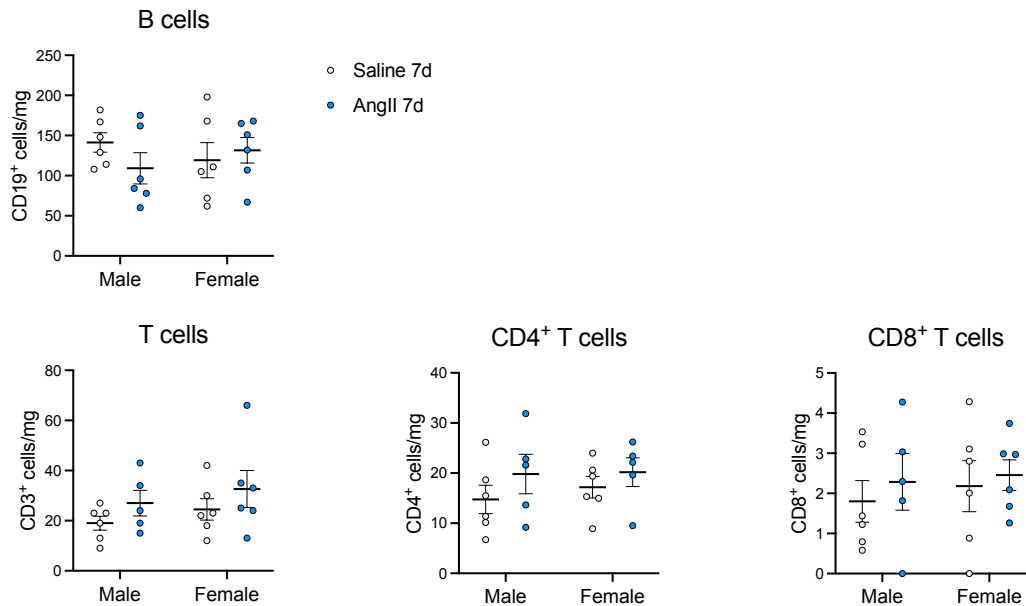


Figure 22 | Cardiac lymphoid subsets upon 7 days of AngII infusion.

Flow cytometric analysis of the number of cardiac lymphoid cell subsets after 7 days of AngII treatment. (n=5-6). Each dot represents a mouse. Data are shown as mean \pm SEM. Two-way ANOVA with Sidak's multiple comparisons; $p < 0.05$ was considered significant.

4.6 AngII-treatment downregulates protective genes in male cardiac macrophages

As an expansion of cardiac macrophages was observed in males after AngII treatment, the transcriptomic profile of cardiac macrophages was assessed via bulk RNA-seq 7 days after AngII infusion. The PCA plot showed a clear clustering between the four groups, with PC1 distinguishing between AngII-treated and saline-treated groups, and PC2 distinguishing between the male and female groups (Figure 23A). Similar to cardiac fibroblasts, the comparison between the AngII-treated and saline-treated group in males resulted in the highest number of DEGs (DEGs=359), followed by the comparison between the AngII-treated and saline-treated group in females (DEGs=220). For the comparison between males and females, 117 DEGs were detected within the saline-treated group, while only 5 DEGs were detected within the AngII-treated group (Figure 23B).

As highlighted in the volcano plots (Figure 23C-D), some of the AngII-induced genes in both male and female mice, in particular *Ccr2*, *Arg1*, *Fn1*, and *Mmp14* are related to the activation of fibrosis and inflammatory signalling.^{52,153,154} Among the downregulated genes in AngII-treated females were *Il1rl1*, *Pik3r6*, and *Klf7*, which are associated with enhanced cardiac remodelling.¹⁵⁵⁻¹⁵⁷ Downregulated genes in the male AngII-treated group included *Lyve1*, *Rhob*, and *Aldh2*, which have been linked to protective effects during cardiac remodelling.¹⁵⁸⁻

The Venn diagram revealed that 117 out of 220 genes (53.2%) were uniquely differentially expressed in AngII-treated females (Figure 23E). In contrast, 256 out of 359 genes (71.3%) were uniquely differentially expressed in AngII-treated males. GO analysis showed that the shared DEGs (47 genes) upregulated in both AngII-treated groups were associated with antigen processing and presentation, cell proliferation, and tissue remodelling. The shared downregulated genes (56 genes) were involved in the regulation of IL-6 production, cardiomyocyte proliferation, and blood vessel diameter maintenance (Figure 24A). Furthermore, the DEGs upregulated uniquely in AngII-treated males were related to innate immune response activation, while the downregulated DEGs were involved in apoptosis, epithelial cell migration, and blood vessel morphogenesis (Figure 24B). On the other hand, the DEGs upregulated uniquely in the female AngII-treated group were associated with cytoplasmic translation, while the downregulated DEGs were involved in intracellular signal transduction and cell differentiation (Figure 24C). Taken together, these results hint towards a more inflammatory phenotype of cardiac macrophages in males after AngII infusion compared to females.

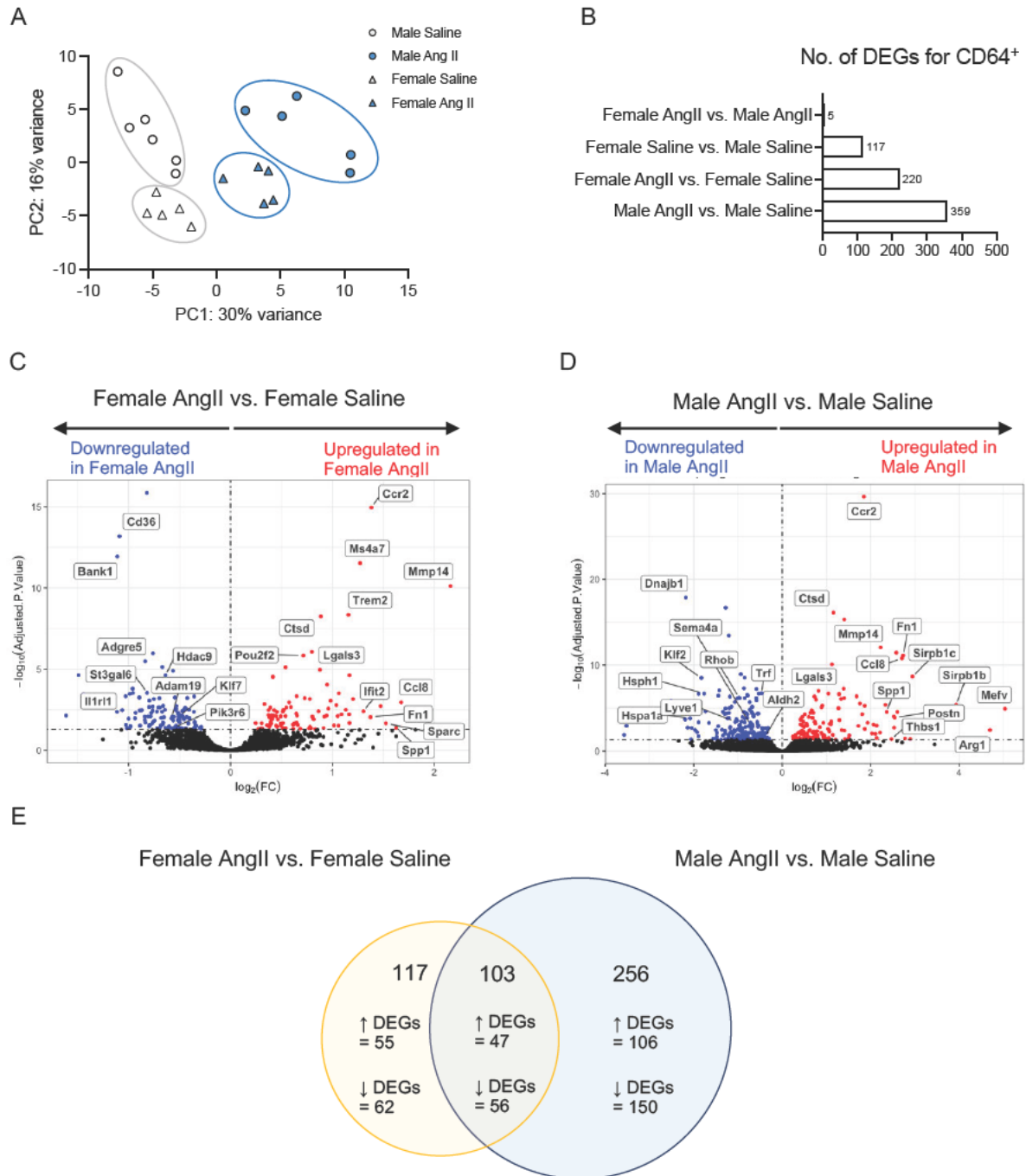


Figure 23 | Bulk RNA-seq analysis of sorted cardiac macrophages upon 7 days of AngII infusion.

Male and female cardiac macrophages were sorted (10,000 cells per sample) for bulk RNA sequencing after 7 days of AngII or vehicle treatment ($n=5-6$ per group). **A.** Principal component analysis (PCA) plot to visualize the heterogeneity of transcriptomic profiles between the experimental groups. Each symbol represents a mouse. **B.** Number of differentially expressed genes (DEGs) with $\text{padj} < 0.05$ and $\text{FC} > \pm 0.2$ for each comparison. **C-D.** Volcano plot with up- (red) and downregulated (blue) DEGs in female AngII (**C**) and male AngII (**D**) compared with their respective saline group. **E.** Venn diagram of DEGs ($\text{padj} < 0.05$) in female AngII (yellow) vs. male AngII (blue). Both the total number of DEGs and the number of up- and downregulated DEGs are indicated.

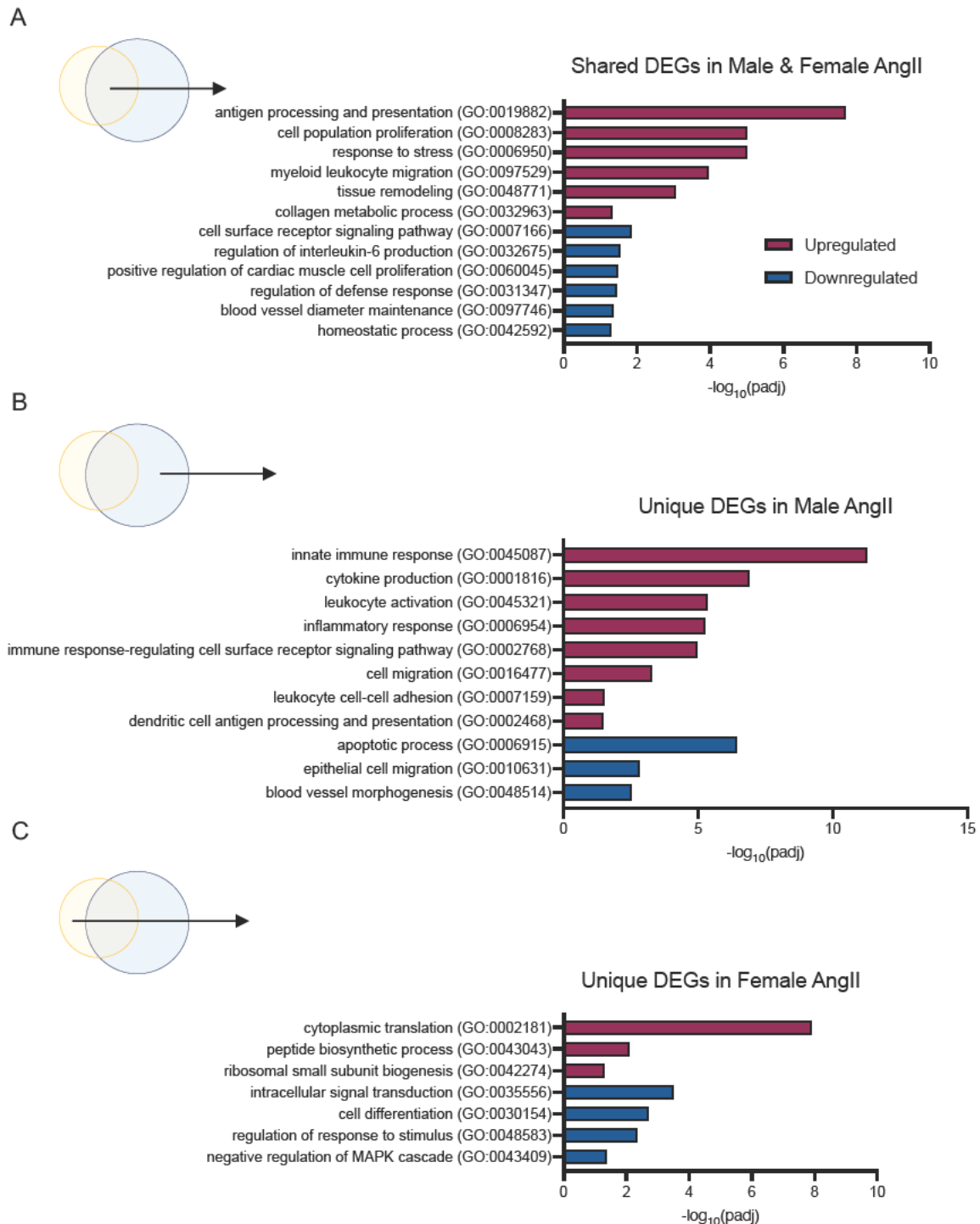


Figure 24 | Bulk RNA-seq analysis of DEGs in cardiac macrophages.

Gene ontology biological process (GOBP) terms associated with shared DEGs in both AngII-treated groups (**A**), unique DEGs in male saline vs. male AngII (**B**) or unique DEGs in female saline vs. female AngII (**C**), performed using g:Profiler based on the results shown in the previous Figure.

4.7 Transcriptomic profiling of circulating Ly6C^{hi} and Ly6C^{lo} monocytes

The shift in the relative proportions of blood and heart monocyte subsets in response to AngII provided the rationale to also perform bulk RNA-seq of Ly6C^{hi} and Ly6C^{lo} monocyte subsets. The number of Ly6C^{int} monocytes was too small for sorting and was therefore not included for transcriptome profiling.

Due to the low number of monocytes in the heart, especially the Ly6C^{lo} monocyte subset, the cells were sorted from the blood (Figure 25A). The PCA plot showed that the PC1 (accounting for 77% of the total variance) clearly separated the Ly6C^{hi} and the Ly6C^{lo} monocytes, while the PC2 (which explains 6% of the variance) distinguished the samples based on sex, although the latter did not form distinctly separated clusters (Figure 25B). To verify the differences between the detected Ly6C^{hi} and Ly6C^{lo} populations, the expression of specific markers previously assigned for each monocyte subset was further investigated. As expected, Ly6C^{hi} monocytes were enriched in *Ccr2* expression while Ly6C^{lo} monocytes had a higher *Cd274* (*Pd-11*) expression level (Figure 25C).^{117,126}

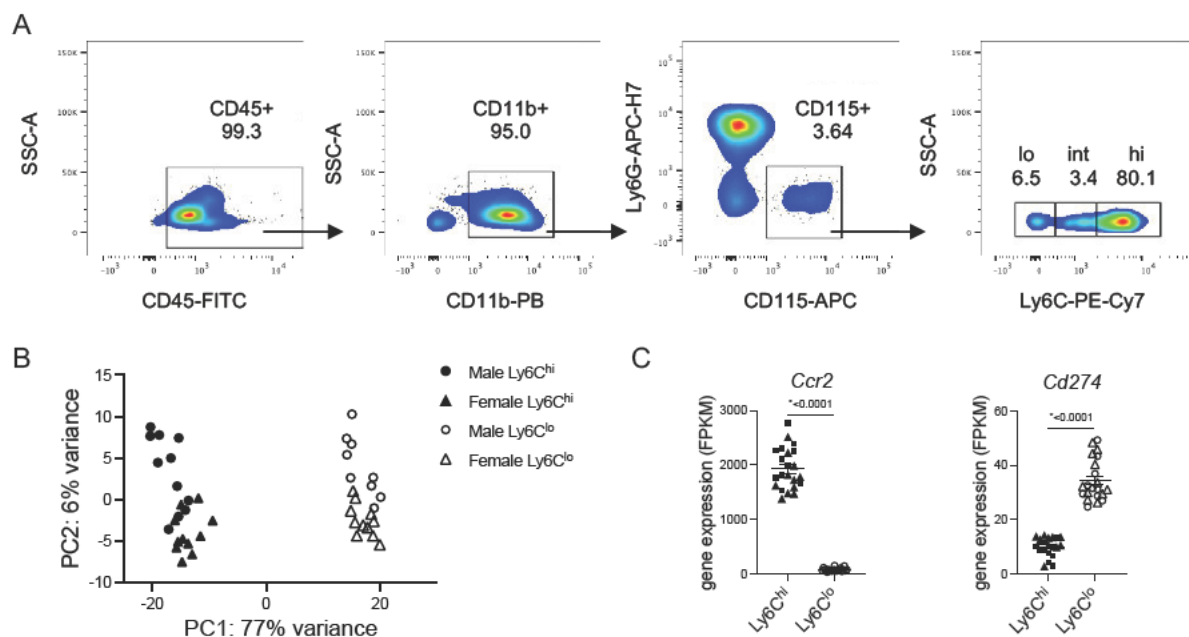


Figure 25 | Transcriptomic profiling of circulating monocyte subsets after 7 days of AngII infusion.

Male and female circulating Ly6C^{hi} and Ly6C^{lo} monocytes were sorted (10,000 cells per sample) for bulk RNA sequencing after 7 days of AngII or vehicle treatment (n=10-12 per group). **A**. Flow cytometry gating for circulating Ly6C^{hi} and Ly6C^{lo} monocytes. **B**. Principal component analysis (PCA) plot to visualize the heterogeneity of transcriptomic profiles between the experimental groups. Each symbol represents a mouse. **C**. C-C chemokine receptor type 2 (*Ccr2*) and programmed death-ligand 1 (*Cd274*) gene expression of circulating Ly6C^{hi} and Ly6C^{lo} monocytes. Data are shown as mean \pm SEM. Unpaired t-test; p<0.05 was considered significant. FPKM=fragments per kilobase of transcript per million mapped reads.

4.8 Ang II treatment upregulates genes linked to antigen presentation and type I interferon response in female Ly6C^{hi} monocytes

To further study the gene expression changes within each monocyte subset, Ly6C^{hi} and Ly6C^{lo} monocyte data were extracted and analysed individually. For the Ly6C^{hi} monocyte subset, the PCA plot did not show a pronounced and distinct separation between the four experimental groups. Nevertheless, PC1 predominantly distinguished between sexes, whereas PC2 generally separated the AngII-treated groups from the saline-treated group (Figure 26A). The comparisons between male and female saline-treated groups gave the highest number of DEGs (DEGs=76), followed by the comparison between male and female AngII-treated groups (DEGs=61). Surprisingly, there were only 9 DEGs detected in the comparison between the AngII-treated and control group in females and no DEGs were detected in males with a cut-off value of $\text{padj} < 0.05$ and minimum fold change ± 0.2 (Figure 26B). Ly6C^{hi} monocytes of female AngII-treated mice had higher gene expression of major histocompatibility class I (MHC I) genes such as *H2-D1*, *H2-K1*, and *H2-Q7* compared to the male AngII-treated group (Figure 26C). GO enrichment analysis revealed that the upregulated genes in the female AngII-treated group were mostly related to antigen processing and presentation (Figure 26D), which aligns with the observed increase in histocompatibility 2, class II antigen A, beta 1 (*H2-Ab1*) expression in the Ly6C^{hi} monocytes (Figure 27A). In addition, the expression of transcription factor *Nr4a1* was significantly higher in females than in males, suggesting that Ly6C^{hi} monocytes in females are more prone to the conversion to Ly6C^{lo} monocytes in the circulation (Figure 27B).¹³⁰

Furthermore, GSEA hinted towards enrichment in genes associated with cellular response to interferon beta and the activation of innate immune response in the female AngII-treated group compared to the male AngII-treated group (Figure 27C). The *Ifnb1* expression in the heart lysate was slightly higher in the female vehicle group compared to the corresponding male group, but lower in females after AngII infusion compared to the sex-matched vehicle group, although these differences did not reach significance (Figure 27D). IFN β production could be linked to a response to cytoplasmic nucleic acid accumulation released from stressed mitochondria via cytosolic GAMP synthase-stimulator of IFN genes (cGAS-STING) signalling.¹⁶¹ In general, Ly6C^{hi} monocytes in females showed an increased expression of the genes involved in type I IFN signalling (*Tlr7*, *Irf5*, *Irf7*, *Janus kinase 2 (Jak2)*, and *Tnf*) (Figure 27E).

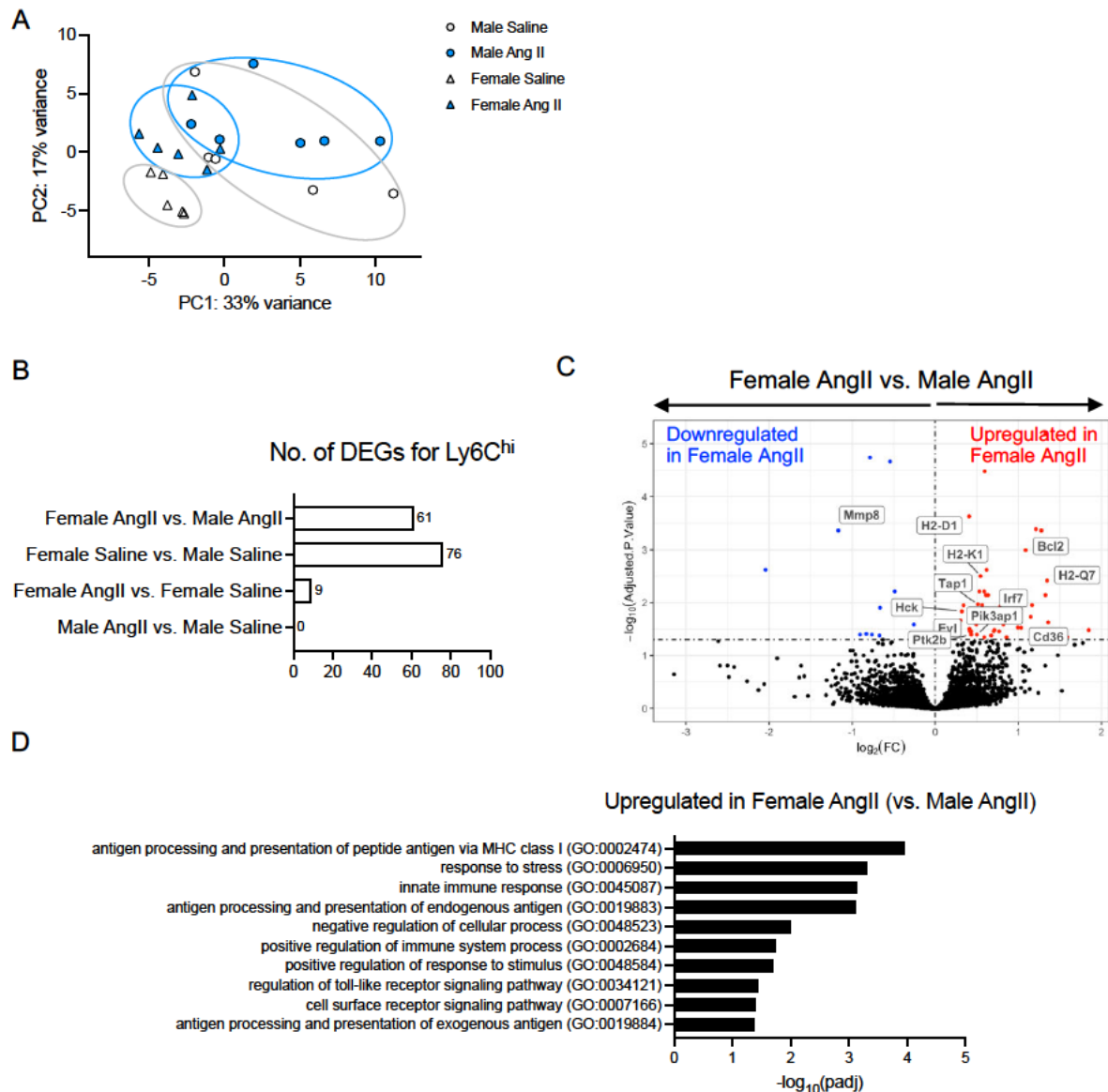


Figure 26 | Bulk RNA-seq analysis of sorted circulating Ly6C^{hi} monocytes after 7 days of AngII infusion.

A. Principal component analysis (PCA) plot of circulating Ly6C^{hi} monocytes to visualize the heterogeneity of transcriptomic profiles between the experimental groups. Each symbol represents a mouse. **B.** Number of differentially expressed genes (DEGs) with $\text{padj} < 0.05$ and $\text{FC} > \pm 0.2$ for each comparison. **C.** Volcano plot with up- (red) and downregulated (blue) DEGs in female AngII compared with male AngII. Sex-linked genes: X-inactive specific transcript (*Xist*) and DEAD-Box Helicase 3 Y-Linked (*Ddx3y*) were removed from the volcano plot to enhance visualisation of other DEGs. **D.** Gene ontology biological process (GOBP) associated with DEGs ($\text{padj} < 0.05$) upregulated in Ly6C^{hi} monocytes of female AngII compared with male AngII (analysed using g:Profiler). (n=5-6).

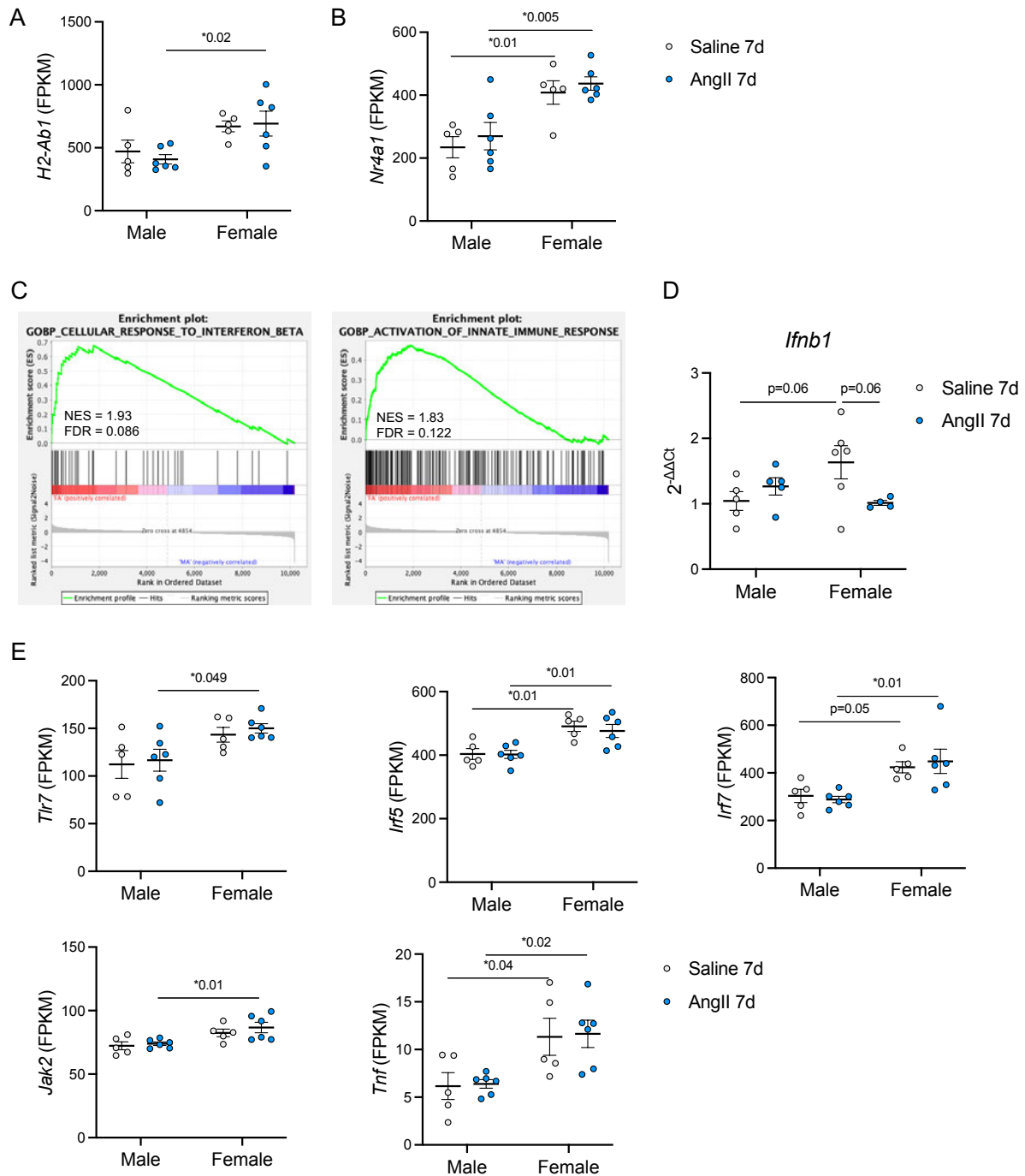


Figure 27 | Type I IFN gene expression in circulating Ly6C^{hi} monocytes after 7 days of AngII infusion.

Gene expression levels (obtained by bulk RNA-seq) of histocompatibility 2, class II antigen A, beta 1 (*H2-Ab1*) (**A**) and nuclear receptor subfamily 4 group A member 1 (*Nr4a1*) (**B**) in circulating Ly6C^{hi} monocytes. **C**. Gene Set Enrichment Analysis (GSEA) of circulating Ly6C^{hi} monocytes of female AngII compared with male AngII. **D**. Expression of interferon beta 1 (*Ifnb1*) in heart lysate measured by RT-qPCR (n=4-5). *Gapdh* was used as the reference gene. Data are normalised over male saline 7d. **E**. mRNA expression levels from the bulk RNA-seq data of Toll-like receptors (*Tlr7*), IFN-regulatory factor 5 (*Ifi5*), IFN-regulatory factor 7 (*Ifi7*), Janus kinase 2 (*Jak2*), and Tumour necrosis factor (*Tnf*) in circulating Ly6C^{hi} monocytes. (n=5-6). Each dot represents a mouse. Data are shown as mean ± SEM. Two-way ANOVA with Sidak's multiple comparisons; p<0.05 was considered significant. FPKM=fragments per kilobase of transcript per million mapped reads.

4.9 Ang II treatment upregulates genes linked to antigen presentation and cell killing in female circulating Ly6C^{lo} monocytes

Next, RNA-seq data from circulating Ly6C^{lo} monocytes were analysed. Similar to Ly6C^{hi} monocytes, the PCA plot did not show a clear separation between the four experimental groups. PC1 (25%) predominantly distinguished between sexes, whereas PC2 (17%) separated the AngII-treated groups from the saline group (Figure 28A). The highest number of DEGs was obtained from the comparison between male and female AngII-treated groups (DEGs=18; Figure 28B). Among these, of particular interest was the elevated expression of *B2m*, *H2-K1*, and *H2-Q7* in the female AngII-treated group (Figure 28C). 9 DEGs were detected when comparing AngII-treated and saline-treated females, followed by 6 DEGs detected when comparing male and female saline-treated groups. No DEGs were found when comparing AngII-treated and saline-treated males (Figure 28B). In addition, both GO analysis and GSEA showed that the genes upregulated in the female AngII-treated group compared to the male AngII-treated group were associated with antigen processing and presentation and positive regulation of cell killing (Figure 29A-B), which aligns with an increased circulating CD8⁺ T cells in AngII-treated females (Figure 20C).

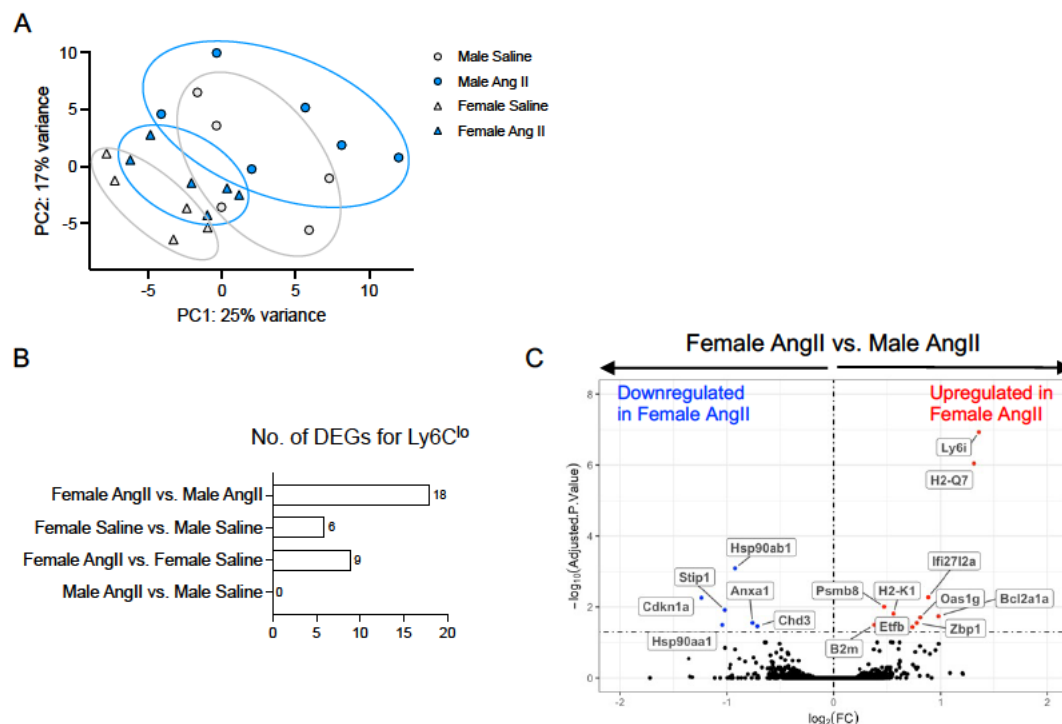
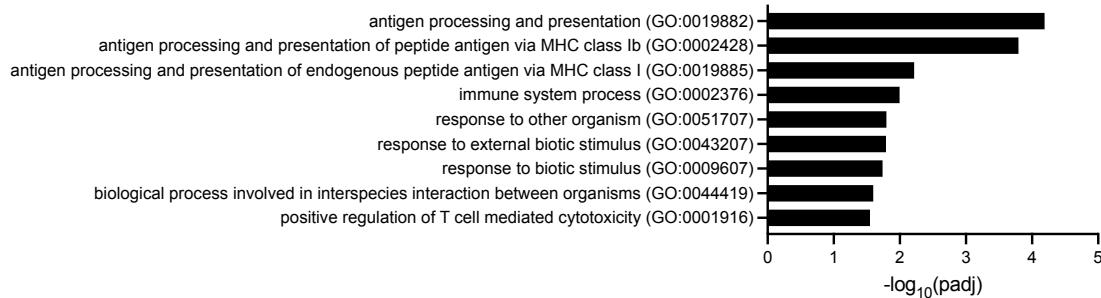


Figure 28 | Bulk RNA-seq analysis of sorted circulating Ly6C^{lo} monocytes after 7 days of AngII infusion.

A. Principal component analysis (PCA) plot of circulating Ly6C^{lo} monocytes to visualize the heterogeneity of transcriptomic profiles between the experimental groups. Each symbol represents a mouse. **B** Number of differentially expressed genes (DEGs) with $\text{padj} < 0.05$ and $\text{FC} > \pm 0.2$ for each comparison. **C.** Volcano plot with up- (red) and downregulated (blue) DEGs in female AngII compared with male AngII. Sex-linked genes: X-inactive specific transcript (*Xist*) and DEAD-Box Helicase 3 Y-Linked (*Ddx3y*) were removed from the volcano plot to enhance visualisation of other DEGs.

A

Upregulated in Female AngII (vs. Male AngII)



B

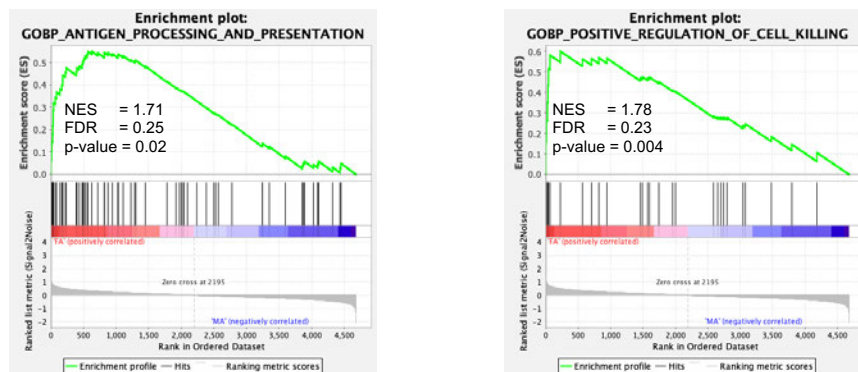


Figure 29 | Gene Ontology biological process analysis in circulating Ly6C^{lo} monocytes after 7 days of AngII infusion.

A. Gene Ontology biological process (GOBP) associated with DEGs ($\text{padj} < 0.05$) upregulated in Ly6C^{lo} monocytes of female AngII compared with male AngII (analysed using g:Profiler). **B.** GOBP enriched in Ly6C^{lo} of female AngII compared with male AngII analysed using Gene Set Enrichment Analysis (GSEA).

4.10 Gene expression of AT1R, ER α , and ER β in various cell types

The cellular expression level of AngII type 1 receptor (AT1R) may affect the magnitude of the AngII downstream signalling and cardiac remodelling. Thus, the fragments per kilobase of transcript per million mapped reads (FPKM) values for the AT1R encoding gene *Agtr1a* in various cell types involved in AngII-induced cardiac remodelling were extracted from the RNA sequencing data and compared. Cardiac fibroblasts expressed the highest level of *Agtr1a*, followed by cardiac macrophages. The expression level of *Agtr1a* in CMs, NCMs, and ECs was very low or non-detectable. However, no significant differences were detected in the gene expression level between the groups for each cell type (Table 13).

Furthermore, various receptors can be involved in oestrogen signalling, depending on the cell type, including ER α (*Esrra*) and ER β (*Esrrb*). This may differentially affect the downstream signalling in male and female mice in this study using young premenopausal mice. Therefore, the RNA sequencing FPKM values of *Esrra* and *Esrrb* were compared between the cell types.

In general, ER α was more expressed than ER β throughout all analysed cell types. While CMs have the highest expression of ER α (Table 14), fibroblasts have the highest expression of ER β , followed closely by cardiac macrophages (Table 15). Similarly, biological sexes and AngII did not significantly affect the expression of ER α and ER β on each cell type.

Table 13 | Gene expression of *Agtr1a* in each cell type

Cell type	Male saline 7d	Male AngII 7d	Female saline 7d	Female AngII 7d
CMs	0.269 \pm 0.3	0.000 \pm 0.0	0.588 \pm 0.4	0.618 \pm 0.3
NCMs	0.127 \pm 0.1	0.250 \pm 0.2	0.000 \pm 0.0	0.109 \pm 0.1
Macrophages	0.960 \pm 0.5	0.594 \pm 0.4	0.989 \pm 0.4	0.475 \pm 0.3
Fibroblasts	2.515 \pm 0.6	1.998 \pm 0.5	4.374 \pm 1.1	3.155 \pm 0.7
ECs	0.000 \pm 0.0	0.000 \pm 0.0	0.095 \pm 0.1	0.096 \pm 0.1

CMs = Classical monocytes (Ly6C^{hi}); NCMs = Non-classical monocytes (Ly6C^{lo}); ECs = Endothelial cells. Data are shown as mean \pm SEM. Two-way ANOVA with Sidak's multiple comparisons; No significance observed between groups.

Table 14 | Gene expression of *Esrra* in each cell type

Cell type	Male saline 7d	Male AngII 7d	Female saline 7d	Female AngII 7d
CMs	78.677 \pm 4.8	79.786 \pm 3.7	84.178 \pm 3.9	76.898 \pm 4.8
NCMs	40.589 \pm 6.7	40.129 \pm 3.5	39.466 \pm 1.0	38.089 \pm 3.2
Macrophages	21.339 \pm 3.7	23.248 \pm 2.1	21.016 \pm 2.7	29.798 \pm 1.9
Fibroblasts	16.837 \pm 2.3	16.687 \pm 0.9	15.302 \pm 1.4	16.263 \pm 1.6
ECs	5.259 \pm 2.3	9.660 \pm 0.4	6.731 \pm 0.8	9.099 \pm 1.6

CMs = Classical monocytes (Ly6C^{hi}); NCMs = Non-classical monocytes (Ly6C^{lo}); ECs = Endothelial cells. Data are shown as mean \pm SEM. Two-way ANOVA with Sidak's multiple comparisons; No significance observed between groups.

Table 15 | Gene expression of *Essrb* in each cell type

Cell type	Male saline 7d	Male AngII 7d	Female saline 7d	Female AngII 7d
CMs	0.764 \pm 0.2	1.056 \pm 0.3	0.809 \pm 0.6	1.255 \pm 0.4
NCMs	0.294 \pm 0.2	0.288 \pm 0.2	0.299 \pm 0.2	1.101 \pm 0.5
Macrophages	2.447 \pm 0.8	3.073 \pm 0.5	1.833 \pm 0.3	2.430 \pm 1.2
Fibroblasts	3.578 \pm 0.9	2.374 \pm 0.6	3.793 \pm 0.7	2.868 \pm 0.7
ECs	0.412 \pm 0.4	0.469 \pm 0.2	0.414 \pm 0.3	0.712 \pm 0.4

CMs = Classical monocytes (Ly6C^{hi}); NCMs = Non-classical monocytes (Ly6C^{lo}); ECs = Endothelial cells. Data are shown as mean \pm SEM. Two-way ANOVA with Sidak's multiple comparisons; No significance observed between groups.

4.11 *Nr4a1se_2*^{-/-} mice as a Ly6C^{lo} monocyte ablation model

To study whether Ly6C^{lo} monocytes play a role in cardiac remodelling in response to AngII treatment, *Nr4a1se_2*^{-/-} mice were used as an NCM ablation model, hereafter referred to as KO mice for simplicity (Figure 30A). The depletion of Ly6C^{lo} monocytes was confirmed by flow cytometry analysis of monocyte subsets in the blood. While around 8% Ly6C^{lo} monocytes were observed in WT mice, less than 0.1% Ly6C^{lo} monocytes were present in KO mice (Figure 30B). To assess whether the ablation of *Nr4a1* super-enhancer subdomain E2 (*Nr4a1se_2*) affects *Nr4a1* expression in other cell types, *Nr4a1* expression was measured in B cells, T cells, cardiac fibroblasts, and cardiac ECs. The *Nr4a1* expression in B cells, T cells, and cardiac ECs in KO mice was comparable between KO and WT mice, while the expression in cardiac fibroblasts was unexpectedly significantly reduced in KO mice (Figure 30C-D). In addition, cardiac fibroblasts in WT females also showed a significantly lower *Nr4a1* expression compared to WT males (Figure 30D). This indicates that the *Nr4a1se_2* is also relevant for the transcriptional regulation of *Nr4a1* in fibroblasts.

Next, to investigate whether *Nr4a1se_2* deficiency affected cardiovascular functional parameters or the body weight under baseline conditions and after AngII treatment, blood pressure, body weight, heart weight, and cardiac functions of the mice were measured after 28 days of AngII infusion. Under baseline conditions, no difference in the systolic and diastolic blood pressure was observed between the groups. However, the KO male mice significantly increased systolic and diastolic blood pressure compared to WT male mice after 28 days of AngII treatment (Figure 32E). While females in general have a lower body weight compared to males independent of the genotype, the AngII-induced increase in normalized heart weight, due to the development of cardiac hypertrophy, was comparable between WT and KO mice (Figure 30F). The evaluation of cardiac functional parameters suggested a more preserved LV function in females subjected to AngII compared to males (Figure 31). However, the only significant differences were found when comparing male and female KO mice subjected to AngII. In particular, ejection fraction and fractional shortening were more preserved in the KO female AngII-treated group compared to the corresponding male group after 28 days of AngII infusion. The latter developed more dilated LV remodelling with higher LV end-diastolic volume (LVEDV), end-systolic volume (LVESV), diastolic (LVID;d) and systolic internal diameter (LVID;s).

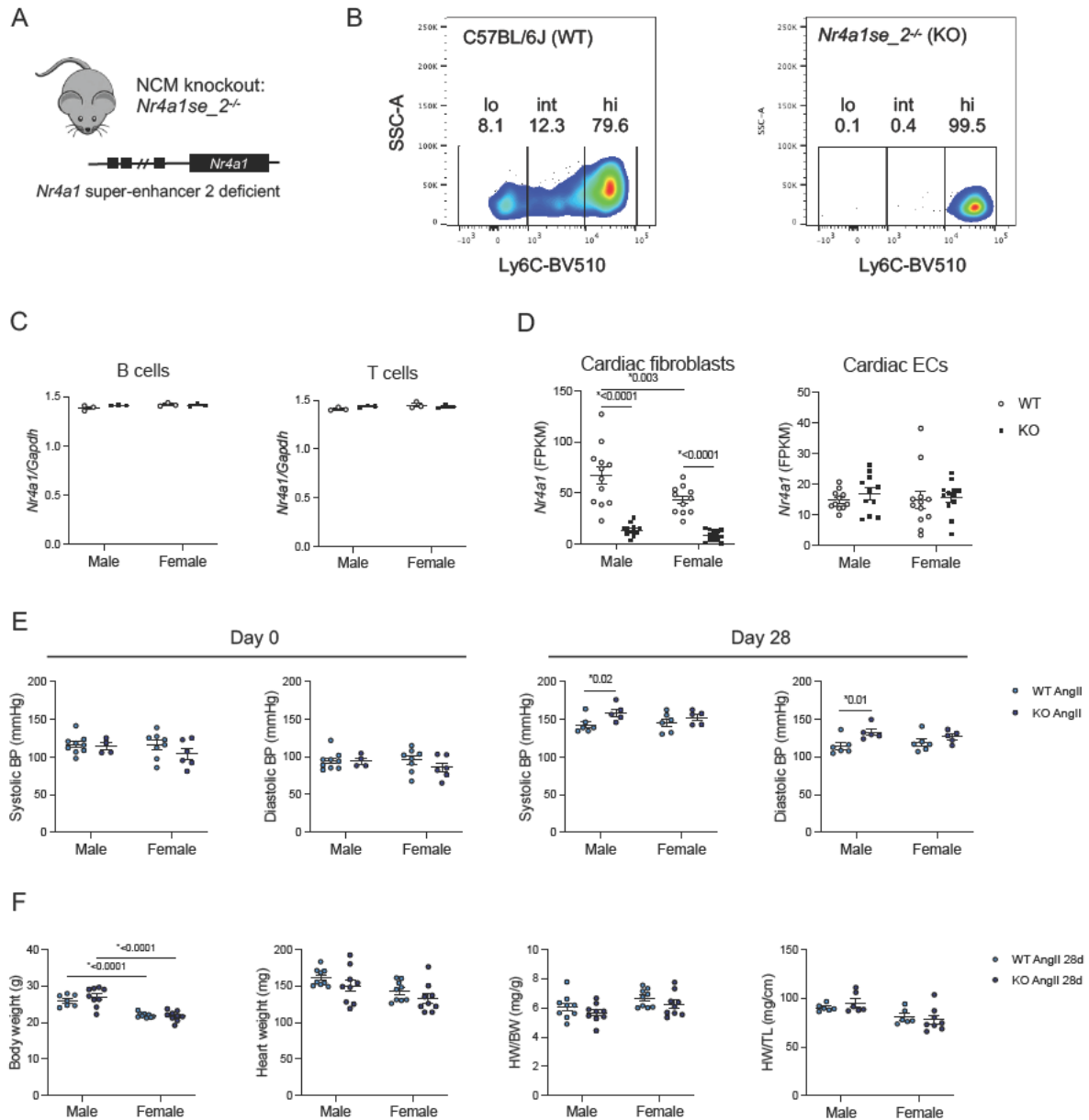


Figure 30 | Phenotypic analysis of *Nr4a1se*^{-/-} mice.

A. Non-classical monocyte (NCM) depletion in mice with global deletion of *Nr4a1* super-enhancer 2. **B.** Representative FACS plots of circulating Ly6C⁺ monocyte subsets in wildtype C57BL/6J (WT) and *Nr4a1se*^{-/-} (KO) mice. **C-D.** *Nr4a1* gene expression normalised to *Gapdh* in B cells and T cells by RT-qPCR (n=3) (**C**) and cardiac fibroblasts, and cardiac endothelial cells (ECs) by RNA-seq (n=10-12) (**D**). **E.** Systolic and diastolic blood pressure (BP) were measured by non-invasive BP monitoring using a tail-cuff at 0- and 28 days of AngII treatment. **F.** Body weight, heart weight, heart weight/body weight ratio (HW/BW), and heart weight/tibia length ratio (HW/TL) were measured after 28 days of AngII treatment. (n=4-9). Each dot represents a mouse. Data are shown as mean ± SEM. Two-way ANOVA with Sidak's multiple comparisons; p<0.05 was considered significant.

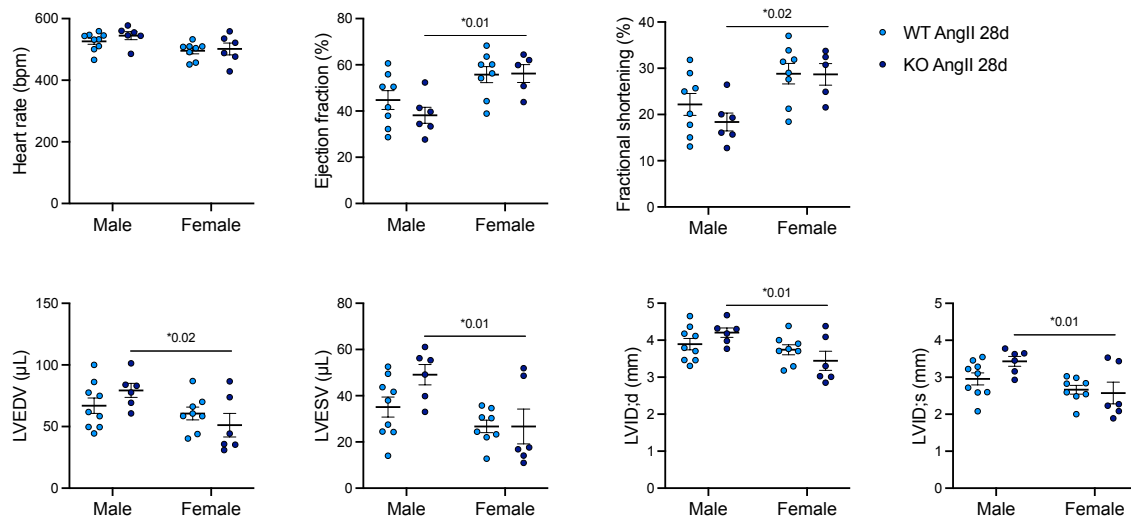


Figure 31 | Echocardiography analysis for cardiac function measurements after 28 days of AngII infusion.

Heart rate, ejection fraction, fractional shortening, left ventricular (LV) end-diastolic volume (LVEDV), LV end-systolic volume (LVESV), LV diastolic internal diameter (ID; LVID;d), and LV systolic ID, (LVID;s) after 28 days of AngII treatment. (n=6-9). Each dot represents a mouse. Data are shown as mean ± SEM. Two-way ANOVA with Sidak's multiple comparisons; p<0.05 was considered significant.

4.12 *Nr4a1se_2* deficiency reverses anti-fibrotic effects in females with AngII infusion

To investigate the effects of *Nr4a1se_2* deficiency on AngII-induced cardiac fibrosis, heart sections were stained with Sirius red solution and cardiac pro-fibrotic gene expression was determined 7 days after AngII infusion. The protection against AngII-induced cardiac fibrosis observed in WT females was not observed in KO females, which presented a similar extent of interstitial fibrosis as observed in WT and KO males. Interestingly, both KO male and female AngII-treated groups showed more pronounced PV fibrosis compared to the sex-matched WT AngII-treated groups. Furthermore, the relative amount of PV fibrosis was higher in KO males compared to KO females (Figure 32A).

The number of cardiac fibroblasts determined by flow cytometry increased only in the WT male AngII-treated group but not in the KO groups (Figure 32B). Gene expression analysis revealed differentially regulated pro-fibrotic gene expression after AngII treatment. While *Col1a2* and *Il-6* were significantly elevated in both KO AngII-treated groups compared to their respective WT AngII-treated group, *Ctgf* was increased only in the KO female AngII-treated group compared to the WT female AngII-treated group. Furthermore, *Col3a1* and *Ccl2* were augmented in the WT male AngII-treated group compared to the corresponding KO group and WT females (Figure 32C). Taken together, these data suggest that *Nr4a1se_2* deficiency reverses the anti-fibrotic effects in females during AngII-induced cardiac remodelling. However, it cannot be

excluded that the enhanced fibrotic response is a consequence of reduced fibroblast *Nr4a1* expression in the KO mice (Figure 30D) rather than the NCM depletion.

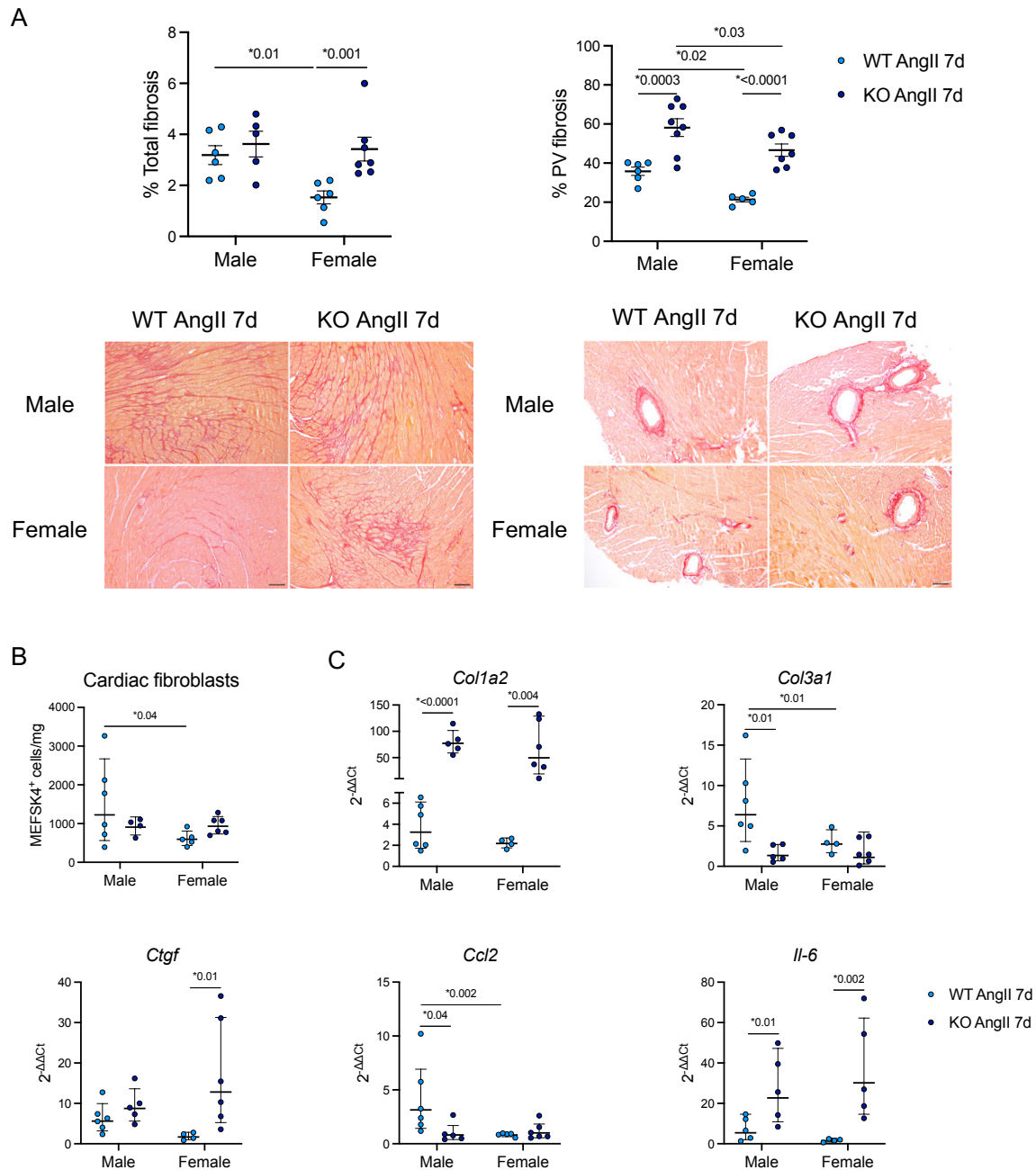


Figure 32 | Impact of *Nr4a1se_2* deficiency on AngII-induced cardiac fibrosis.

A. Total and perivascular (PV) fibrosis were measured after 7 days of AngII treatment. Representative images of Sirius red staining of midventricular transverse sections were taken in 10x magnification (scale bar=100 μ m). Tile scans taken in 10x magnification for each sample were used for total fibrosis measurement. Three vessels per mouse heart were measured for PV fibrosis. Data are shown as mean \pm SEM. **B.** Flow cytometric analysis of the number of cardiac fibroblasts per mg heart after 7 days of AngII treatment. **C.** RT-qPCR analysis of collagen 1a2 (*Col1a2*), collagen 3a1 (*Col3a1*), connective tissue growth factor (*Ctgf*), C-C motif chemokine ligand 2 (*Ccl2*), and interleukin 6 (*Il-6*) of heart lysate after 7 days of AngII treatment. *Gapdh* was used as the reference gene. Data are normalised over male saline 7d (data not shown). (n=4-6). Each dot represents a mouse. Data are shown as geometric mean \pm geometric SD. Two-way ANOVA with Sidak's multiple comparisons; $p < 0.05$ was considered significant.

4.13 *Nr4a1se_2* deficiency promotes the AngII-induced expansion of recruited macrophages in females

To assess the impact of *Nr4a1se_2* deficiency on circulating and cardiac leukocyte subpopulations, flow cytometry analysis was performed after 7 days of AngII infusion. Apart from the expected reduction of circulating Ly6C^{int} and Ly6C^{lo} monocytes in *Nr4a1se_2*^{-/-} mice, other circulating and cardiac immune cells were not affected by the genotype, neither in males nor females (Table 16-17). Furthermore, an increase in the number of cardiac recruited macrophages was observed only in the KO AngII-treated female group, but not in the WT AngII-treated female group compared to the corresponding saline-treated group (Figure 33).

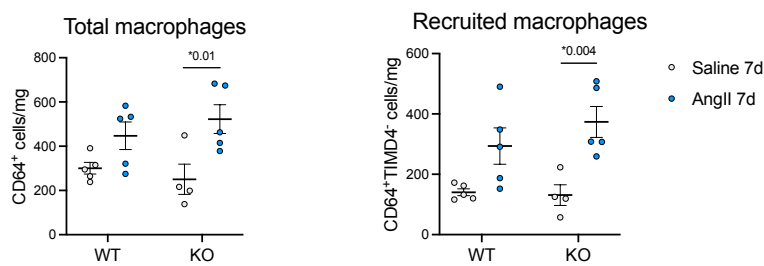


Figure 33 | Cardiac leukocyte quantification in females after 7 days of AngII infusion.

Flow cytometric analysis of total cardiac macrophages (CD64⁺) and recruited macrophages (CD64⁺TIMD4⁻) normalised to heart weight after 7 days of AngII treatment in females (n=4-5). Each dot represents a mouse. Data are shown as mean \pm SEM. Two-way ANOVA with Sidak's multiple comparisons; p<0.05 was considered significant.

Table 16 | Circulating immune cell counts in WT and *Nr4a1se_2*^{-/-} mice after 7 days of AngII infusion

Cell type	WT Male AngII	KO Male AngII	WT Female AngII	KO Female AngII
Leukocytes	1.6x10 ⁵ \pm 1.8x10 ⁴	1.7x10 ⁵ \pm 3.1x10 ⁴	1.6x10 ⁵ \pm 5.4x10 ⁴	2.0 x10 ⁵ \pm 4.0x10 ⁴
Myeloid cells	5.8x10 ⁴ \pm 9.2x10 ³	5.6x10 ⁴ \pm 1.0x10 ⁴	3.8x10 ⁴ \pm 1.2x10 ⁴	4.9x10 ⁴ \pm 1.2x10 ⁴
Lymphocytes	1.2x10 ⁵ \pm 2.0x10 ⁴	1.1x10 ⁵ \pm 2.2x10 ⁴	1.2x10 ⁵ \pm 4.1x10 ⁴	1.4 x10 ⁵ \pm 2.8x10 ⁴
Neutrophils	3.2x10 ⁴ \pm 6.7x10 ³	2.8x10 ⁴ \pm 4.6x10 ³	1.5x10 ⁴ \pm 5.2x10 ³	2.2x10 ⁴ \pm 5.9x10 ³
Monocytes	1.3x10 ⁴ \pm 2.2x10 ³	1.6x10 ⁴ \pm 4.2x10 ³	1.0x10 ⁴ \pm 4.2x10 ³	1.2x10 ⁴ \pm 3.0x10 ³
Ly6C ^{hi}	1.2x10 ⁴ \pm 2.2x10 ³	1.6x10 ⁴ \pm 4.2x10 ³	9.9x10 ³ \pm 4.0x10 ³	1.2x10 ⁴ \pm 3.0x10 ³
Ly6C ^{int}	353 \pm 64	99 \pm 22	275 \pm 79	78 \pm 17 *
Ly6C ^{lo}	408 \pm 69	87 \pm 41	309 \pm 96	70 \pm 23 *
B cells	5.0x10 ⁵ \pm 1.0x10 ⁵	5.7x10 ⁵ \pm 6.5x10 ⁴	5.2x10 ⁵ \pm 8.0x10 ⁴	5.5 x10 ⁵ \pm 7.0x10 ⁴
T cells	2.8x10 ⁵ \pm 4.3x10 ⁴	3.0x10 ⁵ \pm 3.5x10 ⁴	4.2x10 ⁵ \pm 4.1x10 ⁴	3.7x10 ⁵ \pm 2.0x10 ⁴
CD4 ⁺ T cells	1.4x10 ⁵ \pm 2.3x10 ⁴	1.5x10 ⁵ \pm 1.7x10 ⁴	2.2x10 ⁵ \pm 2.3x10 ⁴	2.0x10 ⁵ \pm 9.7x10 ³
CD8 ⁺ T cells	1.0x10 ⁵ \pm 1.7x10 ⁴	1.1x10 ⁵ \pm 1.6x10 ⁴	1.5 x10 ⁵ \pm 1.9x10 ⁴	1.4x10 ⁵ \pm 1.1x10 ⁴

Data are shown as cells/mL (n=6-8). mean \pm SEM; Two-way ANOVA with Sidak's multiple comparisons; *p<0.05 vs. corresponding WT AngII.

Table 17 | Cardiac immune cell counts in WT and *Nr4a1se_2*^{-/-} mice after 7 days of AngII infusion

Cell type	WT Male AngII	KO Male AngII	WT Female AngII	KO Female AngII
Leukocytes	1622 ± 252	1457 ± 181	887 ± 83	1031 ± 106
Myeloid cells	1266 ± 204	1046 ± 127	550 ± 72	688 ± 82
Macrophages	1058 ± 199	826 ± 91	447 ± 62	523 ± 65
TIMD4 ⁺	205 ± 28	172 ± 8	154 ± 26	149 ± 21
TIMD4 ⁻	853 ± 196	654 ± 91	294 ± 60	374 ± 51
Neutrophils	41 ± 9	58 ± 17	19 ± 2	25 ± 5
Monocytes	36 ± 10	38 ± 12	24 ± 4	29 ± 4
Ly6C ^{hi}	20 ± 7	28 ± 9	7 ± 2	16 ± 3
Ly6C ^{int}	8 ± 2	6 ± 2	8 ± 2	6 ± 1
Ly6C ^{lo}	8 ± 2	5 ± 1	9 ± 1	8 ± 1
Lymphocytes	158 ± 31	206 ± 64	194 ± 27	188 ± 20
B cells	99 ± 20	141 ± 42	132 ± 16	121 ± 16
T cells	27 ± 5	27 ± 8	26 ± 4	28 ± 4
CD4 ⁺ T cells	20 ± 4	19 ± 5	20 ± 3	24 ± 4
CD8 ⁺ T cells	2 ± 1	3 ± 2	2 ± 0.4	1 ± 0.5

Data are shown as cells/mg (n=4-6). mean ± SEM; Two-way ANOVA with Sidak's multiple comparisons; No significance observed between groups.

4.14 *Nr4a1se_2* deficiency promotes vascular permeability after AngII infusion in females

Previous experimental studies have reported patrolling functions of NCMs that are important for maintaining vascular endothelial integrity.^{123,127} Thus, cardiac ECs were sorted for bulk RNA-seq to investigate phenotypical and functional changes in cardiac ECs upon Ly6C^{lo} monocyte ablation (Figure 34A). In the PCA plot, PC1 (14% variance) showed a clear separation between the genotypes. However, no pronounced separation for PC2 (8% variance), which distinguished between sexes, was observed. In addition, treatment did not contribute to a distinct separation between AngII-treated and saline-treated groups (Figure 34B). Therefore, the samples were pooled for downstream analysis and split into only two groups, namely WT and KO, for further transcriptomic analysis. The volcano plot revealed that *Nr4a1se_2*^{-/-} mice upregulated genes such as *mt-Nd1*, *mt-Nd5*, and *mt-Co1*, which are associated with elevated response to oxidative stress when subjected to GOBP analysis (Figure 34C-D).

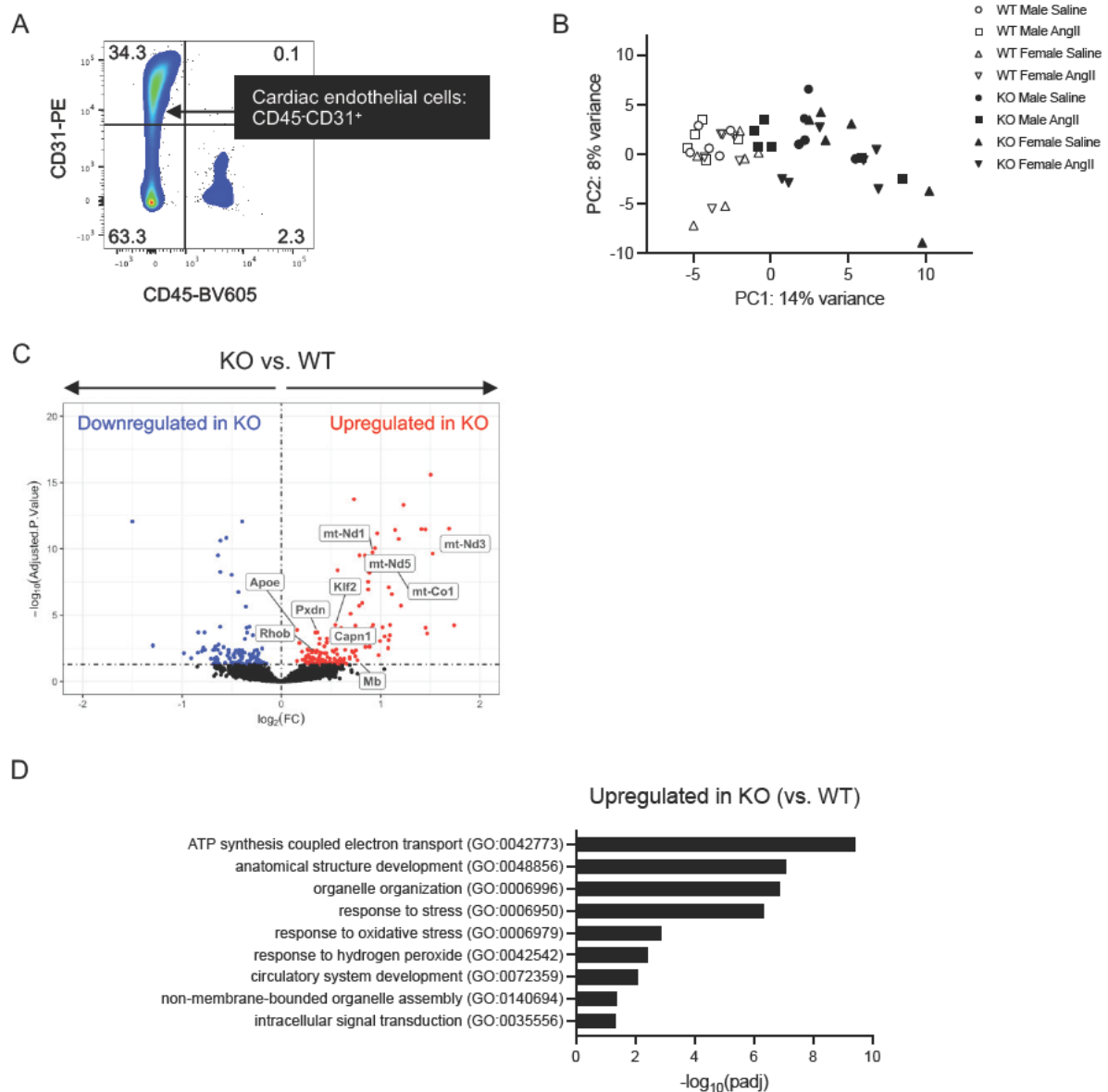


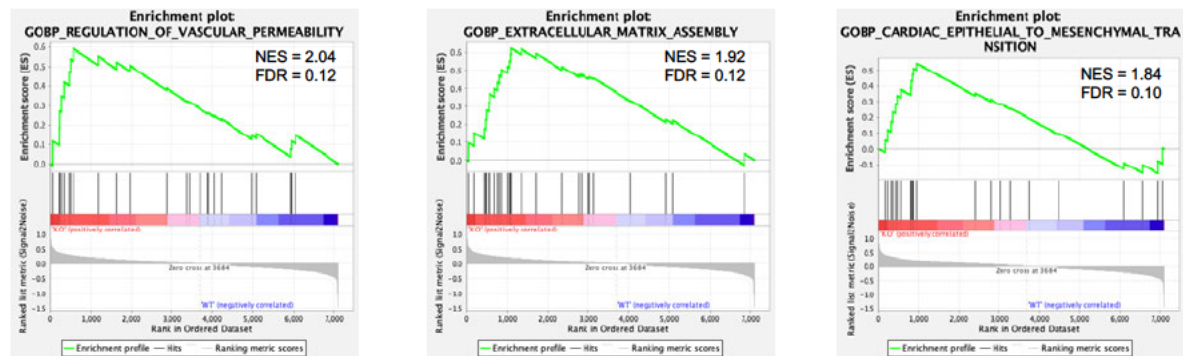
Figure 34 | Bulk RNA-seq analysis of sorted cardiac endothelial cells after 7 days of AngII infusion.

Male and female cardiac endothelial cells (ECs) were sorted (10,000 cells per sample) for bulk RNA sequencing after 7 days of AngII treatment (n=5-6). **A.** Flow cytometry gating for cardiac ECs (CD45⁺CD31⁺). **B.** Principal component analysis (PCA) plot to visualize the heterogeneity of transcriptomic profiles between the experimental groups. Each symbol represents a mouse. **C.** Volcano plot with up- (red) and downregulated (blue) DEGs in KO mice when compared with WT mice. **D.** Gene ontology biological process (GOBP) terms associated with DEGs (padj<0.05) upregulated in cardiac ECs of KO mice compared with WT mice (analysed using g:Profiler).

Moreover, GSEA showed enrichment for gene sets linked to the regulation of vascular permeability, extracellular matrix assembly, and cardiac epithelial-to-mesenchymal transition in KO cardiac ECs (Figure 35A). To functionally confirm a disruption of endothelial integrity in *Nr4a1se⁻²* mice, vascular permeability was tested in WT and KO female mice 7 days after AngII treatment. As expected, significantly elevated Evans blue relative fluorescence units

were observed after dye extraction from KO hearts compared to WT hearts, indicating an increase in vascular permeability (Figure 35B). These data suggest that *Nr4a1se_2* deficiency promotes vascular permeability and the expansion of recruited macrophages and cardiac fibroblasts during AngII-induced cardiac remodelling in females.

A



B

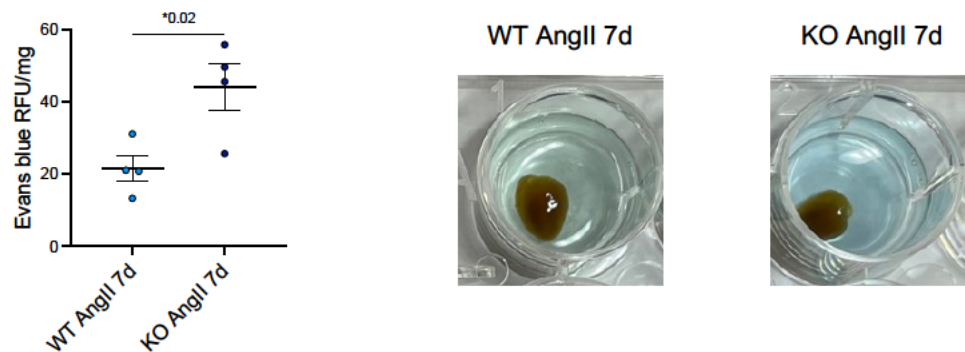


Figure 35 | Gene set enrichment analysis of cardiac ECs and Evans blue assay after 7 days of AngII infusion.

A. GOBP enriched in cardiac endothelial cells of KO mice compared with WT mice by Gene Set Enrichment Analysis (GSEA). (n=5-6). **B.** After 7 days of AngII treatment, Evans blue (40 mg/kg) was administered into the tail vein of female WT and KO mice. Hearts were collected for dye extraction 70 min after injection to measure relative fluorescence units (RFU), which were normalised to heart weight. Formamide was used as blank. (n=4). Each dot represents a mouse. Data are shown as mean \pm SEM. Unpaired t-test; $p < 0.05$ was considered significant.

5. Discussion

Sex differences in the clinical characteristics and pathophysiology of HF have been described in clinical studies, with women more prone to HFpEF, and men more susceptible to HFrEF.^{19,20} However, animal models of HF often focus on just one sex, which could restrict their applicability for translation to human disease context. Chronic hypertension is a risk factor for both HFpEF and HFrEF development and promotes the pathogenesis of HHD, which is the second leading cause of HF after ischaemic heart disease.³⁴ Therefore, this project aimed to study sex-specific differences during chronic hypertension-induced cardiac remodelling by AngII infusion in mice. Chronic AT1R stimulation by AngII in this mouse model results in vasoconstriction and elevated blood pressure.¹³⁶

5.1 Female mice are protected from adverse cardiac fibrosis during AngII infusion

Data presented in this thesis show that AngII infusion promoted cardiac and cardiomyocyte hypertrophy independent of sex. However, previous studies have revealed that patients with hypertension show different features of cardiac hypertrophy, where women are more prone towards concentric hypertrophy while men are oriented towards eccentric hypertrophy with chamber dilatation.^{162,163} Interestingly, in the present study, AngII-induced cardiac fibrosis occurred only in male mice, with elevated pro-fibrotic gene expression and cardiac fibroblast expansion. This result is consistent with data from patients with pressure overload, where men have a more frequent occurrence of cardiac fibrosis, with more pronounced pro-fibrotic marker activation in men compared to women.^{56,164} Consistent with these observations in human patients, the RNA-seq data presented in this thesis reveal a profound alteration of the transcriptomic profile in male cardiac fibroblasts subjected to AngII compared to female fibroblasts. Furthermore, cardiac fibroblasts in AngII-treated males downregulated genes related to detoxifying ROS, which could enhance ECM assembly by promoting cardiac fibroblast proliferation. On the other hand, AngII treatment in females led to a downregulation of genes associated with fibroblast activation and signalling, thus preventing excessive collagen deposition during cardiac remodelling.

In addition, the higher number of recruited macrophages into the myocardium of AngII-treated male mice, as observed in this study, could contribute to the release of pro-fibrotic mediators such as TGF- β , interleukin-10, and platelet-derived growth factor that directly stimulate the proliferation and activation of cardiac fibroblasts, resulting in increased collagen deposition.^{165,166} Macrophages can also secrete TIMPs that inhibit ECM degradation, thereby facilitating microscar formation and the progression of adverse cardiac remodelling.¹⁶⁷ Transcriptomic profiling of cardiac macrophages highlighted that AngII infusion in males

downregulated genes related to cardioprotective mechanisms – primarily the heat shock proteins¹⁶⁸ – in line with the worse cardiac outcome in males. In contrast, the genes downregulated in the female AngII-treated group were associated with maladaptive cardiac remodelling, thereby protecting females against cardiac inflammation and fibrosis. Together, the difference in the extent of cardiac fibrosis could be mainly attributed to the number of cardiac fibroblasts and pro-inflammatory macrophages in the myocardium and the relative proportion of resting and activated fibroblasts.

5.2 AngII promotes antigen processing and presentation in Ly6C^{hi} and Ly6C^{lo} monocytes during cardiac remodelling in females

Another key finding of this thesis was that the relative proportion of Ly6C^{lo} monocytes increased significantly in females upon AngII infusion, which was not observed in males. This could be due to a higher expression of *Nr4a1* in Ly6C^{hi} monocytes of females, promoting the conversion of Ly6C^{hi} to Ly6C^{lo} monocytes in the circulation.

Furthermore, the upregulated genes in Ly6C^{hi} and Ly6C^{lo} monocytes in AngII-treated females were mainly related to antigen processing and presentation via MHC class I. This data is also supported by the observed increase in circulating CD8⁺ T cells in the female AngII-treated group. MHC I plays a crucial role in mediating cytotoxic T-cell adaptive immune response to eliminate viral, pathogens and tumour cells.¹⁶⁹ Cancer studies in mice revealed that the loss of MHC I antigen presentation machinery helps the tumour cells to evade immune surveillance and eradication.¹⁷⁰ Therefore, lower expression of the genes associated with MHC I antigen processing and presentation in monocytes of male AngII-treated mice may fail to induce damage responses to danger signals that normally help maintain tissue homeostasis. Insufficient clearance of damaged vascular ECs and cell debris, in turn, may induce cardiac inflammation and fibrosis, as observed in male mice subjected to chronic AngII infusion.

5.3 AngII induces TLR7 signalling in female Ly6C^{hi} monocytes

Transcriptomic data from circulating Ly6C^{hi} monocytes revealed a significant increase of genes associated with the TLR7 signalling pathway in females independent of treatment received compared to males. An experimental mouse model of lipopolysaccharide-induced kidney injury showed that the exposure of TLR7 to damage-associated molecular patterns promotes fractalkine expression on NCMs and thereby enhances intravascular retention of NCMs. Prolonged contact of NCMs with the endothelium via TLR7 activation triggered the recruitment of neutrophils to mediate focal necrosis of the damaged endothelial cells. NCMs, in turn, scavenged the cellular debris, maintaining the vascular integrity and homeostasis of

the vasculature.¹²² Although the transcriptomic data presented in this thesis suggest that TLR7 signalling *per se* is stronger in female monocytes, no evidence for upregulation of the TLR signalling pathway after AngII infusion was observed, at least at the gene expression level.

5.4 Impact of global *Nr4a1se_2* deficiency on various cell types

The increased relative proportion of NCMs and attenuated cardiac fibrosis in females after AngII treatment led to the hypothesis that NCMs may provide cardioprotective effects during cardiac remodelling. To study the role of NCMs during AngII-induced cardiac remodelling, the *Nr4a1se_2*^{-/-} mouse model with Ly6C^{lo} monocyte ablation was utilised in this thesis. The depletion of NCMs in the circulation was validated through flow cytometry, and no morphological abnormalities were observed in the KO mice. Since *Nr4a1* is expressed by various cell types, it was important to clarify whether global *Nr4a1se_2* deficiency only affected NCMs, without changing the *Nr4a1* expression level in other cells. While *Nr4a1* expression in *Nr4a1se_2*^{-/-} mice was not affected in B cells, T cells, and cardiac ECs, its expression in cardiac fibroblasts was significantly reduced in *Nr4a1se_2*^{-/-} mice compared to WT mice. Studies have shown that NR4A1 is crucial to dampen macrophage inflammatory responses, while global *Nr4a1* deficiency facilitates cell migration and enhances phagocytic activity¹²⁹. *Nr4a1* deficiency was also reported to enhance CCR2 expression on Ly6C^{hi} monocytes, facilitating myocardial infiltration and the differentiation to inflammatory macrophages that contribute to adverse cardiac outcomes.¹³⁰ Furthermore, elevated *Nr4a1* expression was shown to inhibit effector T cell differentiation, while *Nr4a1* deficiency could overcome T cell tolerance and amplify effector function.¹³¹ In reference to the previous study reporting the establishment of the *Nr4a1se_2*^{-/-} mouse model, *Nr4a1se_2* deletion did not affect *Nr4a1* expression in lung alveolar macrophages, large and small peritoneal macrophages. However, the *Nr4a1* expression in splenic red pulp macrophages and circulating Ly6C^{hi} monocytes was significantly reduced.¹³³ These results suggested that the effects of *Nr4a1se_2* deletion on *Nr4a1* expression are dependent on the cell types and tissue origin.

5.5 *Nr4a1se_2* deficiency promotes perivascular fibrosis

Unlike WT females, *Nr4a1se_2*^{-/-} females showed a similar degree of cardiac fibrosis to males when subjected to AngII treatment. This result suggests a cardioprotective role of NCM in females during cardiac remodelling. In addition, certain pro-fibrotic mediators such as *Col1a2*, *Ctgf*, and *Il-6* were significantly elevated and more pronounced perivascular fibrosis was observed in *Nr4a1se_2*^{-/-} mice compared to WT mice after AngII infusion. As NCMs have been described as patrolling monocytes that are responsible for maintaining vasculature homeostasis and immune surveillance,¹¹⁶ aggravated perivascular fibrosis in *Nr4a1se_2*^{-/-}

mice after AngII treatment may be due to the disturbance of vascular integrity in the absence of NCMs. However, the interpretation of these results as to whether the effect is indeed due to NCM depletion or rather the direct effects of the genetic modification on fibroblasts is complicated by the fact that *Nr4a1se_2* depletion also affects *Nr4a1* expression levels in these cells. Studies in patients with systemic sclerosis, as well as mice with liver fibrosis and idiopathic pulmonary fibrosis, revealed that NR4A1 is involved in TGF- β signalling and the inhibition of NR4A1 expression and activation worsens the disease outcome.¹⁷¹

5.6 *Nr4a1se_2* deficiency increases endothelial permeability and oxidative stress

Bulk RNA-seq data of cardiac ECs presented in this thesis revealed a significant alteration in the transcriptomic profile of *Nr4a1se_2*^{-/-} mice compared to WT mice. *Nr4a1se_2* deficiency leads to elevated gene expression associated with increased vascular permeability, EndMT, ECM assembly, and increased oxidative stress. These results were further supported by the functional Evans blue assay showing aggravated vascular permeability in *Nr4a1se_2*^{-/-} females after AngII treatment. In addition, flow cytometry analysis also revealed an expansion of recruited macrophages and cardiac fibroblast in female AngII-treated KO mice compared to their corresponding saline-treated group. In patients with chronic hypertension, endothelial dysfunction and oxidative stress are frequently observed.¹⁷²

Under physiological conditions, reactive oxygen species (ROS) such as superoxide anion ($O_2^{\bullet-}$), hydrogen peroxide (H_2O_2), hydroxyl radical (OH^{\bullet}), and peroxynitrite ($ONOO^-$) act as second messengers in transducing intracellular signalling for a variety of biological processes.¹⁷³ However, when the production of ROS exceeds the capability of the antioxidant defence system, oxidative stress occurs, leading to vascular and myocardial damage.^{174,175} Nitric oxide (NO) plays a critical role in maintaining vascular homeostasis. Disturbance in NO bioavailability via superoxide anion leads to decreased NO generation or elevated NO degradation, contributing to the onset of endothelial dysfunction.¹⁷³ Chronic stimulation of AT1R through AngII infusion promotes the activity of nicotinamide adenine dinucleotide phosphate (NADPH) oxidase (NOX) in endothelial and smooth muscle cells, generating large amounts of superoxide anion.¹⁷⁶ Further amplification of ROS production through the mitochondrial electron transport chain can trigger maladaptive cardiac remodelling and diastolic dysfunction in response to AngII treatment, as previously reported.¹⁷⁷ In addition, endothelial nitric oxide synthase (eNOS) that is normally responsible for NO production can be uncoupled by peroxynitrite during AngII-induced hypertension, which oxidises the eNOS cofactor tetrahydrobiopterin (BH_4) to 7,8-dihydrobiopterin (BH_2), facilitating superoxide anion formation (Figure 38).¹⁷⁶ Together, the presence of NCMs may help to encounter the adverse effects of AngII-induced oxidative stress, thereby mitigating endothelial dysfunction and

perivascular fibrosis. The underlying mechanisms of how NCMs may counterbalance ROS production remain to be clarified.

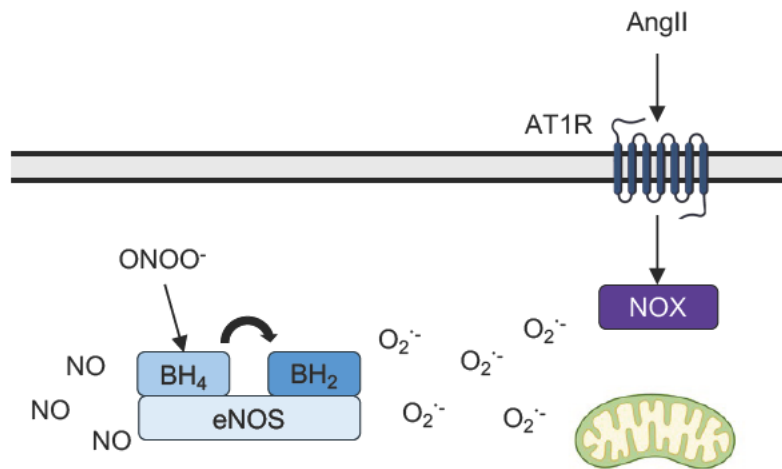


Figure 38 | Contribution of reactive oxidative species in endothelial dysfunction.

Chronic angiotensin II (AngII) stimulation of the AngII type I receptor (AT1R) activates nicotinamide adenine dinucleotide phosphate oxidase (NOX) in endothelial cells, which generates large amounts of superoxide anion ($O_2^{\cdot-}$). Mitochondria also contribute to the production of $O_2^{\cdot-}$ via the electron transport chain. Under steady state, endothelial nitric oxide synthase (eNOS) releases nitric oxide (NO), which helps in maintaining endothelial homeostasis. Increased oxidative stress triggers the uncoupling of eNOS cofactor tetrahydrobiopterin (BH_4) by peroxynitrite ($ONOO^-$) via oxidation to 7,8-dihydrobiopterin (BH_2), resulting in $O_2^{\cdot-}$ synthesis.¹⁷³ (generated using BioRender.com)

5.7 Study limitations and future perspectives

The main finding of this thesis is that biological sex has an impact on the manifestation and disease progression of AngII-induced cardiac remodelling in this experimental mouse model, with females being protected against the development of cardiac fibrosis. Previous studies have revealed that sex hormones crucially affect the pathogenesis of HF.^{18,25,56,178} However, their specific contribution to the observed phenotype was not investigated in this project. Sex hormones have been demonstrated to modulate the expression and activity of the RAAS.¹⁷⁹ Oestrogen favours the vasodilatory arm of the RAAS by promoting the generation of angiotensinogen, ACE2, AngII type 2 receptor (AT2R), and eNOS, whereas testosterone stimulates the increased production of renin, ACE, and AT1R, favouring the vasoconstrictor arm of the RAAS.^{180,181} In a setting of pressure overload, the binding of oestrogen on female cardiac fibroblasts preferentially phosphorylates $ER\alpha$, repressing collagen production. In contrast, oestrogen predominantly phosphorylates $ER\beta$ in male cardiac fibroblasts, which facilitates collagen synthesis, thereby leading to a greater extent of myocardial fibrosis.¹⁸² Furthermore, infiltrated inflammatory cells, especially recruited macrophages, express TGF- β receptors that are involved in modulating the inflammatory response. $ER\beta$ binding by oestrogen on female cardiac fibroblasts inhibits TGF- β production, preventing TGF- β receptor

activation that promotes the conversion of fibroblasts to myofibroblasts.^{183,184} Although the expression of ER α and ER β in each cell type assessed by RNA sequencing did not show significant differences between males and females, the effects of a higher concentration of oestrogen in females during cardiac remodelling cannot be ruled out. Therefore, gonadectomy could be used in future studies to dissect the effects of sex hormones on cardiac remodelling.

In addition, the results of this thesis also demonstrated that WT females had a higher proportion of NCMs with better cardiac outcomes upon AngII infusion. However, the attempts to reverse the adverse cardiac fibrosis in *Nr4a1se_2*^{-/-} mice by adoptive transfer of WT female NCMs in this study have so far proved unsuccessful (data not shown). Another strategy that could help to shed light on the protective role of female NCMs could be the transplantation of female bone marrow into irradiated male mice to investigate if the protective effect against AngII-induced cardiac fibrosis is transferable. This experiment could also provide insights into the question of whether the preferential expansion of NCMs upon AngII-induced stress is an intrinsic effect of the monocytes or rather triggered by sex-specific differences in endothelial cells.

Finally, although the *Nr4a1se_2*^{-/-} mouse model has improved in retaining *Nr4a1* expression and functions on most of the cell types analysed, *Nr4a1* expression in cardiac fibroblasts was unfortunately affected by *Nr4a1se_2* depletion. Thus, a mouse model that specifically ablates the NCMs without affecting the phenotypes and functions of other cell types, for example by using bone marrow chimeric mice, transplanted with bone marrow from WT vs *Nr4a1se_2*^{-/-} mice, should be considered.

6. Conclusion

In conclusion, males and females presented sex-specific differences in regulating AngII-induced cardiac remodelling. A better cardiac outcome observed in WT females is associated with an elevated relative proportion of NCMs. *Nr4a1se_2* depletion has demonstrated that NCMs are pivotal in maintaining vascular homeostasis. Therefore, these findings suggest that the increased percentage of NCMs in WT females upon AngII treatment may contribute to the maintenance of cardiac endothelial integrity, reducing oxidative stress in the vasculature and limiting inflammatory cell infiltration. A lower number of inflammatory cardiac macrophages could inhibit the activation of cardiac fibroblasts, thus mitigating AngII-induced cardiac fibrosis (Figure 39). The underlying mechanisms leading to a preferential cardiac NCM expansion in females, but not males when subjected to chronic AngII infusion and implications for human pathophysiology deserve further investigation.

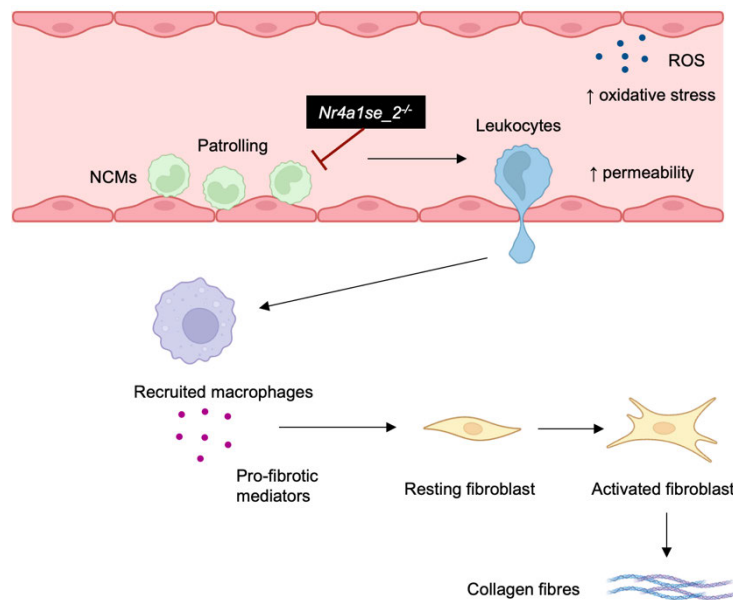


Figure 39 | Role of NCMs in AngII-induced cardiac remodelling

Non-classical monocytes (NCMs) patrol the endothelium to maintain vascular homeostasis. Ablation of NCMs by *Nr4a1se_2*^{-/-} disrupts vascular integrity and increases reactive oxidative species (ROS) production and vascular permeability. Recruited macrophages release pro-fibrotic mediators, activating cardiac fibroblasts that lead to excess collagen fibre deposition. (generated using BioRender.com)

7. References

- 1 Y. X. Shia, J. D., S.-L. Puhl, S. Steffens in *DGK Herztage 2024* (Deutschen Gesellschaft für Kardiologie, Hamburg, 2024).
- 2 Global, regional, and national incidence, prevalence, and years lived with disability for 354 diseases and injuries for 195 countries and territories, 1990-2017: a systematic analysis for the Global Burden of Disease Study 2017. *Lancet* **392**, 1789-1858, doi:10.1016/s0140-6736(18)32279-7 (2018).
- 3 McDonagh, T. A., Gardner, R. S., Clark, A. L. & Dargie, H. *Oxford textbook of heart failure*. (Oxford University Press, 2011).
- 4 Khan, M. S. *et al.* Global epidemiology of heart failure. *Nature Reviews Cardiology*, doi:10.1038/s41569-024-01046-6 (2024).
- 5 Konstam, M. A. & Abboud, F. M. Ejection Fraction. *Circulation* **135**, 717-719, doi:10.1161/CIRCULATIONAHA.116.025795 (2017).
- 6 Savarese, G. *et al.* Prevalence and Prognostic Implications of Longitudinal Ejection Fraction Change in Heart Failure. *JACC Heart Fail* **7**, 306-317, doi:10.1016/j.jchf.2018.11.019 (2019).
- 7 Lopatin, Y. Heart Failure with Mid-Range Ejection Fraction and How to Treat It. *Card Fail Rev* **4**, 9-13, doi:10.15420/cfr.2018:10:1 (2018).
- 8 Bloom, M. W. *et al.* Heart failure with reduced ejection fraction. *Nature Reviews Disease Primers* **3**, 17058, doi:10.1038/nrdp.2017.58 (2017).
- 9 Kawaguchi, M., Hay, I., Fetcs, B. & Kass, D. A. Combined ventricular systolic and arterial stiffening in patients with heart failure and preserved ejection fraction: implications for systolic and diastolic reserve limitations. *Circulation* **107**, 714-720, doi:10.1161/01.cir.0000048123.22359.a0 (2003).
- 10 Westermann, D. *et al.* Role of left ventricular stiffness in heart failure with normal ejection fraction. *Circulation* **117**, 2051-2060, doi:10.1161/circulationaha.107.716886 (2008).
- 11 Borlaug, B. A. The pathophysiology of heart failure with preserved ejection fraction. *Nature Reviews Cardiology* **11**, 507-515, doi:10.1038/nrcardio.2014.83 (2014).
- 12 Simmonds, S. J., Cuijpers, I., Heymans, S. & Jones, E. A. V. Cellular and Molecular Differences between HFpEF and HFrEF: A Step Ahead in an Improved Pathological Understanding. *Cells* **9**, doi:10.3390/cells9010242 (2020).
- 13 Lilly, L. S. *Pathophysiology of heart disease: a collaborative project of medical students and faculty*. (Lippincott Williams & Wilkins, 2012).
- 14 Miller, W. L. Fluid Volume Overload and Congestion in Heart Failure. *Circulation: Heart Failure* **9**, e002922, doi:10.1161/CIRCHEARTFAILURE.115.002922 (2016).
- 15 Louridas, G. E. & Lourida, K. G. Heart Failure in Patients with Preserved Ejection Fraction: Questions Concerning Clinical Progression. *J Cardiovasc Dev Dis* **3**, doi:10.3390/jcdd3030027 (2016).
- 16 McDonagh, T. A. *et al.* 2023 Focused Update of the 2021 ESC Guidelines for the diagnosis and treatment of acute and chronic heart failure: Developed by the task force for the diagnosis and treatment of acute and chronic heart failure of the European Society of Cardiology (ESC) With the special contribution of the Heart Failure Association (HFA) of the ESC. *European Heart Journal* **44**, 3627-3639, doi:10.1093/eurheartj/ehad195 (2023).
- 17 Anker, S. D. *et al.* Empagliflozin in Heart Failure with a Preserved Ejection Fraction. *New England Journal of Medicine* **385**, 1451-1461, doi:10.1056/NEJMoa2107038 (2021).
- 18 Arata, A. *et al.* Sex Differences in Heart Failure: What Do We Know? *J Cardiovasc Dev Dis* **10**, doi:10.3390/jcdd10070277 (2023).
- 19 Ho, J. E. *et al.* Predictors of new-onset heart failure: differences in preserved versus reduced ejection fraction. *Circulation: heart failure* **6**, 279-286 (2013).

- 20 Dewan, P. *et al.* Differential Impact of Heart Failure With Reduced Ejection Fraction on Men and Women. *Journal of the American College of Cardiology* **73**, 29-40, doi:10.1016/j.jacc.2018.09.081 (2019).
- 21 Beale, A. L., Meyer, P., Marwick, T. H., Lam, C. S. P. & Kaye, D. M. Sex Differences in Cardiovascular Pathophysiology. *Circulation* **138**, 198-205, doi:10.1161/CIRCULATIONAHA.118.034271 (2018).
- 22 Chung, A. K. *et al.* Women have higher left ventricular ejection fractions than men independent of differences in left ventricular volume: the Dallas Heart Study. *Circulation* **113**, 1597-1604, doi:10.1161/circulationaha.105.574400 (2006).
- 23 Petersen, S. E. *et al.* Reference ranges for cardiac structure and function using cardiovascular magnetic resonance (CMR) in Caucasians from the UK Biobank population cohort. *J Cardiovasc Magn Reson* **19**, 18, doi:10.1186/s12968-017-0327-9 (2017).
- 24 Salton, C. J. *et al.* Gender differences and normal left ventricular anatomy in an adult population free of hypertension. A cardiovascular magnetic resonance study of the Framingham Heart Study Offspring cohort. *J Am Coll Cardiol* **39**, 1055-1060, doi:10.1016/s0735-1097(02)01712-6 (2002).
- 25 Luchner, A. *et al.* Gender-specific differences of cardiac remodeling in subjects with left ventricular dysfunction: a population-based study. *Cardiovasc Res* **53**, 720-727, doi:10.1016/s0008-6363(01)00510-7 (2002).
- 26 Redfield, M. M., Jacobsen, S. J., Borlaug, B. A., Rodeheffer, R. J. & Kass, D. A. Age- and gender-related ventricular-vascular stiffening: a community-based study. *Circulation* **112**, 2254-2262, doi:10.1161/circulationaha.105.541078 (2005).
- 27 Roth, G. A. *et al.* Global Burden of Cardiovascular Diseases and Risk Factors, 1990-2019: Update From the GBD 2019 Study. *J Am Coll Cardiol* **76**, 2982-3021, doi:10.1016/j.jacc.2020.11.010 (2020).
- 28 Conrad, N. *et al.* Temporal trends and patterns in heart failure incidence: a population-based study of 4 million individuals. *Lancet* **391**, 572-580, doi:10.1016/s0140-6736(17)32520-5 (2018).
- 29 Rapsomaniki, E. *et al.* Blood pressure and incidence of twelve cardiovascular diseases: lifetime risks, healthy life-years lost, and age-specific associations in 1·25 million people. *Lancet* **383**, 1899-1911, doi:10.1016/s0140-6736(14)60685-1 (2014).
- 30 Frohlich, E. D. *et al.* The heart in hypertension. *N Engl J Med* **327**, 998-1008, doi:10.1056/nejm199210013271406 (1992).
- 31 Messerli, F. H., Rimoldi, S. F. & Bangalore, S. The Transition From Hypertension to Heart Failure: Contemporary Update. *JACC Heart Fail* **5**, 543-551, doi:10.1016/j.jchf.2017.04.012 (2017).
- 32 Rizzoni, D. *et al.* Immune System and Microvascular Remodeling in Humans. *Hypertension* **79**, 691-705, doi:10.1161/hypertensionaha.121.17955 (2022).
- 33 Griendling, K. K. *et al.* Oxidative Stress and Hypertension. *Circ Res* **128**, 993-1020, doi:10.1161/circresaha.121.318063 (2021).
- 34 Bragazzi, N. L. *et al.* Burden of heart failure and underlying causes in 195 countries and territories from 1990 to 2017. *Eur J Prev Cardiol* **28**, 1682-1690, doi:10.1093/eurjpc/zwaa147 (2021).
- 35 Díez, J. & Butler, J. Growing Heart Failure Burden of Hypertensive Heart Disease: A Call to Action. *Hypertension* **80**, 13-21, doi:10.1161/HYPERTENSIONAHA.122.19373 (2023).
- 36 Schiattarella, G. G. & Hill, J. A. Inhibition of hypertrophy is a good therapeutic strategy in ventricular pressure overload. *Circulation* **131**, 1435-1447, doi:10.1161/circulationaha.115.013894 (2015).
- 37 Azevedo, P. S., Polegato, B. F., Minicucci, M. F., Paiva, S. A. & Zornoff, L. A. Cardiac Remodeling: Concepts, Clinical Impact, Pathophysiological Mechanisms and Pharmacologic Treatment. *Arq Bras Cardiol* **106**, 62-69, doi:10.5935/abc.20160005 (2016).

- 38 Burchfield, J. S., Xie, M. & Hill, J. A. Pathological Ventricular Remodeling. *Circulation* **128**, 388-400, doi:doi:10.1161/CIRCULATIONAHA.113.001878 (2013).
- 39 González, A. *et al.* Myocardial Remodeling in Hypertension. *Hypertension* **72**, 549-558, doi:doi:10.1161/HYPERTENSIONAHA.118.11125 (2018).
- 40 Zhou, P. & Pu, W. T. Recounting Cardiac Cellular Composition. *Circ Res* **118**, 368-370, doi:10.1161/circresaha.116.308139 (2016).
- 41 Zile, M. R. *et al.* Myocardial stiffness in patients with heart failure and a preserved ejection fraction: contributions of collagen and titin. *Circulation* **131**, 1247-1259 (2015).
- 42 Sawada, K. & Kawamura, K. Architecture of myocardial cells in human cardiac ventricles with concentric and eccentric hypertrophy as demonstrated by quantitative scanning electron microscopy. *Heart Vessels* **6**, 129-142, doi:10.1007/bf02058278 (1991).
- 43 Miyata, S., Minobe, W., Bristow, M. R. & Leinwand, L. A. Myosin Heavy Chain Isoform Expression in the Failing and Nonfailing Human Heart. *Circulation Research* **86**, 386-390, doi:doi:10.1161/01.RES.86.4.386 (2000).
- 44 Díez, J., González, A. & Kovacic, J. C. Myocardial Interstitial Fibrosis in Nonischemic Heart Disease, Part 3/4: JACC Focus Seminar. *Journal of the American College of Cardiology* **75**, 2204-2218, doi:https://doi.org/10.1016/j.jacc.2020.03.019 (2020).
- 45 Martin, M. L. & Blaxall, B. C. Cardiac intercellular communication: are myocytes and fibroblasts fair-weather friends? *J Cardiovasc Transl Res* **5**, 768-782, doi:10.1007/s12265-012-9404-5 (2012).
- 46 Assomull, R. G. *et al.* Cardiovascular magnetic resonance, fibrosis, and prognosis in dilated cardiomyopathy. *Journal of the American College of Cardiology* **48**, 1977-1985 (2006).
- 47 Kong, P., Christia, P. & Frangogiannis, N. G. The pathogenesis of cardiac fibrosis. *Cell Mol Life Sci* **71**, 549-574, doi:10.1007/s00018-013-1349-6 (2014).
- 48 Koitabashi, N. *et al.* Pivotal role of cardiomyocyte TGF- β signaling in the murine pathological response to sustained pressure overload. *The Journal of clinical investigation* **121**, 2301-2312 (2011).
- 49 Hartupée, J. & Mann, D. L. Neurohormonal activation in heart failure with reduced ejection fraction. *Nature Reviews Cardiology* **14**, 30-38, doi:10.1038/nrcardio.2016.163 (2017).
- 50 Tham, Y. K., Bernardo, B. C., Ooi, J. Y., Weeks, K. L. & McMullen, J. R. Pathophysiology of cardiac hypertrophy and heart failure: signaling pathways and novel therapeutic targets. *Arch Toxicol* **89**, 1401-1438, doi:10.1007/s00204-015-1477-x (2015).
- 51 Spinale, F. G. Myocardial matrix remodeling and the matrix metalloproteinases: influence on cardiac form and function. *Physiological reviews* **87**, 1285-1342 (2007).
- 52 López, B. *et al.* Diffuse myocardial fibrosis: mechanisms, diagnosis and therapeutic approaches. *Nat Rev Cardiol* **18**, 479-498, doi:10.1038/s41569-020-00504-1 (2021).
- 53 Martin, T. G. & Leinwand, L. A. Hearts apart: sex differences in cardiac remodeling in health and disease. *J Clin Invest* **134**, doi:10.1172/jci180074 (2024).
- 54 Appiah, D. *et al.* Association of Age at Menopause With Incident Heart Failure: A Prospective Cohort Study and Meta-Analysis. *J Am Heart Assoc* **5**, doi:10.1161/jaha.116.003769 (2016).
- 55 Liu, C. Y. *et al.* Evaluation of age-related interstitial myocardial fibrosis with cardiac magnetic resonance contrast-enhanced T1 mapping: MESA (Multi-Ethnic Study of Atherosclerosis). *J Am Coll Cardiol* **62**, 1280-1287, doi:10.1016/j.jacc.2013.05.078 (2013).
- 56 Kararigas, G. *et al.* Sex-dependent regulation of fibrosis and inflammation in human left ventricular remodelling under pressure overload. *Eur J Heart Fail* **16**, 1160-1167, doi:10.1002/ehf.171 (2014).
- 57 Montalvo, C. *et al.* Androgens contribute to sex differences in myocardial remodeling under pressure overload by a mechanism involving TGF- β . *PLoS One* **7**, e35635, doi:10.1371/journal.pone.0035635 (2012).

- 58 Kararigas, G. *et al.* Comparative proteomic analysis reveals sex and estrogen receptor β effects in the pressure overloaded heart. *J Proteome Res* **13**, 5829-5836, doi:10.1021/pr500749j (2014).
- 59 Kararigas, G., Fliegner, D., Gustafsson, J. & Regitz-Zagrosek, V. Role of the estrogen/estrogen-receptor-beta axis in the genomic response to pressure overload-induced hypertrophy. *Physiol Genomics* **43**, 438-446, doi:10.1152/physiolgenomics.00199.2010 (2011).
- 60 Anderson, K. R., Sutton, M. G. & Lie, J. T. Histopathological types of cardiac fibrosis in myocardial disease. *J Pathol* **128**, 79-85, doi:10.1002/path.1711280205 (1979).
- 61 Galati, G. *et al.* Histological and Histometric Characterization of Myocardial Fibrosis in End-Stage Hypertrophic Cardiomyopathy: A Clinical-Pathological Study of 30 Explanted Hearts. *Circ Heart Fail* **9**, doi:10.1161/cirheartfailure.116.003090 (2016).
- 62 Ongstad, E. & Kohl, P. Fibroblast-myocyte coupling in the heart: Potential relevance for therapeutic interventions. *J Mol Cell Cardiol* **91**, 238-246, doi:10.1016/j.yjmcc.2016.01.010 (2016).
- 63 Kohl, P. & Gourdie, R. G. Fibroblast-myocyte electrotonic coupling: does it occur in native cardiac tissue? *J Mol Cell Cardiol* **70**, 37-46, doi:10.1016/j.yjmcc.2013.12.024 (2014).
- 64 Talman, V. & Ruskoaho, H. Cardiac fibrosis in myocardial infarction-from repair and remodeling to regeneration. *Cell Tissue Res* **365**, 563-581, doi:10.1007/s00441-016-2431-9 (2016).
- 65 Pesce, M. *et al.* Cardiac fibroblasts and mechanosensation in heart development, health and disease. *Nature Reviews Cardiology* **20**, 309-324, doi:10.1038/s41569-022-00799-2 (2023).
- 66 Eghbali, M. *et al.* Collagen chain mRNAs in isolated heart cells from young and adult rats. *J Mol Cell Cardiol* **20**, 267-276, doi:10.1016/s0022-2828(88)80059-2 (1988).
- 67 Herum, K. M., Choppe, J., Kumar, A., Engler, A. J. & McCulloch, A. D. Mechanical regulation of cardiac fibroblast profibrotic phenotypes. *Mol Biol Cell* **28**, 1871-1882, doi:10.1091/mbc.E17-01-0014 (2017).
- 68 Gladka, M. M. *et al.* Single-Cell Sequencing of the Healthy and Diseased Heart Reveals Cytoskeleton-Associated Protein 4 as a New Modulator of Fibroblasts Activation. *Circulation* **138**, 166-180, doi:10.1161/circulationaha.117.030742 (2018).
- 69 Khalil, H. *et al.* Fibroblast-specific TGF- β -Smad2/3 signaling underlies cardiac fibrosis. *J Clin Invest* **127**, 3770-3783, doi:10.1172/jci94753 (2017).
- 70 Kuwahara, F. *et al.* Transforming growth factor-beta function blocking prevents myocardial fibrosis and diastolic dysfunction in pressure-overloaded rats. *Circulation* **106**, 130-135, doi:10.1161/01.cir.0000020689.12472.e0 (2002).
- 71 Hall, C., Gehmlich, K., Denning, C. & Pavlovic, D. Complex Relationship Between Cardiac Fibroblasts and Cardiomyocytes in Health and Disease. *Journal of the American Heart Association* **10**, e019338, doi:10.1161/JAHA.120.019338 (2021).
- 72 Van Linthout, S., Miteva, K. & Tschöpe, C. Crosstalk between fibroblasts and inflammatory cells. *Cardiovasc Res* **102**, 258-269, doi:10.1093/cvr/cvu062 (2014).
- 73 Steffens, S. *et al.* Stimulating pro-reparative immune responses to prevent adverse cardiac remodelling: consensus document from the joint 2019 meeting of the ESC Working Groups of cellular biology of the heart and myocardial function. *Cardiovasc Res* **116**, 1850-1862, doi:10.1093/cvr/cvaa137 (2020).
- 74 Wu, Y. *et al.* S100a8/a9 released by CD11b+Gr1+ neutrophils activates cardiac fibroblasts to initiate angiotensin II-Induced cardiac inflammation and injury. *Hypertension* **63**, 1241-1250, doi:10.1161/hypertensionaha.113.02843 (2014).
- 75 Lindner, D. *et al.* Cardiac fibroblasts support cardiac inflammation in heart failure. *Basic Res Cardiol* **109**, 428, doi:10.1007/s00395-014-0428-7 (2014).
- 76 Pappritz, K. *et al.* Cardiac (myo)fibroblasts modulate the migration of monocyte subsets. *Sci Rep* **8**, 5575, doi:10.1038/s41598-018-23881-7 (2018).

- 77 Segers, V. F. M., Brutsaert, D. L. & De Keulenaer, G. W. Cardiac Remodeling: Endothelial Cells Have More to Say Than Just NO. *Front Physiol* **9**, 382, doi:10.3389/fphys.2018.00382 (2018).
- 78 Li, Y., Lui, K. O. & Zhou, B. Reassessing endothelial-to-mesenchymal transition in cardiovascular diseases. *Nature Reviews Cardiology* **15**, 445-456, doi:10.1038/s41569-018-0023-y (2018).
- 79 Sun, X., Nkenkor, B., Mastikhina, O., Soon, K. & Nunes, S. S. Endothelium-mediated contributions to fibrosis. *Semin Cell Dev Biol* **101**, 78-86, doi:10.1016/j.semcdb.2019.10.015 (2020).
- 80 Salvador, A. M. *et al.* Intercellular Adhesion Molecule 1 Regulates Left Ventricular Leukocyte Infiltration, Cardiac Remodeling, and Function in Pressure Overload-Induced Heart Failure. *J Am Heart Assoc* **5**, e003126, doi:10.1161/jaha.115.003126 (2016).
- 81 Palazzo, A. J. *et al.* Myocardial ischemia-reperfusion injury in CD18- and ICAM-1-deficient mice. *Am J Physiol* **275**, H2300-2307, doi:10.1152/ajpheart.1998.275.6.H2300 (1998).
- 82 Adiarto, S. *et al.* ET-1 from endothelial cells is required for complete angiotensin II-induced cardiac fibrosis and hypertrophy. *Life Sci* **91**, 651-657, doi:10.1016/j.lfs.2012.02.006 (2012).
- 83 Mohammed, S. F. *et al.* Coronary microvascular rarefaction and myocardial fibrosis in heart failure with preserved ejection fraction. *Circulation* **131**, 550-559, doi:10.1161/circulationaha.114.009625 (2015).
- 84 von Gise, A. & Pu, W. T. Endocardial and Epicardial Epithelial to Mesenchymal Transitions in Heart Development and Disease. *Circulation Research* **110**, 1628-1645, doi:10.1161/CIRCRESAHA.111.259960 (2012).
- 85 Moore-Morris, T. *et al.* Resident fibroblast lineages mediate pressure overload-induced cardiac fibrosis. *J Clin Invest* **124**, 2921-2934, doi:10.1172/jci74783 (2014).
- 86 Thiery, J. P., Acloque, H., Huang, R. Y. & Nieto, M. A. Epithelial-mesenchymal transitions in development and disease. *Cell* **139**, 871-890, doi:10.1016/j.cell.2009.11.007 (2009).
- 87 Nieto, M. A., Huang, R. Y., Jackson, R. A. & Thiery, J. P. EMT: 2016. *Cell* **166**, 21-45, doi:10.1016/j.cell.2016.06.028 (2016).
- 88 Ubil, E. *et al.* Mesenchymal-endothelial transition contributes to cardiac neovascularization. *Nature* **514**, 585-590, doi:10.1038/nature13839 (2014).
- 89 McMaster, W. G., Kirabo, A., Madhur, M. S. & Harrison, D. G. Inflammation, immunity, and hypertensive end-organ damage. *Circulation research* **116**, 1022-1033 (2015).
- 90 González, A. *et al.* Myocardial remodeling in hypertension: toward a new view of hypertensive heart disease. *Hypertension* **72**, 549-558 (2018).
- 91 Ghigo, A., Franco, I., Morello, F. & Hirsch, E. Myocyte signalling in leucocyte recruitment to the heart. *Cardiovascular research* **102**, 270-280 (2014).
- 92 Frantz, S. & Nahrendorf, M. Cardiac macrophages and their role in ischaemic heart disease. *Cardiovascular research* **102**, 240-248 (2014).
- 93 Klein, S. L. & Flanagan, K. L. Sex differences in immune responses. *Nature Reviews Immunology* **16**, 626-638, doi:10.1038/nri.2016.90 (2016).
- 94 Hannah, M. F., Bajic, V. B. & Klein, S. L. Sex differences in the recognition of and innate antiviral responses to Seoul virus in Norway rats. *Brain Behav Immun* **22**, 503-516, doi:10.1016/j.bbi.2007.10.005 (2008).
- 95 Klein, S. L., Jedlicka, A. & Pekosz, A. The Xs and Y of immune responses to viral vaccines. *Lancet Infect Dis* **10**, 338-349, doi:10.1016/s1473-3099(10)70049-9 (2010).
- 96 Pisitkun, P. *et al.* Autoreactive B cell responses to RNA-related antigens due to TLR7 gene duplication. *Science* **312**, 1669-1672, doi:10.1126/science.1124978 (2006).
- 97 Berghöfer, B. *et al.* TLR7 ligands induce higher IFN-alpha production in females. *J Immunol* **177**, 2088-2096, doi:10.4049/jimmunol.177.4.2088 (2006).

- 98 Griesbeck, M. *et al.* Sex Differences in Plasmacytoid Dendritic Cell Levels of IRF5 Drive Higher IFN- α Production in Women. *J Immunol* **195**, 5327-5336, doi:10.4049/jimmunol.1501684 (2015).
- 99 Spitzer, J. A. Gender differences in some host defense mechanisms. *Lupus* **8**, 380-383, doi:10.1177/096120339900800510 (1999).
- 100 Weinstein, Y., Ran, S. & Segal, S. Sex-associated differences in the regulation of immune responses controlled by the MHC of the mouse. *J Immunol* **132**, 656-661 (1984).
- 101 Rettew, J. A., Huet-Hudson, Y. M. & Marriott, I. Testosterone reduces macrophage expression in the mouse of toll-like receptor 4, a trigger for inflammation and innate immunity. *Biol Reprod* **78**, 432-437, doi:10.1095/biolreprod.107.063545 (2008).
- 102 Zaman, R. *et al.* Selective loss of resident macrophage-derived insulin-like growth factor-1 abolishes adaptive cardiac growth to stress. *Immunity* **54**, 2057-2071.e2056, doi:10.1016/j.immuni.2021.07.006 (2021).
- 103 Heidt, T. *et al.* Differential contribution of monocytes to heart macrophages in steady-state and after myocardial infarction. *Circ Res* **115**, 284-295, doi:10.1161/circresaha.115.303567 (2014).
- 104 Hulsmans, M. *et al.* Macrophages Facilitate Electrical Conduction in the Heart. *Cell* **169**, 510-522.e520, doi:10.1016/j.cell.2017.03.050 (2017).
- 105 Peet, C., Ivetic, A., Bromage, D. I. & Shah, A. M. Cardiac monocytes and macrophages after myocardial infarction. *Cardiovascular Research* **116**, 1101-1112, doi:10.1093/cvr/cvz336 (2019).
- 106 Swirski, F. K. & Nahrendorf, M. Cardioimmunology: the immune system in cardiac homeostasis and disease. *Nat Rev Immunol* **18**, 733-744, doi:10.1038/s41577-018-0065-8 (2018).
- 107 Dick, S. A. *et al.* Self-renewing resident cardiac macrophages limit adverse remodeling following myocardial infarction. *Nat Immunol* **20**, 29-39, doi:10.1038/s41590-018-0272-2 (2019).
- 108 Epelman, S. *et al.* Embryonic and adult-derived resident cardiac macrophages are maintained through distinct mechanisms at steady state and during inflammation. *Immunity* **40**, 91-104, doi:10.1016/j.immuni.2013.11.019 (2014).
- 109 Lavin, Y. *et al.* Tissue-resident macrophage enhancer landscapes are shaped by the local microenvironment. *Cell* **159**, 1312-1326, doi:10.1016/j.cell.2014.11.018 (2014).
- 110 Leuschner, F. & Nahrendorf, M. Novel functions of macrophages in the heart: insights into electrical conduction, stress, and diastolic dysfunction. *European Heart Journal* **41**, 989-994, doi:10.1093/eurheartj/ehz159 (2019).
- 111 Bajpai, G. *et al.* The human heart contains distinct macrophage subsets with divergent origins and functions. *Nature Medicine* **24**, 1234-1245, doi:10.1038/s41591-018-0059-x (2018).
- 112 Bajpai, G. *et al.* Tissue Resident CCR2⁻ and CCR2⁺ Cardiac Macrophages Differentially Orchestrate Monocyte Recruitment and Fate Specification Following Myocardial Injury. *Circulation Research* **124**, 263-278, doi:doi:10.1161/CIRCRESAHA.118.314028 (2019).
- 113 Kain, D. *et al.* Macrophages dictate the progression and manifestation of hypertensive heart disease. *Int J Cardiol* **203**, 381-395, doi:10.1016/j.ijcard.2015.10.126 (2016).
- 114 Liao, X. *et al.* Distinct roles of resident and nonresident macrophages in nonischemic cardiomyopathy. *Proc Natl Acad Sci U S A* **115**, E4661-e4669, doi:10.1073/pnas.1720065115 (2018).
- 115 Yona, S. *et al.* Fate mapping reveals origins and dynamics of monocytes and tissue macrophages under homeostasis. *Immunity* **38**, 79-91, doi:10.1016/j.immuni.2012.12.001 (2013).
- 116 Thomas, G., Tacke, R., Hedrick, C. C. & Hanna, R. N. Nonclassical Patrolling Monocyte Function in the Vasculature. *Arteriosclerosis, Thrombosis, and Vascular Biology* **35**, 1306-1316, doi:doi:10.1161/ATVBAHA.114.304650 (2015).

- 117 Geissmann, F., Jung, S. & Littman, D. R. Blood monocytes consist of two principal subsets with distinct migratory properties. *Immunity* **19**, 71-82, doi:10.1016/s1074-7613(03)00174-2 (2003).
- 118 Thierry, G. R. *et al.* Non-classical monocytes scavenge the growth factor CSF1 from endothelial cells in the peripheral vascular tree to ensure survival and homeostasis. *Immunity* **57**, 2108-2121.e2106, doi:10.1016/j.immuni.2024.07.005 (2024).
- 119 Cros, J. *et al.* Human CD14dim monocytes patrol and sense nucleic acids and viruses via TLR7 and TLR8 receptors. *Immunity* **33**, 375-386, doi:10.1016/j.immuni.2010.08.012 (2010).
- 120 Passlick, B., Flieger, D. & Ziegler-Heitbrock, H. W. Identification and characterization of a novel monocyte subpopulation in human peripheral blood. *Blood* **74**, 2527-2534 (1989).
- 121 Jakubzick, C. *et al.* Minimal differentiation of classical monocytes as they survey steady-state tissues and transport antigen to lymph nodes. *Immunity* **39**, 599-610, doi:10.1016/j.immuni.2013.08.007 (2013).
- 122 Carlin, L. M. *et al.* Nr4a1-dependent Ly6C(low) monocytes monitor endothelial cells and orchestrate their disposal. *Cell* **153**, 362-375, doi:10.1016/j.cell.2013.03.010 (2013).
- 123 Auffray, C. *et al.* Monitoring of blood vessels and tissues by a population of monocytes with patrolling behavior. *Science* **317**, 666-670, doi:10.1126/science.1142883 (2007).
- 124 Schyns, J. *et al.* Non-classical tissue monocytes and two functionally distinct populations of interstitial macrophages populate the mouse lung. *Nat Commun* **10**, 3964, doi:10.1038/s41467-019-11843-0 (2019).
- 125 Chakarov, S. *et al.* Two distinct interstitial macrophage populations coexist across tissues in specific subtissular niches. *Science* **363**, doi:10.1126/science.aau0964 (2019).
- 126 Bianchini, M. *et al.* PD-L1 expression on nonclassical monocytes reveals their origin and immunoregulatory function. *Sci Immunol* **4**, doi:10.1126/sciimmunol.aar3054 (2019).
- 127 Nahrendorf, M. *et al.* The healing myocardium sequentially mobilizes two monocyte subsets with divergent and complementary functions. *J Exp Med* **204**, 3037-3047, doi:10.1084/jem.20070885 (2007).
- 128 Hanna, R. N. *et al.* The transcription factor NR4A1 (Nur77) controls bone marrow differentiation and the survival of Ly6C[−] monocytes. *Nature Immunology* **12**, 778-785, doi:10.1038/ni.2063 (2011).
- 129 Lith, S. C. *et al.* Nuclear receptor Nur77 regulates immunomechanics of macrophages. *Eur J Cell Biol* **103**, 151419, doi:10.1016/j.ejcb.2024.151419 (2024).
- 130 Hilgendorf, I. *et al.* Ly-6Chigh monocytes depend on Nr4a1 to balance both inflammatory and reparative phases in the infarcted myocardium. *Circ Res* **114**, 1611-1622, doi:10.1161/circresaha.114.303204 (2014).
- 131 Liu, X. *et al.* Genome-wide analysis identifies NR4A1 as a key mediator of T cell dysfunction. *Nature* **567**, 525-529, doi:10.1038/s41586-019-0979-8 (2019).
- 132 Brooks, J. F. *et al.* Negative feedback by NUR77/*Nr4a1* restrains B cell clonal dominance during early T-dependent immune responses. *Cell Reports* **36**, doi:10.1016/j.celrep.2021.109645 (2021).
- 133 Thomas, G. D. *et al.* Deleting an Nr4a1 Super-Enhancer Subdomain Ablates Ly6C(low) Monocytes while Preserving Macrophage Gene Function. *Immunity* **45**, 975-987, doi:10.1016/j.immuni.2016.10.011 (2016).
- 134 Riehle, C. & Bauersachs, J. Small animal models of heart failure. *Cardiovascular Research* **115**, 1838-1849, doi:10.1093/cvr/cvz161 (2019).
- 135 Weir, M. R. & Dzau, V. J. The renin-angiotensin-aldosterone system: a specific target for hypertension management. *Am J Hypertens* **12**, 205s-213s, doi:10.1016/s0895-7061(99)00103-x (1999).

- 136 Ma, T. K., Kam, K. K., Yan, B. P. & Lam, Y. Y. Renin-angiotensin-aldosterone system blockade for cardiovascular diseases: current status. *Br J Pharmacol* **160**, 1273-1292, doi:10.1111/j.1476-5381.2010.00750.x (2010).
- 137 Janjic, A. *et al.* Prime-seq, efficient and powerful bulk RNA sequencing. *Genome Biology* **23**, 88, doi:10.1186/s13059-022-02660-8 (2022).
- 138 Dobin, A. *et al.* STAR: ultrafast universal RNA-seq aligner. *Bioinformatics* **29**, 15-21, doi:10.1093/bioinformatics/bts635 (2013).
- 139 Kolberg, L. *et al.* g:Profiler-interoperable web service for functional enrichment analysis and gene identifier mapping (2023 update). *Nucleic Acids Res* **51**, W207-w212, doi:10.1093/nar/gkad347 (2023).
- 140 Subramanian, A. *et al.* Gene set enrichment analysis: A knowledge-based approach for interpreting genome-wide expression profiles. *Proceedings of the National Academy of Sciences* **102**, 15545-15550, doi:doi:10.1073/pnas.0506580102 (2005).
- 141 Mootha, V. K. *et al.* PGC-1 α -responsive genes involved in oxidative phosphorylation are coordinately downregulated in human diabetes. *Nature Genetics* **34**, 267-273, doi:10.1038/ng1180 (2003).
- 142 Liberzon, A. *et al.* The Molecular Signatures Database (MSigDB) hallmark gene set collection. *Cell Syst* **1**, 417-425, doi:10.1016/j.cels.2015.12.004 (2015).
- 143 Hulsen, T., de Vlieg, J. & Alkema, W. BioVenn – a web application for the comparison and visualization of biological lists using area-proportional Venn diagrams. *BMC Genomics* **9**, 488, doi:10.1186/1471-2164-9-488 (2008).
- 144 Cleutjens, J. P., Verluyten, M. J., Smiths, J. F. & Daemen, M. J. Collagen remodeling after myocardial infarction in the rat heart. *Am J Pathol* **147**, 325-338 (1995).
- 145 Bonnans, C., Chou, J. & Werb, Z. Remodelling the extracellular matrix in development and disease. *Nat Rev Mol Cell Biol* **15**, 786-801, doi:10.1038/nrm3904 (2014).
- 146 Spada, S., Tocci, A., Di Modugno, F. & Nisticò, P. Fibronectin as a multiregulatory molecule crucial in tumor matrisome: from structural and functional features to clinical practice in oncology. *Journal of Experimental & Clinical Cancer Research* **40**, 102, doi:10.1186/s13046-021-01908-8 (2021).
- 147 Bime, C. *et al.* Reactive oxygen species-associated molecular signature predicts survival in patients with sepsis. *Pulm Circ* **6**, 196-201, doi:10.1086/685547 (2016).
- 148 Pei, J. *et al.* GPX3 and GSTT1 as biomarkers related to oxidative stress during renal ischemia reperfusion injuries and their relationship with immune infiltration. *Front Immunol* **14**, 1136146, doi:10.3389/fimmu.2023.1136146 (2023).
- 149 Frudd, K., Burgoyne, T. & Burgoyne, J. R. Oxidation of Atg3 and Atg7 mediates inhibition of autophagy. *Nature Communications* **9**, 95, doi:10.1038/s41467-017-02352-z (2018).
- 150 Hanna, A., Humeres, C. & Frangogiannis, N. G. The role of Smad signaling cascades in cardiac fibrosis. *Cell Signal* **77**, 109826, doi:10.1016/j.cellsig.2020.109826 (2021).
- 151 Pollak Nina, M., Hoffman, M., Goldberg Ira, J. & Drosatos, K. Krüppel-Like Factors. *JACC: Basic to Translational Science* **3**, 132-156, doi:10.1016/j.jacbts.2017.09.001 (2018).
- 152 George, M., Vijayakumar, A., Dhanesh, S. B., James, J. & Shivakumar, K. Molecular basis and functional significance of Angiotensin II-induced increase in Discoidin Domain Receptor 2 gene expression in cardiac fibroblasts. *J Mol Cell Cardiol* **90**, 59-69, doi:10.1016/j.yjmcc.2015.12.004 (2016).
- 153 Xu, J. *et al.* CCR2 mediates the uptake of bone marrow-derived fibroblast precursors in angiotensin II-induced cardiac fibrosis. *Am J Physiol Heart Circ Physiol* **301**, H538-547, doi:10.1152/ajpheart.01114.2010 (2011).
- 154 Chen, S. *et al.* Modulation of anti-cardiac fibrosis immune responses by changing M2 macrophages into M1 macrophages. *Molecular Medicine* **30**, 88, doi:10.1186/s10020-024-00858-z (2024).
- 155 Shah, R. V. & Januzzi, J. L., Jr. ST2: a novel remodeling biomarker in acute and chronic heart failure. *Curr Heart Fail Rep* **7**, 9-14, doi:10.1007/s11897-010-0005-9 (2010).

- 156 Wang, C. *et al.* The KLF7/PFKFB3/ACADL axis modulates cardiac metabolic remodelling during cardiac hypertrophy in male mice. *Nature Communications* **14**, 959, doi:10.1038/s41467-023-36712-9 (2023).
- 157 Durrant, T. N. & Hers, I. PI3K inhibitors in thrombosis and cardiovascular disease. *Clin Transl Med* **9**, 8, doi:10.1186/s40169-020-0261-6 (2020).
- 158 Vieira, J. M. *et al.* The cardiac lymphatic system stimulates resolution of inflammation following myocardial infarction. *J Clin Invest* **128**, 3402-3412, doi:10.1172/jci97192 (2018).
- 159 Wojciak-Stothard, B. *et al.* Role of RhoB in the regulation of pulmonary endothelial and smooth muscle cell responses to hypoxia. *Circ Res* **110**, 1423-1434, doi:10.1161/circresaha.112.264473 (2012).
- 160 Choi, H., Tostes, R. C. & Webb, R. C. Mitochondrial aldehyde dehydrogenase prevents ROS-induced vascular contraction in angiotensin-II hypertensive mice. *J Am Soc Hypertens* **5**, 154-160, doi:10.1016/j.jash.2011.02.005 (2011).
- 161 McNab, F., Mayer-Barber, K., Sher, A., Wack, A. & O'Garra, A. Type I interferons in infectious disease. *Nature Reviews Immunology* **15**, 87-103, doi:10.1038/nri3787 (2015).
- 162 Ponikowski, P. *et al.* 2016 ESC Guidelines for the diagnosis and treatment of acute and chronic heart failure: The Task Force for the diagnosis and treatment of acute and chronic heart failure of the European Society of Cardiology (ESC) Developed with the special contribution of the Heart Failure Association (HFA) of the ESC. *Eur Heart J* **37**, 2129-2200, doi:10.1093/eurheartj/ehw128 (2016).
- 163 Regitz-Zagrosek, V. *et al.* Gender in cardiovascular diseases: impact on clinical manifestations, management, and outcomes. *Eur Heart J* **37**, 24-34, doi:10.1093/eurheartj/ehv598 (2016).
- 164 Petrov, G. *et al.* Maladaptive remodeling is associated with impaired survival in women but not in men after aortic valve replacement. *JACC Cardiovasc Imaging* **7**, 1073-1080, doi:10.1016/j.jcmg.2014.06.017 (2014).
- 165 Buechler, M. B., Fu, W. & Turley, S. J. Fibroblast-macrophage reciprocal interactions in health, fibrosis, and cancer. *Immunity* **54**, 903-915, doi:10.1016/j.immuni.2021.04.021 (2021).
- 166 Kuppe, C. *et al.* Spatial multi-omic map of human myocardial infarction. *Nature* **608**, 766-777, doi:10.1038/s41586-022-05060-x (2022).
- 167 Maruyama, K. & Imanaka-Yoshida, K. The Pathogenesis of Cardiac Fibrosis: A Review of Recent Progress. *Int J Mol Sci* **23**, doi:10.3390/ijms23052617 (2022).
- 168 Latchman, D. S. Heat shock proteins and cardiac protection. *Cardiovascular Research* **51**, 637-646, doi:10.1016/s0008-6363(01)00354-6 (2001).
- 169 Leone, P. *et al.* MHC Class I Antigen Processing and Presenting Machinery: Organization, Function, and Defects in Tumor Cells. *JNCI: Journal of the National Cancer Institute* **105**, 1172-1187, doi:10.1093/jnci/djt184 (2013).
- 170 Dhatchinamoorthy, K., Colbert, J. D. & Rock, K. L. Cancer Immune Evasion Through Loss of MHC Class I Antigen Presentation. *Front Immunol* **12**, 636568, doi:10.3389/fimmu.2021.636568 (2021).
- 171 Palumbo-Zerr, K. *et al.* Orphan nuclear receptor NR4A1 regulates transforming growth factor- β signaling and fibrosis. *Nature Medicine* **21**, 150-158, doi:10.1038/nm.3777 (2015).
- 172 Schulz, E., Gori, T. & Münzel, T. Oxidative stress and endothelial dysfunction in hypertension. *Hypertension Research* **34**, 665-673, doi:10.1038/hr.2011.39 (2011).
- 173 Incalza, M. A. *et al.* Oxidative stress and reactive oxygen species in endothelial dysfunction associated with cardiovascular and metabolic diseases. *Vascul Pharmacol* **100**, 1-19, doi:10.1016/j.vph.2017.05.005 (2018).
- 174 Gori, T. & Münzel, T. Oxidative stress and endothelial dysfunction: therapeutic implications. *Ann Med* **43**, 259-272, doi:10.3109/07853890.2010.543920 (2011).

- 175 Maack, C. *et al.* Oxygen free radical release in human failing myocardium is associated with increased activity of rac1-GTPase and represents a target for statin treatment. *Circulation* **108**, 1567-1574, doi:10.1161/01.Cir.0000091084.46500.Bb (2003).
- 176 Mollnau, H. *et al.* Effects of Angiotensin II Infusion on the Expression and Function of NAD(P)H Oxidase and Components of Nitric Oxide/cGMP Signaling. *Circulation Research* **90**, e58-e65, doi:10.1161/01.RES.0000012569.55432.02 (2002).
- 177 Maack, C. & Böhm, M. Targeting Mitochondrial Oxidative Stress in Heart Failure. *Journal of the American College of Cardiology* **58**, 83-86, doi:10.1016/j.jacc.2011.01.032 (2011).
- 178 Regitz-Zagrosek, V. Sex and Gender Differences in Heart Failure. *Int J Heart Fail* **2**, 157-181, doi:10.36628/ijhf.2020.0004 (2020).
- 179 Te Riet, L., van Esch, J. H., Roks, A. J., van den Meiracker, A. H. & Danser, A. H. Hypertension: renin-angiotensin-aldosterone system alterations. *Circ Res* **116**, 960-975, doi:10.1161/circresaha.116.303587 (2015).
- 180 Schunkert, H. *et al.* Effects of estrogen replacement therapy on the renin-angiotensin system in postmenopausal women. *Circulation* **95**, 39-45, doi:10.1161/01.cir.95.1.39 (1997).
- 181 Hilliard, L. M., Sampson, A. K., Brown, R. D. & Denton, K. M. The "his and hers" of the renin-angiotensin system. *Curr Hypertens Rep* **15**, 71-79, doi:10.1007/s11906-012-0319-y (2013).
- 182 Dworatzek, E. *et al.* Sex-specific regulation of collagen I and III expression by 17 β -Estradiol in cardiac fibroblasts: role of estrogen receptors. *Cardiovasc Res* **115**, 315-327, doi:10.1093/cvr/cvy185 (2019).
- 183 Dobaczewski, M., Chen, W. & Frangogiannis, N. G. Transforming growth factor (TGF)- β signaling in cardiac remodeling. *J Mol Cell Cardiol* **51**, 600-606, doi:10.1016/j.yjmcc.2010.10.033 (2011).
- 184 Pedram, A., Razandi, M., O'Mahony, F., Lubahn, D. & Levin, E. R. Estrogen receptor-beta prevents cardiac fibrosis. *Mol Endocrinol* **24**, 2152-2165, doi:10.1210/me.2010-0154 (2010).

8. Acknowledgements

First and foremost, I would like to express my gratitude to my supervisor, Prof. Sabine Steffens, for giving me the opportunity to join the lab as an intern and continue with my journey as a PhD student. Thank you for providing me with the freedom to explore and the space to grow while always being available to offer support and guidance whenever needed. Your gentle and caring approach has made me feel secure and motivated, making the often-challenging journey much easier and more enjoyable. I would also like to thank my TAC members, Prof. Christian Schulz and Dr. Johan Duchene. Thank you for providing invaluable scientific insight and suggestions for the project.

Next, I would like to express my gratitude to Dr. Sarah-Lena Puhl. Thank you for introducing me to the world of scientific research. Your passion for science and your pursuit of perfection have profoundly inspired me to strive for excellence and aim higher.

I am also thankful to Dr. Sabrina Bortoluzzi for your valuable insights into experimental design and data analysis, as well as your assistance in revising my thesis.




I would also like to extend my thanks to Anna Kaltenbach for being such a great benchmate. Your help with troubleshooting and dealing with ZVH was invaluable, and I truly enjoyed every moment of working alongside you.

In addition, I would also like to thank Emma Buller for being my internship student. Thank you for allowing me to experience the transition from learning to teaching.

I am also grateful for the help and support of all other members of AG Steffens: Prof. Alexander Faussner, Yong Wang, Bingni Chen, George Shakir, Guo Li, Aishvarya Prabhu, Martina Geiger, Srishti Ramanathan, and Shiyu Cao. Thank you for creating such a friendly and enriching lab environment in which I have felt very comfortable working.

Last but not least, my deepest gratitude to my family for accompanying me through this journey.

9. Affidavit

	LUDWIG- MAXIMILIANS- UNIVERSITÄT MÜNCHEN	Promotionsbüro Medizinische Fakultät		
Affidavit				

Shia, Yi Xuan

Surname, first name

Pettenkoferstraße 9b

Street

80336, München, Deutschland

Zip code, town, country

I hereby declare, that the submitted thesis entitled:

Role of non-classical monocytes in angiotensin II-induced cardiac remodelling

.....

is my own work. I have only used the sources indicated and have not made unauthorised use of services of a third party. Where the work of others has been quoted or reproduced, the source is always given.

I further declare that the dissertation presented here has not been submitted in the same or similar form to any other institution for the purpose of obtaining an academic degree.





Munich, 05.12.2024

place, date

Yi Xuan Shia

Signature doctoral candidate

10. Confirmation of congruency

			
Confirmation of congruency between printed and electronic version of the doctoral thesis			

Shia, Yi Xuan

Surname, first name

Pettenkoferstraße 9b

Street

80336, München, Deutschland

Zip code, town, country

I hereby declare, that the submitted thesis entitled:

Role of non-classical monocytes in angiotensin II-induced cardiac remodelling

.....

is congruent with the printed version both in content and format.

Munich, 05.12.2024

place, date

Yi Xuan Shia

Signature doctoral candidate

12. Publications and abstract presentations

12.1 List of publications

1. **Y. X. Shia**, K. Pappritz, A. C. Kaltenbach, G. Li, V. Fardella, S. Van Linthout, D. Carnevale, S. Steffens, S.-L. Puhl. Pericardial adipose tissue promotes transition to heart failure with reduced ejection fraction upon pressure-overload in mice. *Basic Research in Cardiology*. (accepted)
2. B. Schopohl, M. Kohlhaas, A. G. Nickel, A.-F. Schiuma, S. L. Maas, E. P. C. van der Vorst, **Y. X. Shia**, C. Maack, S. Steffens, S.-L. Puhl (2024) Gpr55 deficiency crucially alters cardiomyocyte homeostasis and counteracts angiotensin II induced maladaptation in female mice. *British Journal of Pharmacology*, 1-22. doi:<https://doi.org/10.1111/bph.17350>.
3. K. Pappritz, S.-L. Puhl, I. Matz, E. Brauer, **Y. X. Shia**, M. El-Shafeey, S. E. Koch, K. Miteva, C. Mucha, G. N. Duda, A. Petersen, S. Steffens, C. Tschöpe, & S. Van Linthout (2023). Sex- and age-related differences in the inflammatory properties of cardiac fibroblasts: impact on the cardiosplenic axis and cardiac fibrosis. *Frontiers in cardiovascular medicine*, 10, 1117419.

12.2 List of abstracts

1. **Y. X. Shia**, J. Duchene, S.-L. Puhl, S. Steffens (2024). Depletion of non-classical monocytes abolishes sex differences in angiotensin II-induced cardiac fibrosis. Poster presentation at the annual autumn meeting of the German Society for Cardiology (Herztage der Deutschen Gesellschaft für Kardiologie; DGK).
2. **Y. X. Shia**, J. Duchene, S.-L. Puhl, S. Steffens (2024). Depletion of non-classical monocytes abolishes sex differences in angiotensin II-induced cardiac fibrosis. Poster presentation at the II. Cardioimmunology Congress, Bad Staffelstein, Germany.
3. **Y. X. Shia**, G. Li, S.-L. Puhl, S. Steffens (2023). Sex-dependent differences in cardiac remodelling and circulating monocyte phenotype in a model of chronic angiotensin II infusion. Poster presentation at the 10th Cardiac Regeneration and Vascular Biology Conference, San Servolo, Venice, Italy.
4. **Y. X. Shia**, G. Li, S.-L. Puhl, S. Steffens (2023). Sex-dependent differences in cardiac remodelling and circulating monocyte phenotype in a model of chronic angiotensin II infusion. Poster presentation at the annual spring meeting of the German Society for Cardiology (Jahrestagung der Deutschen Gesellschaft für Kardiologie; DGK).
5. **Y. X. Shia**, J. Duchene, S.-L. Puhl, S. Steffens (2022). Role of non-classical monocytes in angiotensin II-induced cardiac remodelling. Poster presentation at the annual autumn meeting of the German Society for Cardiology (Herztage der Deutschen Gesellschaft für Kardiologie; DGK).